IMAGE: A MAP OF THE STARS OF THE ORION CONSTELLATION

Print ISSN: 2631-8490 Online ISSN: 2631-8504

JournalPreview

London Journal of Research in Science: Natural and Formal
Volume 23 | Issue 2 | Compilation 1.0

Great Britain Journals Press

WWW.JOURNALSPRESS.COM

Journal Content
In this Issue

Great Britain Journals Press

Review of Fundamentals of Covariant Quantum Mechanics in the Dual 4-Dimensional Space-Time : Substance of Wave Function, the Origin of Quantum Probability and the Cause of Quantum Superposition State

Zhao Guoqiu & Zhao Cancan

Huazhong University of Science and Technology

ABSTRACT

Microscopic objects have some spatial distribution, which influences quantum phenomena. The particle model does not apply to the microworld. In this work, we use a rotating field matter sphere model. The size of the sphere changes along with the movement state, harmonizing with special relativity. Thus, we independently construct a dual 4-dimensional space-time to describe the microscopic quantum phenomenon and establish the objective reality of plural description, which has obvious theoretical advantages. In the dual 4-dimensional space-time, the wave function describes matter waves as physical waves. Which is the physical basis of quantum communication. Quantum probability originates from the tangible structure and matter density distribution of the microscopic objects and is reflected in the transformation of space-time. Matter waves and probability waves can be transformed by using Fourier transformation.

Keywords: field matter sphere; model; matter wave; quantum probability; origin; transformation of representation.

Classification: DDC Code: 530.12 LCC Code: QC174.12

Language: English

Great Britain Journals Press

LJP Copyright ID: 925611
Print ISSN: 2631-8490
Online ISSN: 2631-8504

London Journal of Research in Science: Natural and Formal

Volume 23 | Issue 2 | Compilation 1.0

Review of Fundamentals of Covariant Quantum Mechanics in the Dual 4-Dimensional Space-Time: Substance of Wave Function, the Origin of Quantum Probability and the Cause of Quantum Superposition State

Zhao Guoqiu[α] & Zhao Cancan[σ]

ABSTRACT

Microscopic objects have some spatial distribution, which influences quantum phenomena. The particle model does not apply to the microworld. In this work, we use a rotating field matter sphere model. The size of the sphere changes along with the movement state, harmonizing with special relativity. Thus, we independently construct a dual 4-dimensional space-time to describe the microscopic quantum phenomenon and establish the objective reality of plural description, which has obvious theoretical advantages. In the dual 4-dimensional space-time, the wave function describes matter waves as physical waves. Which is the physical basis of quantum communication. Quantum probability originates from the tangible structure and matter density distribution of the microscopic objects and is reflected in the transformation of space-time. Matter waves and probability waves can be transformed by using Fourier transformation.

Keywords: field matter sphere; model; matter wave; quantum probability; origin; transformation of representation.

Author α: HUST-WISCO Joint Laboratory, Huazhong University of Science and Technology, Wuhan, Hubei, China.
σ: Department of Materials Science and Engineering, Southern University of Science and Technology, Shenzhen, Guangdong, China.

I. INTRODUCTION

The physical meaning of the wave function and the origin of quantum probability are two of the most concerning problems of quantum mechanics. For the physical meaning of the wave function, The realist school, represented by Einstein, De Broglie, and Schrodinger, indicates that the wave function has a physical meaning and describes physical reality; The indeterminist school, represented by Bohr, Born, Heisenberg, and Dirac, believes that the wave function has no physical meaning but just describes the probability distribution of the microscopic particle, the square of the absolute value of the wave function describes the probability density of the microscopic particle appearing in space and time. The indeterminist school considers that the wave functions are knowledge of the cognitive world (cognitivism), known as the school of nondeterminism. [1]

Some scholars even directly believe that the wave function is a mathematical reality. Thus, there are two opposite opinions about the origin of quantum probability. One school represented by Einstein believes that “God does not play dice”, thus quantum probability derives from external uncertainties, which are defined as "hidden variables" by Bohm [1]. The other school, represented by Bohr, believes that microscopic particles have natural uncertainty, and quantum probability originates from the nature of particles [1].

London Journal of Research in Science: Natural and Formal

For the difficulty of quantum mechanics, Thom [2], Sakata [3], and Yukawa [4] believed that microscopic objects could not be treated as point particles in microworld. The superstring theory should be considered as a non-point model, which was a great success. Up to now, although the superstring theory is hard to be determined experimentally, it continues to grow [5]. The basic research of quantum mechanics is still developing.

At the 2019 International Symposium on Fundamentals of Quantum Mechanics, Peter J. Lewis, professor of Dartmouth College, focusing on the measurement-induced collapse problem, pointed out three main viewpoints for realism: Spontaneous collapse, pilot-wave theory, and Many worlds theory. However, the defects of these models could also lead to problems, such as insufficiently deterministic, non-local, probability, dimension, and self-interaction. To address the dilemma of realism, cognitivism proposes that wave function is not a description of the world, but a theory about information, knowledge, and belief. The four theoretical forms are ψ- cognitivism, Quantum Information, Quantum Bayesianism, and Quantum pragmatism [6]. In this cognitive route, it is difficult to achieve unification on the nature of wave function, the origin of quantum probability, the matter basis of Over light speed and quantum communication in quantum measurement, etc.

In this work, we abandoned the point model and adopted the rotating field matter sphere model, to establish a dual 4-dimensional space-time for describing the microscopic quantum phenomena. In the dual 4-dimensional space-time, wave function describes matter waves as physical waves. In the present model, the microscopic quantum objects could be described using complex numbers. Quantum probability originates from the physical structure and matter density distribution of the microscopic objects. Quantum measurement introduces new continuous interactions through local transformation to eliminate fixed phase differences, leading to the transformation of doal 4 -dimensional space-time to classical space-time description, and the evolution of matter waves into probability waves [7]. It is of great significance to discuss the physical nature of quantum entanglement and quantum communication.

II. GEOMETRICAL CONSTRUCTION OF THE MICROSCOPIC QUANTUM OBJECT AND ESTABLISHMENT OF THE DUAL 4-DIMENSIONAL SPACE-TIME

Let's review the basic concepts of space-time. For space-time and philosophy, we advocate that matter and space-time are inseparable. For space-time and geometry, Euclidean geometry, Minkowski geometry, and Riemannian geometry are included. For space-time and physics, we believe that physical space-time has construction characteristics. Newtonian space-time is physical space-time, using Euclidean geometry as geometric background. The space-time of special relativity is also physical, using Minkowski geometry as geometric background. The space-time of general relativity is physical space-time and its geometric background is Riemannian geometry. The dual 4-dimensional space-time of quantum mechanics is also physical, we chose complex numbers extension of Minkowski's geometry as geometric background.

The foundation of the dual 4-dimensional space-time covariant quantum mechanics consists of three parts. Firstly, philosophical foundation: establishment of the interaction realism; Secondly, is a modification of the physical model, adopting the rotating field matter sphere model (rotating curvature vector). Thirdly, establishing the dual 4-dimensional space-time to describe the microscopic quantum phenomena. This word focuses on the last two parts.

2.1 Matter sphere model of rotating field in the dual 4-dimensional space-time covariant quantum mechanics

Previous research reveals that, in modern physics, spatial coordinates of microscopic objects should not be smaller than the Compton wavelength λ_c ($\lambda_c=h/mc$) [8]. Furthermore, the radius of the electron shows good agreement with the Compton wavelength [9], which was experimentally proved.

2.1.1 Experimental Evidence of the Field Matter Sphere Model

1. Study on electronic dipole moment of advanced cold molecules

Doyle's team [10] found that an Electron is a perfect sphere. This research provides an important experimental basis for applying the field matter sphere model in the basic theory of the dual 4-dimensional space-time covariant quantum mechanics.

2. Comparison between experimental and theoretical values of Hofstadter particle radius $R_0=\hbar/m_0c$, $R_4=\hbar/mc$ take this as a theoretical value of the microcosmic object distribution "radius". A comparison of the theoretical values with the experimental values is shown in the following table:

Table 1: Comparison of experimental values of electron, proton, and neutron radii with theoretical values of Compton wavelength (static -- R_0, dynamic -- R_4) [9]

Category	Proton (static) (R0)	Neutron (static) (R0)	Static electron (R0)	Moving electron (20Gev) (R4)	Moving electron (60Gev) (R4)
Theoretical value	0.21×10^{-15}m	0.21×10^{-15}m	3.86×10^{-11}cm	0.93×10^{-15}cm	3.1×10^{-16}cm
Experimental value	1.1×10^{-15}m	1.1×10^{-15}m	Accord with estimate	$< 10^{-15}$cm	$< 10^{-16}$cm

The theoretical values show good agreement with experimental values. However, Ding's measurement accuracy was improved to 10^{-17}cm, still proving that electrons are not points.

The microscopic objects are not point particles, but have a certain "spatial distribution", and the distribution radius R decreases with increased movement speed. The comparison of experimental and theoretical values shows that it is reasonable to use Compton wavelength λ_0 (λ_4) to construct the extension distribution of the static (dynamic) microscopic objects.

3. Uncertainty of Landau's single mechanical quantity

In 1930 Landau indicated that there were two uncertainties for measuring a single mechanical quantity, position measurement uncertainty ($\triangle X_o = \hbar/m_0c$) and momentum uncertainty ($\triangle P_o = m_0c$).[11] The uncertainty of electronic position is the theoretical value of the "radius" of electronic Distribution

$$R_o = \hbar / m_0c$$

Landau's explanation of $\triangle x_0$ should come from the point particle hypothesis. But an electron is not a point particle, and a true distribution radius R_0 is exist for the electron. If the electron is regarded as a "point", then the "point" must be dispersed in a range of cycles with a diameter of $2R_0$. An electron couldn't be positive more accurate than $2R_0$, meanwhile, the electron's position is uncertain. This is an important theoretical basis for the field matter sphere model provided by Landau.

2.12 Geometrical construction of the microscopic objects

State description of the microscopic objects in the sphere model [7] : In static status, the radius of curvature is

$$R_o = \hbar / m_o c \tag{1}$$

M_o is defined as the static mass of the matter field, and R_o shows the extension of the matter distribution in the intrinsic rotating field of a static microscopic object. And the curvature K_o is determined as

$$K_0 = 1/R_0 = m_0 c/h \tag{2}$$

R_o and K_o define the microscopic object. They are two invariants for any reference frame, independent of position x in space. The microscopic object represented by R_o and K_o is similar to the physical noumenon. A physical noumenon cannot be observed directly, but it is real. Observations are all phenomenal entities. K_o is called the quantum curvature of the microscopic object.

In dynamic status, the radius of curvature is defined as

$$R_4 = \hbar /mc \tag{3}$$

Curvature is defined as

$$K_4 = 1/R_4 = mc/\hbar \tag{4}$$

Where m is the motion mass. As m increases, the radius of curvature decreases, and the curvature increases. A sphere of matter is a quantum object of variable form. In translation and spin rotation, the linear velocity of the edge of the sphere does not exceed the speed of light, which is coordinated with the relativity theory. It is a physical entity [7] in the theory of physics.

In three-dimensional (four-dimensional) space mapping, curvature radius is defined as

$$R_i = \hbar/mv_i \tag{5}$$

Curvature is defined as

$$K_i = mv_i/\hbar \tag{6}$$

$P_i = mv_i$ is relativistic momentum, which is observable. $i = 1,2,3$.

R_i and K_i are "representations" of physical noumenon R_o and K_o in physical space, respectively. Physical noumenon cannot be observed directly, but "representation" can be observed. Quantum "motion" carries all quantum phenomena.

Rotation frequency is defined as

$$\nu_0=E_0/h,\ \nu_4=E/h,\ (\nu_i=E_i/h) \tag{7}$$

$E_o= m_oc^2$, $E=mc^2$, ($E_i=m_ov_i^2/2$ or $E_i=mv_i^2/2$), which is consistent with the basic assumptions of quantum mechanics and relativity.

The field matter density is defined as

$$\eta = m/V = \eta(k) \tag{8}$$

V is the volume of the field matter sphere, V=V(R), R=R(k), and η, the density of the matter field, is a function of the curvature k. $k = k_0, k_4, k_i$. It can be proved that with a decrease or increase of V, k and η increase or decrease, respectively. η (k) is positively correlated with k.

According to our understanding, R_0 and R_4 should not be less than the Planck length, and the field matter density and energy density of the field matter sphere cannot be infinite. Thus, the problem of infinite curvature of point particle theory is solved.

In the rotating field matter sphere model, we can establish the attachment relationship of the waves to the rotating field matter sphere, which is similar to the relationship hypothesis between energy, momentum, wavelength, and frequency in the Einstein and De Broglie point model. Here, the equations of E=hν, p=h/ λ will evolve into the real physical process of field matter sphere movement, as show as follow:

$$E = h\nu = \hbar\omega$$
$$p = h/\lambda = \hbar k$$

The physical state corresponding to the spherical model is described by the above formulas. ω denotes the rotational frequency of the field matter sphere, k= P/ħ denotes the curvature of the field matter sphere ($k=K_0, k_4, k_i$), which describes the density change of the field matter sphere. But the corresponding physical model is the rotating field matter sphere, not a point particle. Hence, matter waves of microscopic objects there is a new definition.

A microscopic object is a rotating field matter sphere with mass evenly distributed, which has a certain spatial distribution. Position *x* is uncertain for the microscopic object. 2R ($2R_0$, $2R_4$) is the uncertainty of position *x*.

If the microscopic object does not move, then $v_i=0$, $K_i=0$, in the physical space-time, the release map of the ontology structure K is 0, there is no change in the morphological structure and field matter density, and the phenomenon of quantum fluctuation disappears. In addition, according to the relativistic momentum (curvature) triangle, the microscopic object does not move, m*v*=0. Meanwhile, the angle between m_0c and *mc* is *a*=0, along the movement direction of the microscopic object. *x*=0 (*v*=*x*/t, *v*=0, *x*=0). The spatial release mapping of ontology R_0 in physical space-time is 0, and the position coordinates do not appear. Although ontology R_0 still exists. Therefore, quantum motion is a necessary condition for K_0 and R_0 to present quantum phenomena in physical space-time. *x* and *k* are the basic variables to describe quantum phenomena, quantum phenomena could be describted in the physical space-time (*x, k*) constructed by the moving microscopic object itself. But the position *x* of the microscopic object is uncertain and within a range.

2.2 The Energy Formula of Special Relativity and the Establishment of the Field Matter Sphere Model and the Dual 4-Dimensional Space-Time in Quantum Mechanics

2.1.1 Revelation of Relativistic Energy Formula

According to the relativistic energy formula of the microscopic objects, as shown as follow:

$$E^2 = (mv_i)^2c^2 + m_0^2c^4, \quad (mc)^2 = (mv_i)^2 + (m_0c)^2 \tag{9}$$

A momentum triangle can be obtained:

$$p_4^2 = p_i^2 + p_0^2 \tag{10}$$

Divide both sides of equation (10) into a $\hbar^2$, resulting in a sphere model curvature triangle:

$$k_4^2 = k_i^2 + K_0^2 , \quad i=1, 2, 3 \tag{11}$$

The vector relation is:

$$K_o = \mathbf{k}_4 - \mathbf{k}_i \tag{12}$$

Therefore, the 4-dimensional curvature space K and the related 4-dimensional coordinate space X of the motion microscopic object can be defined.

2.2.2 Establishment of Double 4-Dimensional Space-Time in Quantum Mechanics

4-dimensional curvature k-space is $k = K(k_4 - k_1 - k_2 - k_3)$ (13)

4-dimensional coordinate x-Space is $x = X(x_4 - x_1 - x_2 - x_3)$ (14)

The spatial invariant of 4-dimensional curvature K is given by formula (12)

$$k_0^2 = k_4^2 - k_1^2 - k_2^2 - k_3^2 \tag{15}$$

4 dimensional coordinate space x invariant is

$$x_0^2 = x_4^2 - x_1^2 - x_2^2 - x_3^2 \tag{16}$$

x_o can be seen as the projection of R_o of the microscopic object associated with k_o onto a 4-dimensional space x. k_o and x_o are invariants under two 4-dimensional coordinate transformations. It just reflects the existence of the microscopic object, that is physical noumenon, independent of space-time transformation. The two Spaces k and $\boldsymbol{x}$ can jointly construct a dual 4- dimensional complex space-time W($\boldsymbol{x},\boldsymbol{k}$) associated with the state description of the moving microscopic object.

$$W = x_\mu + ik_\mu \quad W^{※} = x_\mu - ik_\mu$$

μ=1,2,3,4, $k_{(1,2,3,4)}$ and $\boldsymbol{x}_{(1,2,3,4)}$ are two 4-dimensional releases of hidden spatial degrees of freedom for the point model [7]. $\boldsymbol{x}_{(1,2,3,4)}$ is the location of the microscopic object and has uncertain properties. x and k are Lorentz covariants. Hence, Dual 4-dimensional space-time is supported by relativity. Let the state wave function describing microscopic quantum phenomena in W(x,k) be:

$$\Psi(x,k) = A(x,k)e^{-ik\mu x\mu} \tag{17}$$

It's a complex function. A_n (x,k) is amplitude, which is complicated. The phase of the wave function is constituted by coordinate $k_\mu x_\mu$, which is dimensionless. The wave function ψ (x,k) is described in the phase space $k_\mu x_\mu$. Wigner's prediction, "the use of complex numbers is in this case not a calculational trick of applied mathematics but comes close to being a necessity in the formulation of the laws of quantum mechanics", is confirmed. [12]

Equation (17) is similar to Penrose's 5-dimensional twisted space, in which the state wave function is described in 2-dimensional complex space and 3-dimensional classical real space. In the present model, the space is the relativistic covariant dual 4-dimensional complex space, the state wave function is described in 4-dimensional imaginary space + 4-dimensional real space. It could be proved that the dual 4-dimensional complex space-time W(x, k) can be generated automatically in the derivation of the wave function. In dual 4-dimensional complex space-time, the value of curvature k represents the particle property, and the change of curvature k (the change of matter density) shows fluctuation. Thus, the matter wave could be described as a physical wave by the wave function which establishes the objective reality of complex numbers. (note 1). The wave-particle duality of microscopic objects could be uniformly and intrinsically understood very well.

The amplitude A(x,k) cannot be compared with that of classical waves, and the image is unimaginable [13]. It is expected to be understood in the derivation of the matter wave function. Wigner gave an expanded form of A(x,k) [14], which could be used to discuss the wave equation in dual 4-dimensional space-time.

Formula (10) and (12) show that the hidden spatial freedom of the microscopic object point model could be released in a 4-dimensional space. The releasement could be observed, and is related to the motion of the microscopic object. This will be demonstrated in the derivation of wave functions in the next section.

2.3 Physical properties and space-time metric of the dual 4-dimensional space-time W(x, k)

Vector K (k_1, k_2, k_3, k_4) describes the spatial structure of the microscopic object itself, presenting the existence form and matter density distribution of the microscopic object.

Vector X(x_1,x_2,x_3,x_4) describes the position of the microscopic object, with uncertainty (or probability). And then uncertainty corresponds to the matter density distribution of the microscopic object.

Further study shows that all quantum phenomena are described in the Dual 4-dimensional complex phase space W(x, k) composed of vectors X and K. The metric tensor of $W(x, k)$ is

$$\begin{aligned} g^{\mu\nu} &= diag(1, -1, -1, -1) \\ x^2 &= x_\mu g^{\mu\nu} x_\nu = x_4^2 - x_1^2 - x_2^2 - x_3^2 \\ k^2 &= k_\mu g^{\mu\nu} k_\nu = k_4^2 - k_1^2 - k_2^2 - k_3^2 \\ |W|^2 &= WW^{※} = x^2 + k^2 \end{aligned} \tag{18}$$

When the microscopic quantum object spins locally

$$k_i = 0,\ x_i = 0,\ i = 1,2,3.$$

$$|W|^2 = A_0^2 = x_4^2 + k_4^2 = x_0^2 + k_0^2$$

A_0 denotes the amplitude of the microscopic quantum object(the physical noumenon——the rotating field matter sphere).

x and k are Lorentz invariants, and the space-time is uniform and flat. Therefore, we consider W(x,k) to be a complex extension of M^4 (x). The Dirac equation is invariant in Lorentz transformation.

III. DERIVATION OF THE MATTER WAVE FUNCTION, MATTER-WAVE EQUATION, AND QUANTUM PROBABILITY IN THE DUAL 4-DIMENSIONAL SPACE-TIME

3.1 Generation and Derivation of the Matter Wave Function in the Dual 4-Dimensional Space- Time

We have defined a static rotating field matter sphere with a radius $R_o=\hbar/ m_oc$ and a curvature $K_o =m_oc/\hbar$. Rotational angular frequency $\omega_o=2\pi\nu_o=2\pi m_oc^2/h$. R_o, k_0, and $\boldsymbol{\omega}_o$ are all constants, the whole space is invariant. A Static rotating field matter sphere is natural object and physical noumenon without observation. Let the wave function of this rotating field material sphere be described with a complex number function

$$\Psi_0=A_0e^{i\omega_0t_0} \tag{19}$$

There are two basic physical quantities, R_o and K_o. R_o represents the space occupation of the sphere and corresponds to the position coordinate $\boldsymbol{x}$, which is uncertain. K_o represents the structure and matter density of the sphere and corresponds to the curvature coordinate $\boldsymbol{k}$. The amplitude A_o of ψ_o should be associated with them, and it's probably complicated, but can be learned through in-depth discussion. Penrose described the microscopic object with a unit circle, letting $A_o=1$, which is simplified, just focus on the phase. But this is just a mathematical representation, without clear physical meaning. Here we take the two-dimensional projection of the field matter sphere -- the rotating field matter circle. I think so. Eq. (19) is expected to be the source of quantum phenomena.

If the coordinate system K_o is built on the "rotating field matter sphere", the sphere moves uniformly along the positive direction of $\boldsymbol{x}$-axis from resting state. Using the Lorentz transformation: $t_o=(t-vx/c^2)/(1-v^2/c^2)^{1/2}$, in the observation system K, we obtain the new plural described matter wave function

$$\Psi=Ae^{i\omega t}=Ae^{i(\boldsymbol{px}-Et)/\hbar} \tag{20}$$

This results from the combination of two different kinds of spatial. The amplitude A is complex and contains new coordinate variables. p, x, E, and t are relativistic quantities. And $P=mv$ $E=mc^2$,m is the motion mass. Under the condition of relativity (classical conditions will be discussed separately) [7,13], Equation (20) is the fluctuating motion of field matter, which is matter waves -- physical waves. It is often mistaken for a probability wave of a point particle in 3 - or 4- dimensional real space. No, it's just the same mathematical version. A little transformation of phase $i(\boldsymbol{px}-Et)/\hbar$ of equation (20) is given

$$i(\boldsymbol{px}-Et)/\hbar=i(k_ix_i-k_4x_4) =-ik_\mu x_\mu$$

k_4 =mc/ħ, x_4 = ct. Wave function equation (20) becomes

$$\Psi=Ae^{i\omega t}=Ae^{i(\boldsymbol{px}-Et)/\hbar}=Ae^{i(k_ix_i-k_4x_4)}=Ae^{-ik_\mu x_\mu} \tag{21}$$

In the present equation (21), x and k are the new phase space coordinate variables. The product of $k_\mu x_\mu$ happens to be dimensionless. It is automatically generated when Lorentz time transform is introduced after the motion of "the field matter sphere", which integrates the complex and real Spaces.

It can be considered that $\boldsymbol{k}_\mu$ is the 4-dimensional physical space-time release of $\boldsymbol{k}_o$, and $\boldsymbol{x}_\mu$ is the 4-dimensional physical space-time release of R_o. The descriptive space-time also becomes a new combination of complex-real space-time -- the dual 4-dimensional complex space-time W(x,k),

instead of Penrose's 5-dimensional twisted subspace. The amplitude A=A (x,k) is A very complicated function. i =1, 2, 3, μ=1, 2, 3, 4, k_4x_4 =mc²t /ħ=(mc/ħ)•ct . It is an important step to write mc2t/ħ as (mc/ħ)•ct, which represents a physical process on the light cone. This is the introduction of the theory of relativity into a new space-time. The phase space $\boldsymbol{k_\mu x_\mu}$ is consistent with the own construction space of the microscopic object sphere model, namely Dual 4- dimensional complex space, as shown as the follow equiptions:

4-dimensional curvature k-space: $K = K(K_4\text{-}K_1\text{-}k_2\text{-}k_3)$

and invariant of 4-dimensional k-space: $K_0^2 = K_4^2\text{-}K_1^2\text{-}K_2^2\text{-}k_3^2$

4-dimensional coordinate x-space: $x = X(x_4\text{-}x_1\text{-}x_2\text{-}x_3)$

and invariants of 4-dimensional x-space: $x_0^2 = x_4^2\text{-}x_1^2\text{-}x_2^2\text{-}x_3^2$

The description space of the wave function ψ is on the phase, as same as that of Equation (17). The wave function equation (17) can be derived from the relativistic Lorentz time transformation through the motion of the quantum object field matter sphere. It is further confirmed theoretically that the wave function ψ is a physical wave. The overall picture of the wave function is complex, where the amplitude is A=A (x,k), and Wigner gives an expanded form. We will apply the expanded form in the derivation of the equations of motion of quantum mechanics in the Dual 4-dimensional space-time In 4-dimensional coordinate x space, x_0 is an invariant of the distance between two points in coordinate transformation. The microscopic object is stationary, P=0, $k_{1,2,3}$=0, k_4=k_0, $x\text{-}_{release\ -\ mapping}$ =0. Meanwhile, $x_{1,2,3}$=0, x_0= x_4, and x_0=R_0, x_0 is the projection of "the field matter sphere of ontology " in coordinate space, which is an invariant and cannot be observed directly, and no observable quantum effects. When P≠0, $k_{1,2,3}$≠0, and k_4≠k_0, $x_{\ release\ –\ mapping}$ is the release and mapping of coordinate x of the moving microscopic object in 3-dimensional or 4-dimensional space. $\boldsymbol{x}_{\ release\ -\ mapping}$ ≠0, at this time, x_0≠x_4, the quantum motion effect of the microscopic object in space-time can be observed. Due to the Lorentz covariant of x and k, relativity and quantum mechanics are unified based on physical models. Special relativity spacetime is extended to the quantum mechanical dual 4-dimensional complex spacetime.

The above analysis shows that the rotating field matter sphere described in the complex number (19) releases four components $x(x_4-x_1-x_2-x_3)$ along the spatial direction x and $k(k_4-k_1-k_2-k_3)$ along the curvature k (P /ħ). It is the ingenious expansion of the space structure of the moving microscopic quantum object in dual 4-dimensional complex space-time. That is, $k_{1,2,3}$ are the 3-dimensional release of k_0, and $x_{1,2,3}$ are the 3-dimensional release of R_0. Since Equation (20) can describe all quantum phenomena, equation (21) can completely describe all quantum phenomena in the Dual 4-dimensional complex space-time W(x,k).

Equation (19) is consistent with Penrose's thought and method of 5-dimensional twisted space, except that we confirm the existence of an in-itself structure R_0 and its "rotation" in complex space, and observe the movement of microscopic objects using relativistic space-time instead of classical Newtonian space-time [7,13]. In fact, from the relativistic momentum triangle, we can know that the expansion of 4-dimensional curvature space and 4-dimensional coordinate space is presented in the electron from "static" to "dynamic". If the electron changes from "moving" to "static", $P_{1,2,3}$=0, that is, $k_{1,2,3}$=0, k_0=k_4, then the included Angle between m0c and mc is 0, so the observation space $x_{\ release\ -\ mapping}$ =0. Quantum phenomena disappear. In our method, through the electron from "static" to "dynamic", it is illation into a unified. Dual 4-dimensional complex space-time describing quantum phenomena. This is a relativistic advance on the Penrose 5 - dimensional twisted subspace.

In addition, it must be noted that although equation (20) is the same as the mathematical form of the wave function in traditional quantum mechanics, the traditional quantum mechanical wave function is only an assumption under the point particle model, with unclear physical significance [13], and is a probabilistic wave in 3d or 4d real space-time $M^4(x)$. This leads to a lot of cognitive contradictions. Here, the wave function formula (20) is derived from the movement of the field matter sphere in the rotating. It describes the fluctuating movement of the rotating field matter and has a clear physical meaning. It is matter waves -- physical waves. It is in the dual 4- dimensional complex space-time $W(x,k)$. A further study shows that the conversion between the dual 4-dimensional complex space-time $W(x,k)$ and the 4-dimensional real space-time $M^4(x)$ is realized by quantum measurement, and the probabilistic properties are shown.

We predict that matter waves, like electromagnetic waves, will have communication and other applications. But it's not electromagnetic waves, which require the movement of charged objects. Matter waves with no need for charged objects. The propagation of matter waves is both realistic and deterministic. Its probabilistic properties need to be represented in quantum measurements. The electromagnetic wave properties of moving electrons and their matter wave properties may be applied separately through experimental design.

3.2 Covariant Quantum Mechanics Equations of Matter-Wave in the Dual 4-Dimensional Space-Time

3.2.1 Establishment of the Classical Wave Equation in the Dual 4-Dimensional Space-Time

The matter wave function described by the dual 4-dimensional space-time $W(x,k)$

$$\begin{aligned}\psi(x,k) &= A(x,k)exp[i(\boldsymbol{k}\cdot\boldsymbol{x}-Et/\hbar)]=A(x,k)exp[i(\boldsymbol{k}\cdot\boldsymbol{x}-mc/\hbar\,.ct)]\\ &=A(x,k)exp[-i(k_4\,.x_4-\boldsymbol{kx})]=A(x,k)exp(-ik_\mu x_\mu)\end{aligned} \tag{22}$$

In the stationary state, $k_\mu = k_{1,2,3}\, x_\mu = x_{1,2,3}$, $A(x,k)$ only depends on the 3-dimensional space coordinates x_μ and the 3-dimensional curvature coordinates k_μ

$$A(x,\,k)=\sum_0^\infty C_n\,A_n(x,\,k),$$

The amplitude of the matter wave is a function of the space coordinate $\boldsymbol{x}$ and the structure space $\boldsymbol{k}$. It satisfies the following differential equation [7]

$$\begin{aligned}&H(x,k)exp[\mathrm{i}/2(\overleftarrow{\partial}_x\overrightarrow{\partial}_k-\overleftarrow{\partial}_k\overrightarrow{\partial}_x)]\,A(x,k)\\ &=H(x,k)\,*\,A(x,k)=EA(x,k)\end{aligned} \tag{23}$$

Where $H(x,k)$ is the classical Hamiltonian function of the system. * The operation is the Moyal product, defined as follows:

$$F(x,y)\,*\,g(x,y)=F(x,y)exp[\mathrm{i}/2(\overleftarrow{\partial}_x\overrightarrow{\partial}_y-\overleftarrow{\partial}_y\overrightarrow{\partial}_x)]\,g(x,\,y)$$

Where y= k, the average of any quantity $F(x,k)$ in this stationary state can be written as

$$<F>=\int_{-\infty}^{\infty} F(x,k)A(x,\,k)\,dxdk \tag{24}$$

The wavelength of the general wave function of a physical system can be defined by the generalized de Broglie relation, which also applies to the wave-motion of the matter field.

The asterisk multiplication operator wave equation is equivalent to the Schrodinger equation and the path integral quantization equation. The forms cannot be transformed into each other, and the results are equivalent. Square wave function Ψ (*x*) the absolute value of | Ψ (*x*) | ² has the same probability. Wigner function transformation formula

$$\Psi（x）=（\int_{-\infty}^{\infty} A(x,k)dk）^{1/2}$$

$$\int_{-\infty}^{\infty} A(x,k)dk=|\Psi（x）|^2=\rho(x)$$

And, $\boldsymbol{\Psi}(\boldsymbol{x})$ of course be the solution to the Schrodinger equation. The form of the Schrodinger equation remains the same.

3.2.2 Discussion

Dirac equation of free electron: When H(*x,k*) is the relativistic Hamiltonian function of the system, the Moyal multiplication rule is adopted to obtain the wave equation of the dual 4- dimensional space-time

$$H(x,k)*A(x,k)=E\ (x,k) \qquad (25),$$

In Equation (25), H(*x,k*) and A(*x,k*) contain x_4(=ct) and k_4. Different from Equation (23), H(*x,k*) is an evolution equation containing time.

In addition, due to the equivalent meaning of wave function ψ, the relativistic quantum mechanical operator [15] is adopted:

$$H=c\boldsymbol{\alpha}\cdot\boldsymbol{p}+\beta m_0c^2 \qquad (26\text{-}1)$$

Static electron p=0

$$H=\beta m_0c^2 \qquad (26\text{-}2)$$

The Dirac equation for the free electron is

$$i\hbar\partial\psi/\partial t=H\psi \qquad (26\text{-}3)$$

So this goes back to the traditional quantum mechanical system.

3.2.3 Wigner Function Method -- Wave Function ψ (X) Position Representation and Wave Function φ (K) Curvature K Representation

The matter wave function of the microscopic object is ψ (*x,k*), which is a physical wave, the amplitude A=A (*x,k*) contains the matter information of the microscopic object, and the phase is composed of coordinate variables. And its motion satisfies the Dirac equation (or Schrodinger equation). And there is a Wigner transformation relation [7]

$$A(x,k)=\int_{-\infty}^{\infty} d\xi e^{-i\xi k}\Psi^{※}(x-½\xi)\Psi(x+½\xi) \qquad (27)$$

$$A(x,k)=\int_{-\infty}^{\infty} d\xi e^{-i\xi x}\Phi^{※}(k-½\xi)\Phi(k+½\xi) \qquad (28)$$

Where ψ (*x*) is the representation of position, and x has an uncertain property for the microscopic object. φ (*k*) is the representation of curvature *k*, corresponding to the property of matter density. So let's integrate these two things.

Eliminating the variable k from Equation (27), the matter wave ψ (x,k) maps to the real part space. The location representation wave function ψ (x) and probability density distribution function ρ(x) are obtained.

$$\Psi(x) = \left(\int_{-\infty}^{\infty} A(x,k)dk\right)^{1/2} \tag{29-1}$$

$$\int_{-\infty}^{\infty} A(x,k)dk = |\Psi(x)|^2 = \rho(x) \tag{29-2}$$

Normalization is expressed as $\int_\tau c\,\rho(x)\,d\tau = \int_\tau c\,|\Psi(x)|^2 d\tau = 1$ (30)

In dual 4-dimensional space-time, the position x has an uncertain（probabilistic）property for the microscopic object, ψ (x) has a probabilistic significance for the microscopic object, and ρ (x) is the probability density of the microscopic object appearing at x. These are equivalent to traditional quantum mechanics. Conventional quantum mechanics defines ψ (x) as the probability amplitude and it makes sense. The microscopic object has a certain size, so $0<\rho(x)<1$.

By eliminating the variable x from Equation (27), the matter waves ψ (x,k) maps to the imaginary k-space. The wave function φ(k) of curvature k and the density distribution function η(k) of the matter field are obtained.

$$\Phi(k) = \left(\int_{-\infty}^{\infty} A(x,k)dx\right)^{1/2} \tag{31-1}$$

$$\int_{-\infty}^{\infty} A(x,k)dx = |\Phi(k)|^2 = \eta(k) \tag{31-2}$$

The normalization is written as

$$\int_v c\,\eta(k)\,dv = \int_v c\,|\Phi(k)|^2\,dv = \int_v c\,dv/v = 1 \tag{32}$$

The midpoint of the dual 4-dimensional complex space-time (x,k) represents: the vector $\mathbf{k}$ (k_1, k_2, k_3, k_4,) describes the spatial structure or matter density distribution of the microscopic object itself; Vector: $\boldsymbol{X}$ (x_1,x_2,x_3,x_4) describes the location of the microscopic object, has a certain spatial distribution, and has uncertain properties.

3.2.4 A New Understanding of Mapping Relationship Between ψ(X,k) and ψ(X) , φ (K)

1. Elimination of the variable k, A(x,k) mapping to the real part of the dual 4-dimensional space- time, and obtain the microscopic object probability density distribution function ρ(x) at x.
2. Elimination of the variable x, A(x,k) mapping to the imaginary part of the dual 4-dimensional space-time, obtain the microscopic object the matter field density distribution function η(k) at x.

If k= constant, the energy level is unchanged, the physical structure of the microscopic object is unchanged, and the matter density is unchanged, it is just equivalent to the probability density distribution of the whole space is unchanged, and it is a monochromatic plane wave.

If k≠ constant, the quantum transition, the density of matter changes, and the probability density will also change. Corresponding to different monochromatic plane waves [7].

3.3 Discussion on the New Theory of the Origin of Quantum Probability

3.3.1 The Uncertainty of Microscopic Object Position-- a New Understanding of the uncertainty relation

The microscopic object is not a point, but the rotating field matter sphere, Uniform distribution of mass, with a certain spatial distribution radius R, and uncertain position x. The uncertainty D depends on R. With a certain mass, the smaller the microscopic quantum object is, the greater the matter density is, and the smaller the position uncertainty D is. On the contrary, the larger R of the same microscopic quantum object is, the smaller the matter density is, and the greater the position uncertainty D is. Discussion:

1. R=0, mass density $\eta=\infty$, the particle model can be adopted, the position is completely determined, uncertainty D=0, the probability of microscopic object appearing at x is $\rho(x)=1$, not belonging to the dual 4-dimensional space-time description object;
2. R=∞, mass density $\eta=0$, position x is completely uncertain, uncertainty D=∞, the existence of microscopic object can not be found, the probability of occurrence at x $\rho(x)=0$, also does not belong to the dual 4-dimensional space-time description object;
3. In the dual 4-dimensional space-time quantum mechanics, the field matter sphere has a certain size, the matter density $0<\eta(k)<\infty$, the position uncertainty $0<D<\infty$, and the probability density $0<\rho(x)<1$ at x.

According to the relationship between the density of field matter and quantum probability, the uncertainty relation in the dual 4-dimensional space-time can be understood as follows: the greater the density of field matter η (k), the smaller the position uncertainty D ;The smaller the field density η (k) is, the greater the position uncertainty D .The uncertainty relationship is easy to understand.

However, in classical mechanics, if the microscopic quantum is treated as a classical particle without external interference, its position x is determined. Thus, the probability distribution phenomenon of quantum measurement is attributed by the Copenhagen school to the "inherent" position uncertainty of the microscopic quantum object themselves. Bohr is the representative of this cognitive route.

Einstein disagreed with the Copenhagen school that God did play dice. The quantum probability phenomenon of the microscopic object must have external and unknown objective reasons. Bohm later called its development a "hidden variable", but Einstein himself was not satisfied. of course, there are also people looking for the objective reason for external interference of quantum probability, but it is still not successful at present.

The dual 4-dimensional space-time quantum mechanics ascribes quantum probability to a certain spatial distribution of the microscopic quantum object. The nature of the position of the microscopic quantum object is uncertain. In other words, for the microscopic quantum object, coordinate x in wave function $\psi(x)$ has the property of uncertainty. This transforms the uncertain cognition of the microscopic quantum object's position into the uncertain attribute of x coordinates of the real part of dual 4-dimensional space-time. This is a transformation from subjective cognition to physical time and space, and realizes the dichotomy of subject and object. It can be seen that the physical properties of the real part of the dual 4-dimensional space-time quantum mechanics ascribe quantum probability to a certain spatial distribution of the microscopic quantum object. The dual 4-dimensional space-time quantum mechanics ascribes quantum probability to a certain spatial distribution of the microscopic quantum object. The dual 4-dimensional space-time is not the same as those of special relativity $M^4(x)$.

3.3.2 Quantum Probability Description in the Dual 4-Dimensional Space-Time

The matter wave ψ (*x*,*k*) of the dual 4-dimensional space-time is mapped to the virtual k-space, and the pure state wave function φ (*k*) of the curvature K representation is obtained. The k representation of the wave function has the property of the matter density.

$$\Phi(k) = [\int_{-\infty}^{\infty} A(x,k)dx]^{1/2} \qquad (a\text{-}1)$$

φ (k) represents the matter density distribution corresponding to the microscopic object at position x, and its value is

$$\eta(k) = \int_{-\infty}^{\infty} A(x,k)dx = |\Phi(k)|^2 \qquad (a\text{-}2)$$

This is a theoretical value in the dual 4-dimensional space-time and cannot be observed directly.

In fact, the imaginary part *K* is the wave-vector space of quantum field theory. $\boldsymbol{k}$ makes the infinite calculation of interaction in quantum field theory stop at the quantum curvature $\boldsymbol{k}_0$ and overcomes the infinite difficulty of the point particle model in quantum field theory.

The matter wave ψ (*x*,*k*) is mapped to the real part space, and the positional representation wave function ψ (*x*), corresponding to the microscopic object, the *x* representation of the wave function has a probabilistic property. Probability amplitude

$$\Psi(x) = [\int_{-\infty}^{\infty} A(x,k)dk]^{1/2} \qquad (a\text{-}3)$$

The position of the microscopic object at *x* is uncertain, and the theoretical probability of occurrence is

$$\rho(x) = \int_{-\infty}^{\infty} A(x,k)dk = |\Psi(x)|^2 \qquad (a\text{-}4)$$

This is also a theoretical value in dual 4-dimensional space-time, again not directly observable.

3.2.3 The Source of Quantum Probability in the Dual 4-Dimensional Space-Time -- Re-Understanding of the Connection Between ψ(X) and φ (K) by Fourier Transform

$$\psi(x) = (2\pi\hbar)^{(-1/2)} \int_{-\infty}^{\infty} \Phi(k)exp(ikx)d(\hbar k) \qquad (33)$$

$$\Phi(k) = (2\pi\hbar)^{(-1/2)} \int_{-\infty}^{\infty} \psi(x)exp(ikx)d(x) \qquad (34)$$

Equations (33) and (34) are the representation transformation of the field matter density distribution and probability density distribution. The density distribution of the field matter and probability density distribution can be transformed into each other. The density of field matter is evenly distributed, and the probability density is evenly distributed. The density distribution of field matter is large and the probability of microscopic objects is high. The field matter density is zero, and the probability density is zero. The density distribution of field matter is the source of quantum probability [7], the primacy of matter is supported. Quantum probability comes from the spatial distribution and mass density distribution of microscopic objects, which is completely objective.

Neither Einstein's god does not play dice nor Copenhagen's subjective understanding of the uncertain nature of particles is needed in a double four-dimensional space-time. The subjective dependence of quantum phenomena on humans can be eliminated by describing the microscopic quantum

phenomena by the dual 4-dimensional space-time W(x,$\boldsymbol{k}$) of quantum mechanics. Just as special relativity does not require a moving object to automatically shrink in length in the direction of motion.

IV. THE DIFFERENCE BETWEEN MACRO AND MICRO CAUSALITY

4.1 On Macroscopic and Microscopic Causality and Quantum Parallelism States

Macroscopic classical world, intrinsic localized causality; Microscopic quantum world, intrinsic nonlocality causality. Quantum measurement can eliminate the nonlocality causality and restore the localized causality. It is wrong to treat the causal relationship between the evolution of macro and micro physical states as the same.

4.1.1 Generation of the Spacelike Interval Between Eigenstates

Quantum transitions take place over time [16], according to a study published on June 3, 2019, in the British journal Nature. We believe that due to the extremely short transition time, the quantum theory system assumes the mutation time t=0, which is still valid, and the quantum theory is established. However, the concept of transition velocity can be defined. If the microscopic object moves in a linear, flat and continuous space-time, s is the transition distance, t is the transition time, and the transition speed can be defined as

$$v=s/t$$

1. Motion properties of the microscopic quantum object in the particle model

A particle has no size. In particle model quantum mechanics, within the scope of the structure of the microscopic object itself, before and after the quantum mutation distance $S\to0=0$, the mutation time $T\to0=0$, ψ_n , ψ_{n+1} appear simultaneously. Motion speed

$$V =s/t=0/0=C \text{ (constant)}$$

In theory, the constant C can be less than, equal to, or greater than the speed of light.

In point particle quantum theory, the mutation time T =0 implies that the transition speed can exceed the speed of light. Exceeding the speed of light is a basic property of microscopic quantum object motion.

This is an additional property that quantum transition and particle models add to microscopic objects. It has human subjectivity and corresponds to the intrinsic specification of point particle theory.

Special relativity uses a point model, where energy changes continuously, there are no energy transitions, t≠0, faster than the speed of light is excluded, which corresponds to a localized causality constraint. According to Einstein's convention in special relativity, the constant C is less than or equal to the speed of light, which just meets the requirement of localized causality.

In the quantum mechanics theory of the point particle model, human subjective suggestion contradicts the convention of special relativity.

(1) Non-locality of space and the shapes of the microscopic object

Real microscopic objects have shape structures. In transition, the minimum transition distance is the overall structure s=2R and R is the field matter sphere radius. The transition distance s≠0, the transition time still stipulates t=0 and the transition speed

$$v=s/t=s/0=\infty$$

Motion, and energy change "faster than light speed"! The quantum transition of the tangible object is accompanied by a space interval s=2R. The sudden insertion of the spacelike partition. The faster-than-light energy change between energy levels has a theoretical basis.

Experiments show that the spacelike compartments between quantum states are Compton waves Long $\lambda_c=\hbar/mc$ of the microscopic object, which undoubtedly provides theoretical and experimental support for the field matter sphere model. The space-like partition defined in the dual 4-dimensional space-time covariant quantum theory is the Compton wavelength of the microscopic object:$\lambda_c=\hbar/mc$, that is, the field matter sphere radius R of the microscopic object. Here the energy is quantized, the localized space is quantized, and the field is quantized.

Under the quantum transition hypothesis, between the quantum states Ψ_n—Ψ_{n+1}, there is an interspace between $\hbar/mc$ that the speed of light cannot communicate [7]. Eigenstates can be superimposed to replace the classical concept that particles cannot be superimposed and to sow the seeds for nonlocalized causality. However, the point model subjectively changes the change of physical space properties caused by objective reasons into the faster-than-light change of energy and motion properties of "point" particles, while the space-time properties remain unchanged, and continue to use the classical space-time, resulting in the disharmony between quantum mechanics and relativity. The fundamental way to eliminate contradictions is to return the subjective to the objective and construct a new physical space-time.

Quantum mechanical space-time is not ordinary Newtonian space-time or special relativity space-time, but a new space-time that satisfies the laws of quantum mechanics and reasonably explains quantum phenomena. It is the dual 4-dimensional quantum mechanical complex space -time. Dual 4-dimensional quantum mechanics can analyze the interrelations among time-like, light-like, and space-like Spaces by adopting the mathematical method of multi-dimensional state space and introducing a light cone graph from relativity. Dual 4-dimensional space-time quantum mechanics and special relativity have internal consistency and can communicate with each other.

(2) In the point particle model, the multi-dimensional state space has the same properties as the background space. The trade-off is that microscopic objects confer faster-than-light properties on motion, contradicting relativity. In the sphere model dual 4-dimensional space-time covariant quantum mechanics, the microscopic object move in space-time, and quantum transition increases the spacelike interval between states, thus changing the physical properties of state space, which is different from point model background space. In the dual 4-dimensional space-time covariant quantum mechanics, the quantization and quantum transition of the microscopic object structure is the root of space-time non-locality.

It can be seen that the physical properties of the state space of the point model and sphere model are different. In the sphere model, the quantum state in the dual 4-dimensional complex space-time, the localized interaction is cut off by the spacelike interval, and the matter waves propagate in the timelike space, which is coordinated with relativity. The quantum state of the point model in 4-dimensional real space-time implies that the particle has faster-than-light motion, which is incompatible with relativity. Spacelike interval and faster-than-light motion are equivalent expressions of the two models in different physical Spaces. To describe quantum phenomena, the sphere model of the dual 4-dimensional complex space-time is more reasonable than the point model of 4-dimensional real space-time.

The point model has localized causality in 4-dimensional real space-time, while the sphere model has non-localized causality in the dual 4-dimensional space-time. Quantum measurement leads to the

introduction of continuous compensating action $U=e^{a(x)}$, the elimination of non- localization of physical spacetime, and the global transformation from the dual 4-dimensional complex space-time to 4-dimensional real space-time. It leads to the transition from sphere model to point model, from quantum field to classical field, and from matter waves to probability wave. The two Spaces can communicate through quantum measurement [7].

There are only two worlds, one is the microscopic quantum world, and the other is the macroscopic classical world. The microscopic quantum world is inherently non-localized causality and has parallel quantum states. Conversely, the state change of the macroscopic world requires the change of interaction and the change of interaction time, and it is impossible to form the existence of parallel quantum states similar to the quantum world because of the inherently localized causality.

In the macroscopic world, internal localized causality, force is the cause, and state change is the effect; The microscopic quantum world is inherently non-localized causality. The spacelike interval is the cause, and the parallel quantum state of the free microscopic object is the effect. The macroscopic world has no parallel worlds with the same meaning as the parallel quantum world.

In the dual 4-dimensional space-time covariant quantum theory, the wave function has matter properties and is a physical wave (confirmed by Shi Baosen et al. [17]). The time evolution of the Schrodinger equation is deterministic, which means that the time evolution of the density or structure of matter is deterministic. The randomness of wave function measurement is only the macroscopic experimental emergence of the probability properties of the wave function in the two types of spatial transformation [7].

4.12 Quantum State Quantum Segmentation Diagram

Plane-wave superposition is the product of continuous function quantum partition (quantu m mutation added into spacelike interval). Matter waves and probability waves are objective descriptions of quantum phenomena, but they are in different physical Spaces. The matter waves are at $W(x,k)$ and the probability waves are at $M^4(x)$. Conversion by quantum measurement.

Fig. 1 shows wave function with continuous energy variation Three-dimensional or four- dimensional flat Spaces, continuous curves, Rutherford atomic model: force action is the cause, the state change is the effect - local causality. The eigenvalues of the quantum state are contained in the continuous curve. As shown in figure 1

Fig. 1: Flat space, continuous curve

As shown as Fig. 2, in the dual 4-dimensional space-time $W(x,k)$, the quantized segmentation of energy and structure -- the intersegment function, the states are truncated by the tangible structure -- the spacelike interval $\lambda_c=\hbar/mc$ is added [7], which breaks the local causality and enters the non- local causality. Spatial non-localized is the cause, microscopic objects move freely, and the parallel existence of states is the effect. The eigenvalues of the quantum state correspond to the quantum parallel state and come from the continuous function quantum state.

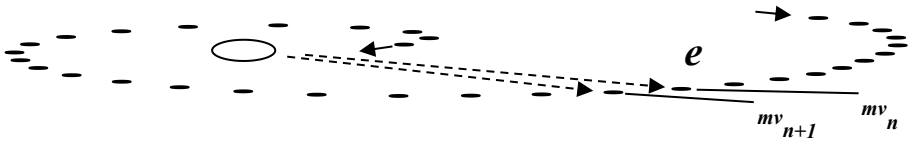

Fig. 2: Flat space, discontinuous function and space - like partition

From Fig. 1 to Fig. 2, it shows that the spacelike interval $\lambda_c=\hbar/mc$ is inserted, the break the mechanical causal chain, the localized causality is destroyed, and the states co-exist simultaneously, $\psi=\Sigma\psi_n$, pure state, and coherence. Cost: the sacrifice of classic local causality. Into the non-local causality and the quantum parallel state. Eigenvalues come from quantum states of continuous functions. The wave function propagates in W(x,k) space.

From Fig. 2 to Fig. 1, it shows that a continuous compensation field U（$U\psi=\Sigma e^{a(x)}\psi_n$ ）is introduced in the measurement, which eliminates the fixed phase difference and breaks the non- local causality into local causality. The physical space-time changes from W(x,k) to $M^4(x)$, the physical model changes, the quantum transition disappears, the continuous mechanical motion resumes, the mixed state is formed, and eliminate the coherence. The eigenvalues are presented in a probabilistic manner, and regression graph 1 continues in the eigenvalues.

V. PROBABILITY MEASUREMENT DISPLAY AND SPACE-TIME CONVERSION

5.1 The Measurement of Quantum Probability

Quantum measurement is understood from three main aspects. Firstly, physical principle. the measurement of the presence or absence of interaction; Secondary, mathematical expression, global, local phase transformation, eigenstate equation; Thirdly, design experimental display, measurement momentum and measurement position.

In the dual 4-dimensional space-time, it is considered that in the measurement statement $A\psi_n(x)=a_n\psi_n^{\ k}(x)$, the left and right wave functions of the equation will not be the same physical space-time considering the interaction factors in measurement. The pure state wave function on the left is in the dual 4-dimensional space-time, and the mixed state wave function on the right is in the 4-dimensional real space-time. At this time, the essence of quantum measurement is to lead to the transformation of cognitive level and the transformation of physical time-space of describing quantum phenomena.

The invariance of the mathematical form of $\psi^{k}(x)$ and $\psi(x)$ just guarantees the invariance of the form of the Schrodinger equation or Dirac equation, describing the microscopic quantum object in two space-times. The mathematical form of $\psi^{k}(x)$ and $\psi(x)$ in the two space-times is unchanged, which indicates that the ontology is continuous without fracture. This is what structural realism and realism of interaction are based on. Kuhn's paradigm is incommensurable and noumenon fracture is wrong. How to realize the probabilistic motion of quantum mechanical matter-wave to point particle involves the physical principle, experiment, and mathematical operation of transforming the dual 4-dimensional space-time into 4-dimensional real space-time [7,8].

5.1.1 Quantum Measurement Mechanics Analysis and Space-Time Transformation in the Dual 4-Dimensional Space-Time

Although the physical model of the microscopic object in the dual 4-dimensional space-time is the field matter sphere, the field matter sphere has been transformed into matter waves $\psi(x)$ in the theoretical description. The phase transformation on $\psi(x)$ will be reflected in the interaction of the microscopic object. In phase transformation, the phase factor $e^{\alpha(x)}$ multiplied by $\psi(x)$ is a mathematical statement of this interaction.

(1) If the multiplied phase factor $\boldsymbol{e^{\alpha(x)}}$, causes the waves function fixed phase difference to disappear, this would be the introduction of a substantial continuum interaction. The pure state waves function $\psi n(x)$ on the left side of the equation is transformed into the mixed state waves function $\psi^{k}(x)$ on the right side of the equation. In this case, $\psi^{k}(x)$ is not in dual 4-dimensional space-time, is purely a quantum probability function of a point particle in 4-dimensional real space, and has no coherence. At this time, the essence of quantum measurement is a space-time transformation, which converts dual 4-dimensional space-time to 4-dimensional real space-time, and the matter-wave evolves into a probability wave, and the mathematical form of wave function remains unchanged. The invariance of the mathematical form of the waves function guarantees the invariance of the form of the Schrodinger equation and Dirac equation in the two space-times before and after the measurement.

The description of space-time has changed, and the physical model will change, too. The sphere model of the dual 4-dimensional space-time has evolved into a point model of 4- dimensional real-time space. The wave phase of the microscopic object evolves into the particle phase. The space-time transformation transforms the probabilistic property of the dual 4- dimensional space-time into the probabilistic motion of point particles in 4-dimensional space- time.

The $\psi(x)$ collapse will reflect the transformation of cognitive level, the transformation of physical space-time describing quantum phenomena, entanglement resonance, and so on. During the space-time transition, there are no collapse process waves and no direct faster-than-light motion of the microscopic object. The single measurement result ak appears, is the microscopic object probability motion and instrument measurement resonance display. Multiple measurements reflect the transformation of the probabilistic properties of space-time into the probabilistic motion of the microscopic objects.

Through measurement, quantum probability can be able to render by cognitive level change, space-time transformation, and physical model change. Its origin is different from both classical thermodynamic probability and macroscopic classical statistical probability. As mentioned earlier, quantum probability derives from the spatial distribution and the matter density distribution properties of the microscopic objects. It doesn't need an implicit variable. In the dual 4- dimensional space-time, matter tells space-time how to have probabilistic properties, and by quantum measurements, space-time tells matter how to make a probabilistic motion.

(2) If the multiplied phase factor $e^{\alpha(x)}$ ($\alpha(x)$ = constant), causes the waves function fixed phase difference to remain, it is the coordinate translation of matter waves. Measure the momentum and let the matter waves pass through the single slit and double slit. At this time, the measurement does not introduce substantial interaction and the space-time where the matter waves are located does not change. After the wave packet "collapses", are still matter waves-pure monochromatic plane waves in the dual 4-dimensional space-time. Using diffraction and interference of wave, its wavelength can be calculated accurately. In the dual 4-dimensional space-time, momentum can be accurately measured.

(1) Unitary transformation

$$\psi = e^{\alpha(x)}\psi(x) \ , \quad \alpha(x) = H(t);$$

The transformation preserves the invariance of the eigenvalues and the trace of the matrix.

(2) The gauge transformation

For the global gauge transformation, $a(x)$ = constant

$$\psi = e^{\alpha(x)}\psi(x) = \sum c_n e^{\alpha(x)}\psi_n(x)$$

After the transformation, there is still a fixed phase difference between the eigenstates, the coherence still exists, and the properties of pure states remain unchanged. It's the coordinate translation of the matter wave, still in the dual 4-dimensional space-time.

For the local gauge transformation, $\alpha(x)$ = variable (function of x)

$$\psi = e^{\alpha(x)}\psi(x) = \sum c_n e^{\alpha(x)}\psi_n(x) = \sum c_n \Phi_n$$

The fixed phase difference between the eigenstates disappears, the interaction is introduced in essence, and the pure state evolves into the mixed state. For electromagnetic action, Lorentz invariance of the Dirac equation can be discussed by adopting vector potential A and introducing

(3) General phase transformation

For the global transformation $a(x) =$ = constant

$$\psi = e^{\alpha(x)}\psi(x) = \sum c_n e^{\alpha(x)}\psi_n(x)$$

After the transformation, there is still a fixed phase difference between the eigenstates, and the coherence properties of the pure states remain unchanged. The global transformation has no substantial interaction involved. But it's also supposed to be a quantum measurement. Matter- wave packets "collapse" into pure monochromatic plane waves [13].

In the equation of eigenstate $A\psi_n(x) = a_n \psi^{k}(x)$, the wave functions $\psi_n(x)$ of the left and right sides of the equation are in the dual 4-dimensional space-time, which are physical waves, pure states, and which are coherent of waves. It is the physical basis for defining the mixed state as pure incoherent mixing. In fact, it's a constructed mixed state, and it's needed in quantum communication. By designing experiments and using the interference effect of plane waves, we can know the exact momentum of the microscopic object from the wavelength. Matter waves can be used to measure the momentum of microscopic objects.

Momentum is knowable in dual four-dimensional space-time. We use it to define curvature coordinates. The action quantity in the path integral is also well defined, and the question of Dirac's student does not exist [1,7,8]. At the same time, according to the sphere model, momentum is large and curvature is large (equivalent matter density large), the uncertainty of position is small; Momentum small, curvature small, position uncertainty large; The momentum is infinitely large, the curvature is infinitely large, and the position of falling on the geometric point is completely determinable; Momentum zero, curvature zero, plane, a position completely uncertain, in the dark. Heisenberg's uncertainty relation has a realist explanation.

For the local transformation, $a(x)$ = variable (function of x)

$$\psi = e^{a(x)}\psi(x) = \sum c_n e^{a(x)}\psi_n(x) = \sum c_n \Phi_n = \Phi$$

The fixed phase difference disappears and the coherence of waves disappears. The pure state evolves into a mixed state. Embodied measurement introduces substantial interactions. It is a nonlinear R process of quantum measurement, which is carried out simultaneously in the whole space, and the invariance of linear equations is destroyed.

Before measurement, the wave function of the measured microscopic object is in a pure state, in $W(x,k)$ space. If $\psi(x) = \Sigma\psi_n(x)$, there is a fixed phase difference between the superposition eigenstates, and there is coherence. Interaction potential $U=e^{a(x)}$ is introduced in the measurement, then.

$$e^{a(x)}\psi(x) = e^{a(x)}\sum c_n\psi_n(x) = \sum c_n e^{a(x)}\psi_n(x) = \sum c_n \Phi_n = \Phi$$

The free motion of the quantum parallel pure state is destroyed and the spacelike interval disappears. The fixed phase difference between the eigenstates disappears simultaneously in the whole space, the phase difference changes continuously, the wave function evolves into a mixed state, and the coherence disappears. The description space is transformed, and people's cognitive level simultaneously enters the 4-dimensional real space $M^4(x)$. The physical essence of the local transformation $e^{a(x)}\psi(x)$ eradicate coherence is that the continuous potential function and the phase change are introduced simultaneously in the whole space. There is no faster-than-light propagation of information, as Einstein called it.

5.2 Interaction of the Microscopic Object in the Dual 4-Dimensional Space-Time and Interpretation of Instrument Measurement Function

Gauge field theory is the cornerstone of the Standard Model. However, in standard field theory, the wave function is given a probabilistic interpretation from the very beginning, and matter waves are probabilistic waves [18]. The gauge transformation in gauge field theory is the mathematical operation of probability function, and the introduced gauge field A is the vector potential of the electromagnetic field and is the auxiliary quantity of electric field (E). Gauge transformation gives more impression of mathematical significance than physical ones. Matter waves in the dual 4-dimensional space-time are physical waves [7]. The gauge transformation of physical waves reveals the real physical significance of the gauge transformation.

5.2.1 Traditional Global Gauge Transformation

The global gauge transformation of the wave function of the charged free microscopic object is carried out [18], a = constant, $\partial a = 0$

$$\psi \to \psi' = e^{-i\alpha}\psi \quad , \quad \overline{\psi} \to \overline{\psi}' = \overline{\psi}\, e^{i\alpha}$$

$$\partial_\mu \psi \to \partial_\mu \psi' = e^{-i\alpha}\partial_\mu \psi$$

ψ、$\overline{\psi}$、$\partial_\mu \psi$ The same rules transformation. Gauge invariance is established, the Lorentz covariant Dirac equation is obtained

$$(ir^\mu \partial_\mu - m)\psi = 0$$

The solution of the Dirac equation confers a probabilistic interpretation. Wave functions are not deterministic and the meaning of physical realism is unclear.

5.2. 2 Traditional local gauge transformation

In the above formula, if the multiplied phase factor α is a function of the space-time coordinate *x*. Local norm transformation of field quantity ψ and its derivative $\partial_\mu\psi$ of charged free microscopic object [18] :

$$\psi \to \psi' = e^{-i\alpha(x)}\psi, \quad \overline{\psi} \to \overline{\psi}' = e^{-i\alpha(x)}\overline{\psi}$$

$$\partial_\mu\psi \to \partial_\mu\psi' = \partial_\mu[e^{-i\alpha(x)}\psi]$$

$$= e^{-i\alpha(x)}\partial_\mu\psi - i\partial_\mu\alpha(x)e^{-i\alpha(x)}\psi \neq e^{-i\alpha(x)}\partial_\mu\psi$$

Traditional analysis shows that the Lorentz covariant Dirac equation cannot be obtained because $\partial\mu\alpha(x) \neq 0$, and the transformation of field quantity and its derivative is inconsistent. By introducing the covariant derivative D_μ

$$\partial_\mu \to D_\mu = \partial_\mu - ieA_\mu$$

The Dirac field equation of the same form can be obtained:

$$(ir^\mu D_\mu - m)\psi = 0$$

It can be seen that by introducing A gauge field A_μ through covariant derivative, the interaction between electromagnetic field and charged the microscopic object can be reflected, and the local gauge transformation gauge invariance can be restored.

Dual 4-dimensional space-time considers that the global gauge transformation is the coordinate translation of free electron matter wave. The electrons are already exposed to the electromagnetic field in a local gauge transformation. Embody $\partial_\mu\alpha(x) \neq 0$. The state of free motion and Lorentz covariation are destroyed, so the form of the Dirac field equation is destroyed. The covariant derivative D_μ introduces the gauge field A_μ to reflect the electromagnetic effect. In fact, it is a physical and mathematical operation to eliminate the effect of the introduced electromagnetic field in the local gauge transformation, eliminate the influence of $\partial_\mu\alpha(x) \neq 0$, restore the free motion state of electrons and Lorentz covariant, and ensure the unchanged form of the Dirac field equation.

Spin in the dual 4-dimensional space-time has a natural physical definition and is no longer a property of point particles [7]. In the experiment of electron spin of the silver atom, the local transformation of the spin wave function ψ(x) is carried out, and the nonuniform magnetic field is the classical electromagnetic coupling effect on electron spin. Electrons go from a pure state to a mixture of the spin up and the spin down. Describes the transformation of space-time from W(x,k) to $M^4(x)$. In the laboratory space, we will observe the fine structure of two lines above and below the orbital motion of the spin up and the spin down mixed state electrons [7,19]. Here, the introduction of an inhomogeneous magnetic field is a quantum measurement involving the Penrolaus nonlinear R process.

If the invariance of the Dirac equation and the electromagnetic action of an electron is discussed in the quantum field, the vector potential A_μ of the electromagnetic field should be adopted, and a series of mathematical physical operations of the covariant derivative is considered.

The weak interaction and quantum chromodynamics are similar. In the interaction of quark and gluon fields, mathematics uses group theory. Considering the physical reality of quark and gluon

fields and the physical significance of their phase, quantum chromodynamics can make the same mechanical analysis. The interaction between quark and gluon fields is also realized in the local gauge transformation, and the introduction by the covariant derivative into the gauge field is only a counteracting effect. The invariance of the form of the Dirac field equation can be guaranteed by the quark's free motion again.

In the dual 4-dimensional space-time, the essence of quantum measurement is to carry out a full-space instantaneous space-time transformation through the introduction of interaction, transforming the dual 4-dimensional space-time into 4-dimensional real space-time, transforming the sphere model into the point model, and transforming matter waves into probability waves. Matter tells space-time how to have probabilistic properties, and by quantum measurements, space-time tells matter how to Probability of movement. In fact, the introduction of a continuous potential $U=e^{\alpha(x)}$, the elimination of spacelike partition, and the space-time transformation in full space are mathematical and physical operations. The transformation of the wave function takes place simultaneously in the whole space, There is no"the converted waves" propagation[7]. The instantaneous propagation of information and the formation of entangled states in quantum entanglement are the results of the simultaneous transformation of wave functions in the whole space.

5.2.3 Mathematical Representation of Decoherence and Local Transformation for Macroscopic Instruments

In the dual 4-dimensional space-time, the macroscopic measurement instrument can be automatically decoherence.

The macroscopic instrument is designed and manufactured by the classical point particle theory of 4-dimensional real space-time. There is no quantum mutation hypothesis and no spacelike partition between states. There is continuous interaction between states. It does not constitute a pure quantum state, but can be written as a mixed state at most. Because of the existence of continuous potential, the instrument has the ability of automatic decoherence.

The state of the macroscopic instrument can be directly observed, and of course, the measurement display can be directly observed. In quantum measurement, the macroscopic instrument not only changes the cognitive level of the system under test but also transforms the describing space-time to return to the classical space-time to record the measurement results. This is the physical essence of instrument translation in quantum measurement. The irreversible evolution from the pure state to the mixed state in the measurement indicates that the macroscopic measuring instrument is unable to make the microscopic measured system automatically return from the mixed state to the microscopic pure quantum state. This is the inevitable result of the establishment of macroscopic instrument theory, design, and manufacturing principles.

According to von Neumann's measurement theory, the initial state of the macroscopic instrument is assumed to be $X_o(x)$. $X_{on}(x)$ is the decomposition pure state, and $X_o(x) = \sum X_{on}(x)$. There is a fixed phase difference between X_{on} and X_{on+1} and there is coherence. The final state of the instrument is $X_n(x)$. $X_{nn}(x)$ is the final pure state of decomposition, and $X_n(x) = \sum X_{nn}(x)$. There is also a fixed phase difference between X_{nn} and X_{nn+1}, and there is also coherence. The instrument is self-coherent.

However, these are purely hypothetical. The self-coherence properties of instruments have never been observed. Instrument auto-coherence is not allowed in measurement, so a variety of automatic instrument decoherence schemes are proposed. But so far there has been no successful case. It would be absurd for decoherence to require the last glance of God or man.

In the dual 4-dimensional space-time, the self-coherence of macroscopic instruments is eliminated automatically in theory and instrument design and production, considering local transformation.

If the macroscopic measuring instrument in quantum mechanics is decomposed into the macroscopic component states, even the microscopic component states, it is clear that the interaction between the component states will be governed by the continuous interaction potential $U=e^{a(x)}$. This shows that the states X_{on}, $X_{on}+1$, or X_{nn} and $X_{nn}+1$ are governed by the continuous interaction potential $U=e^{a(x),}$ which is automatically constituted by a local transformation

$$X_0(x)\rightarrow X_0(x)' \quad =e^{a(x)}X_0(x)=e^{a(x)}\sum X_{0n}\ (x)=\sum e^{a(x)}X_{0n}(x)=\sum X_{0n\Phi}=X_{0\Phi}$$

$$X_n\ (x)\rightarrow X_n(x)' \quad =e^{a(x)}X_n\ (x)=e^{a(x)}\sum X_{nn}\ (x)=\sum e^{a(x)}X_{nn}\ (x)=\sum X_{nn\Phi}=X_{n\Phi}$$

$\boldsymbol{\Phi}$ is the mixed state mark. $X_{0n\Phi}$ and $X_{nn\Phi}$ are the mixed components of the initial and final states. Under the action of continuous potential $U=e^{a(x)}$, the initial and final states of the macroscopic instrument automatically evolve into mixed states $X_{0\Phi}$ and $X_{n\Phi}$. Analog wave Function

$$\psi\rightarrow\psi' \quad =e^{a(x)}\psi=e^{a(x)}\sum c_n\psi_n=\sum e^{a(x)}c_n\psi_n=\sum c_n\Phi_n \qquad (35)$$

The local transformation. The interaction could be a classical potential.

Inside the macroscopic instruments, the continuous interaction potential $U=e^{a(x)}$ exists, the fixed phase difference between the internal states do not exist at all, and the phase interference of waves does not exist. The states $X_o(x)$ and $X_n\ (x)$ of the macroscopic instruments can only appear in the form of mixed states $X_{o\Phi}$ and $X_{n\Phi}$. Therefore, there is a theoretical basis for the absence of self-coherence in the macroscopic instruments. In von Neumann's measurement entanglement model, there are some problems with the pure state assumption of the macroscopic instrument, and the physical essence of the intrinsic continuous interaction and local transformation of the instrument is not taken into account. Therefore, any other assumptions about the automatic decoherence of the instrument are redundant.

The biological and physiological organs of the Schrodinger cat, even if observed down to the molecular and atomic level, are dominated by macroscopic continuous interaction. The macroscopic cat can only be a mixed state Φ_n, there is no dead cat, live cat parallel pure state existence. Its decoherence is self-completed by biological mechanisms, and the mathematical expression is also an equation (35). There are also theoretical reasons why we don't observe the phase interference of waves of the macroscopic cat.

VI. CONCLUSION

The physical model of quantum mechanics is a rotating field of matter ball, particle model is not applicable. The physical space-time describing quantum phenomena is dual 4-dimensional space-time, which has the characteristics of construction [20]. It is equivalent to Newtonian space-time, special relativity space-time, and gravitational space-time in describing nature.

1. The wave function can be derived strictly from the motion of the field matter ball. Matter waves are physical waves. The traditional cognitive confusion of wave function can be completely eliminated and has new physical applications [21,22]. Such as the coulomb blocking Matter wave cognitive

experiment (electronic wave barrier-free through the Coulomb blocking), matter-wave chip engrave technology experiment, matter-wave communication technology experiment, and so on.

2. Matter tells space-time how to have probabilistic properties, and space-time tells matter how to behave in probabilistic motion.
3. The spatial distribution and mass density distribution of microscopic objects are the origins of quantum probability. Quantum probability is completely different from thermodynamic probability and classical statistical probability.
4. Different macro and micro physical mechanisms and different causal relationships. Quantum superposition states have microscopic physical mechanisms to follow. Quantum measurement changes the nature of causality correlation, and the pure state becomes a mixed state. It is crucial to thoroughly understand the physical mechanism of phase transformation of the wave function.
5. In dual 4-dimensional space-time, the calculation of field interaction cutoff is at the curvature K0, and there is no infinite divergence difficulty.
6. The deep application of the Wigner function method based on dual 4-dimensional space-time covariant quantum mechanics penetrates the new understanding of many important physical meanings of the quantum mechanical formal system. The cognitive difficulties in the traditional quantum mechanical formal system are almost eliminated. Wigner Moyal product (*) wave equation is equivalent to Schrodinger equation, Diracequation, and Feynman path integral equation.

ACKNOWLEDGMENTS

Thanks to many scholars experts and leaders different periods for their discussion, care, support, and guidance on theoretical development. Professor Li Hongfang of the University of Chinese Academy of Sciences proofread the English translation of this paper.

Note

Note 1: China university of science and technology of Jian-wei Pan, Zhao-yang Lu, Xiao-bo Zhu, and professor at the university of Seville, Spain Cabello, using ultra-high precision superconducting quantum circuits for deterministic entwine exchange, at more than 43 standard deviations of the experiment proved that the precision of real number cannot complete description standard quantum mechanics, established the objective reality of complex numbers description. The findings were published as an "editor's recommendation" in Physical Review Letters. Viewpoint and News & Views were respectively invited by the website of American Physical Society Physics and the journal Nature. (China University of Science and Technology News Network Mozi Salon 2022-01-30 16:06)

Note 2: Some important nouns: 1) interaction realism, 2) time-like space, 3) spacelike space , 4) phenomena, 5)sphere model, 6) particle model, 7) microscopic quantum object, 8) matter waves, 9) rotating field matter sphere, 10) physical space-time, 11) dual 4-dimensional space-time, 12) macroscopic object.

Note 3: about the author: Zhao Guo-qiu, 1944.10.--, male, researcher, 1969.8. Graduated from Huazhong University of Science and Technology. Research directions: Philosophy of Physics, basis of quantum mechanics, basis of modern Science in Traditional Chinese Medicine basis Theory.

REFERENCES

1. Jammer, M. Philosophy of Quantum Mechanics. the interpretations of quantum mechanics in historical perspective. (Wiley, 1974).
2. Thom, R. CATASTROPHE THEORY (Wiley, 1978).
3. Sakata, S. Shoichi Sakata: Scientific Works. (Publication Committee of Scientific, 1977).
4. Yukawa, H. Theory of Elementary Particles Extended in Space-time. (Kyoto University, 1979).
5. Smolin, L. The trouble with physics: the rise of string theory, the fall of a science, and what comes next. (HMH, 2007).
6. Lewis, P. J. Quantum ontology: A guide to the metaphysics of quantum mechanics. (Oxford University Press, 2016).
7. Zhao, Guo-qiu. Quantum Mechanics Foundation in Dual 4-Dimensional Space-Time—Space-Time Origins of Quantum Probability. (Scientific Reasearch Publishing, 2016).
8. Zhao, Guo-qiu. Fundamentals of Covariant Quantum Mechanics in dual 4-dimensional space-time. (Hubei Science and Technology Press, 2022).
9. Zhang, Y. Quantum Free-talk. (Tsing hua University Press, 2016).
10. Collaboration, A. et al. Order of magnitude smaller limit on the electric dipole moment of the electron. Science 343, 269-272 (2014).
11. Landau, L. & Peierls, R. Quantum electrodynamics in configuration space. Zeit. f. Phys **62**, 188-200 (1930).
12. Wigner, E. 2). The unreasonable effectiveness of mathematics in the natural sciences. Richard Courant lecture in mathematical sciences delivered at New York University, May 11, 1959. Communications on Pure and Applied Mathematics **13**, 1-14 (1960).
13. Inman, F. W. & Miller, C. E. Contemporary Physics. (Macmillan, 1975).
14. Li, K., Wang, J., Dulat, S. & Ma, K. Wigner functions for Klein-Gordon oscillators in non-commutative space. International Journal of Theoretical Physics **49**, 134-143 (2010).
15. Penrose, R. The road to reality. (Random house, 2006).
16. Minev, Z. K. et al. To catch and reverse a quantum jump mid-flight. Nature **570**, 200-204 (2019).
17. Zhao, Guo-qiu. Meaning of the Wave Function and the Origin of Probability in Quantum Mechanics. International Journal of Quantum Foundations **1**, 32-45 (2019).
18. Zhou, Z.-Y. et al. Quantum twisted double-slits experiments: confirming wavefunctions' physical reality. Science Bulletin 62, 1185-1192 (2017). https://doi.org:https://doi.org/10.1016/j.scib.2017.08.024
19. Hu, Y. Gauge Theory of Field. (Publishing House of East China Normal University, 1984).
20. Zhao, Guo-qiu. A new study on the role of covariant derivative Dμ in local gauge transformation. *Modern Physics* **11**, 77-79 (2021).
21. Zhao, Guo-qiu. Quantum Mechanics description of dual 4-Dimensional Space-Time. *Modern Physics* 8, 150 (2013).
22. Zhao Guo-qiu Quantum mechanical description and ontological basis of wave function in dual 4-dimensiona l Space-Time. Modern Physics Journal, Vol. 05, No. 16, 2014, p. 51066.

Determination of the Hydrological Parameter of the Curve Number (NC) for the Las Cañas Stream in the Siscunsí Paramo by means of Geographic Information Systems

Julián David Segura –Pena, Sully Segura-Pena, Harricson Steve Penagos Barreto, Diego Felipe García-Corredor & Diana Catalina Gomez-Castaneda

Universidad Santo Tomás Seccional Tunja

ABSTRACT

In this study, the curve number parameter is automatically determined in the micro-watershed of the Las Cañas stream of the Siscunsí paramo, in the department of Boyacá, Colombia, using the method of the Soil Conservation Service of the United States, which has the capacity to estimate the amount of runoff in an established hydrographic basin. This procedure is based on the use of geographic information systems, and thus create new maps of the curve number at regional scale, using algorithms of the same programs. Likewise, a multitemporal analysis of the vegetation cover and land use identified in the area was conducted to analyze the presence of anthropogenic activities such as agriculture, making it possible to evaluate the type of soil, precipitation, and flow rates. Finally, the results of the flow simulation obtained using GIS software were compared with the flows provided by the rational method based on the intensities calculated by the Dick Peschke and Frederich Bell models using historical precipitation records from climatic stations adjacent to the micro basin.

Keywords: curve number, GIS, precipitation, flow, remote sensing.

Classification: DDC Code: 530.14301516 LCC Code: QC174.17.G46

Language: English

Great Britain Journals Press

LJP Copyright ID: 925612
Print ISSN: 2631-8490
Online ISSN: 2631-8504

London Journal of Research in Science: Natural and Formal

Volume 23 | Issue 2 | Compilation 1.0

Determination of the Hydrological Parameter of the Curve Number (NC) for the Las Cañas Stream in the Siscunsí Paramo by means of Geographic Information Systems

Determinación Del Parámetro Hidrológico Del Número De Curva (NC) Para La Quebrada Las Cañas Del Páramo De Siscunsí Por Medio De Sistemas De Información Geográfica

Julián David Segura –Peña[α] , Sully Segura-Peña[σ] , Harricson Steve Penagos Barreto[ρ]
Diego Felipe García-Corredor[Ↄ] & Diana Catalina Gómez-Castañeda[¥]

RESUMEN

En este estudio se determina, de manera automática, el parámetro del número de curva en la microcuenca de la quebrada Las Cañas del páramo de Siscunsí, en el departamento de Boyacá, Colombia, empleando el método de la Soil Conservation Service de los Estados Unidos, el cual tiene la capacidad de estimar la precipitación efectiva en una cuenca hidrográfica establecida. Este procedimiento está basado en usar sistemas de información geográfica, y así crear nuevos mapas del número de curva a escala regional, por medio de algoritmos de los mismos programas. Asimismo, se realizó un análisis multitemporal de las coberturas vegetales y usos del suelo identificados en la zona que permiten analizar la presencia de actividades antrópicas como la agricultura permitiendo evaluar el tipo de suelo, precipitación, y caudales. Finalmente, se compararon los resultados de la simulación de los caudales obtenidos mediante software SIG con los caudales entregados por medio del método racional a partir de las intensidades calculadas por los modelos de Dick Peschke y Frederich Bell empleando los registros históricos de precipitación de estaciones climáticas aferentes a la microcuenca.

Palabras clave: número de curva, SIG, precipitación, caudal, sensores remotos.

ABSTRACT

In this study, the curve number parameter is automatically determined in the micro-watershed of the Las Cañas stream of the Siscunsí paramo, in the department of Boyacá, Colombia, using the method of the Soil Conservation Service of the United States, which has the capacity to estimate the amount of runoff in an established hydrographic basin. This procedure is based on the use of geographic information systems, and thus create new maps of the curve number at regional scale, using algorithms of the same programs. Likewise, a multitemporal analysis of the vegetation cover and land use identified in the area was conducted to analyze the presence of anthropogenic activities such as agriculture, making it possible to evaluate the type of soil, precipitation, and flow rates. Finally, the results of the flow simulation obtained using GIS software were compared with the flows provided by the rational method based on the intensities calculated by the Dick Peschke and Frederich Bell models using historical precipitation records from climatic stations adjacent to the micro basin.

Keywords: curve number, GIS, precipitation, flow, remote sensing.

Author α σ ρ: Departamento de Ciencias Básicas, Universidad Santo Tomás Seccional Tunja.
Ↄ ¥: Facultad de Ingeniería Ambiental, Universidad Santo Tomás Seccional Tunja.

London Journal of Research in Science: Natural and Formal

I. INTRODUCCIÓN

La hidrología y los SIG (Sistemas de información geográfica) se han constituidos como dos áreas que comparten una gran variedad de información (Morad, 2001). Por tal motivo, ha sido de gran interés el estudio de las relaciones y vínculos que existen entre los SIG y el modelamiento hidrológico (Castro López, 2011). El método del número de curva (CN) es uno de los vínculos que presentan estos dos campos de investigación. Esta metodología fue desarrollada por SCS (Soil Conservation Service) de los Estados Unidos con la finalidad de determinar la precipitación efectiva de una cuenca a partir del tipo de cobertura y uso de suelo, la lluvia acumulada y las condiciones de humedad de la zona (Ven Te, 1984); es decir, a partir de estas características físicas del territorio, este parámetro hidrológico permite establecer el potencial de escorrentía de la cuenca (Díaz Carvajal , 2017).

De acuerdo con (Romano Castillo, 2007) el CN es el método más adecuado para transformar la precipitación total en precipitación efectiva debido a que tiene en cuenta una de las principales etapas del ciclo del agua, como lo es la infiltración, la cual influye notablemente en la dinámica hidrológica. Este proceso se presenta cuando el agua precipitada se mueve de manera vertical a través de la superficie del suelo generando el incremento en la humedad en esta matriz (Calvache, 2010).

A pesar de que la metodología del SCS se ha convertido en una de las principales herramientas para la modelación hidrológica y ambiental (Sánchez Palomino, 2015), el número de curva ha generado gran interés en las diferentes investigaciones debido a que permite establecer y describir las condiciones geográficas generales de una zona de estudio (Sedano Cruz, 2013) al tiempo que indica el potencial de escorrentía de una superficie determinada.

Para la estimación del número de curva en una cuenca hidrográfica, se han aplicado los SIG y la teledetección como herramientas de gran utilidad para determinar las condiciones generales de la cobertura vegetal y del uso del suelo(Lao Ramos, 2018). (Deshmukh *et.al.*, 2013) emplearon y procesaron imágenes satelitales por medio de un software SIG con el fin de identificar la transformación del CN que se ha presentado en tres cuencas hidrográficas ubicadas en India. Por medio de los resultados obtenidos se pudo concluir que este parámetro hidrológico se ha incrementado en la zona a raíz del crecimiento desmesurado de la frontera agrícola.

Por su parte, (Rodríguez *et.al.*, 2012) establecieron mediante la zonificación del CN, el impacto ambiental que se presenta en un escenario determinado, en cuanto a la ocupación del territorio, por medio de uso de las herramientas SIG. En Colombia, se llevó a cabo un estudio en la subcuenca de Betancí, ubicada en el departamento de Córdoba. Debido a los diferentes servicios ecosistémicos que ofrece esta ciénaga en el territorio y a la diversidad que se encuentra en ella, es considerada como uno de los ecosistemas estratégicos del departamento. Sin embargo, a causa de las diferentes actividades antrópicas que se han presentado alrededor de la ciénaga de Betancí se ha presentado una transformación del uso del suelo en la zona como consecuencia de la expansión de la frontera agrícola y ganadera, lo cual ha generado la pérdida casi total del bosque secundario (Díaz Carvajal , 2017).

Por otra parte, Colombia es uno de los principales países latinoamericanos que se caracterizan por sus abundantes recursos naturales presentes en los diferentes ecosistemas del territorio. Los servicios ambientales proveídos por estos ecosistemas han contribuido al desarrollo humano y social de la población colombiana. Sin embargo, las diferentes actividades antrópicas que se ha desarrollado dentro de estos ecosistemas estratégicos han generado una transformación en la cobertura vegetal y el uso del suelo en diferentes zonas, debido a un aprovechamiento inadecuado de los recursos. Este esquema de desarrollo insostenible ha producido grandes impactos ambientales que ponen en riesgo la estabilidad y el bienestar de las presentes y futuras generaciones (Sánchez Pérez, 2018).

Los páramos son uno de los ecosistemas estratégicos que presentan un bajo nivel de freático por lo que son considerados muy quebradizos , esto debido a que aproximadamente un 75% del terreno corresponde a agua (Cuervo Barahona, Cely Reyes, & Moreno Pérez, 2016). En este contexto, las actividades productivas como la ganadería presentan efectos negativos en la estructura del páramo debido a la pérdida de las propiedades retenedoras de agua y carbono en la matriz del suelo y la compactación de este como producto del pisoteo del ganado (Rivera Ospina, 2013). Los suelos del páramo se caracterizan por contener tres veces más reservas de CO en comparación con la biomasa presente sobre la tierra, además, contienen el doble de carbono que el que se registra en la atmósfera; por tal motivo, la materia orgánica del suelo en este tipo de ecosistemas es una fuente peligrosa para la generación de dióxido de carbono lo cual contribuye a una de las principales problemáticas ambientales como el calentamiento global (García Portilla, 2003).

A partir de la fragilidad de los ecosistemas de páramo dentro de territorio colombiano se han generado diferentes normativas para su protección y preservación, como lo es el artículo 173 de la Ley 1753 del 2015, en el cual se estipuló que en estas zonas no se pueden desarrollar actividades productivas que involucren el uso de recursos naturales no renovables. Con base en lo anterior, la población que se encuentra asentada en este tipo de ecosistemas no puede continuar con sus actividades económicas tradicionales. Por lo anterior, es indispensable formular alternativas laborales para las comunidades campesinas residentes en estos ecosistemas (Rubiano Galvis, 2015).

El páramo del Siscunsí, ubicado al sur oriente del municipio de Sogamoso, es uno de los principales ecosistemas estratégico del departamento de Boyacá ya que presenta una extensión de 5.942 ha (Sánchez Pérez, 2018). El principal afluente del páramo es la quebrada La Iglesia, también conocida como quebrada Las Cañas, la cual es uno de los principales drenajes que alimentan al Rio Cusiana dentro del departamento.

Considerando lo anteriormente expuesto, es claro que existe la necesidad de conocer el potencial actual de generación de escorrentía en este ecosistema estratégico, y de este modo que las autoridades competentes cuenten con acceso a herramientas e información científica para tener la capacidad de formular acciones de remediación al impacto ambiental provocado sobre este ecosistema de páramo. De esta manera, los objetivos del presente estudio fueron determinar el CN en la microcuenca de la quebrada Las Cañas del páramo de Siscunsí y así reconocer la dinámica hidrológica de este ecosistema en cuanto al potencial de generación de escorrentía, así como identificar las coberturas del suelo a partir de un mosaico multitemporal de imágenes LANDSAT, asignar los grupos hidrológicos del suelo y comparar los resultados de los caudales obtenidos para los diferentes años de estudio a partir del método racional empleando los modelos de Frederich Bell y Dick Peschke para el cálculo de las intensidades, con los resultados entregados por las medias aritméticas analizados a partir del software QGIS de las imágenes ráster de la escorrentía superficial.

II. MATERIALES Y MÉTODOS

2.1 Identificación del cambio de coberturas vegetales y uso del suelo

2.1.1 Delimitación de la cuenca de estudio

Para obtener las imágenes satelitales se realizó la descarga del Modelo de Elevación Digital (DEM, por sus siglas en inglés), obtenido del Servicio de Satélites de Alaska (Alaska Satellite Facility), la cual tiene una resolución espacial por píxel de 12.5 metros. Por medio de la red de drenajes obtenida a partir del procesamiento del DEM y de la información suministrada por el Instituto Geográfico Agustín Codazzi (IGAC), se realizó la delimitación la microcuenca de la quebrada Las Cañas. Estos datos fueron procesados por medio del software QGIS 2.18, donde se realizó la corrección de píxeles, así como la

determinación de la dirección y acumulación de flujo y el respectivo análisis de cuenca. En la figura 1, se observa el mapa de localización y delimitación del área de estudio.

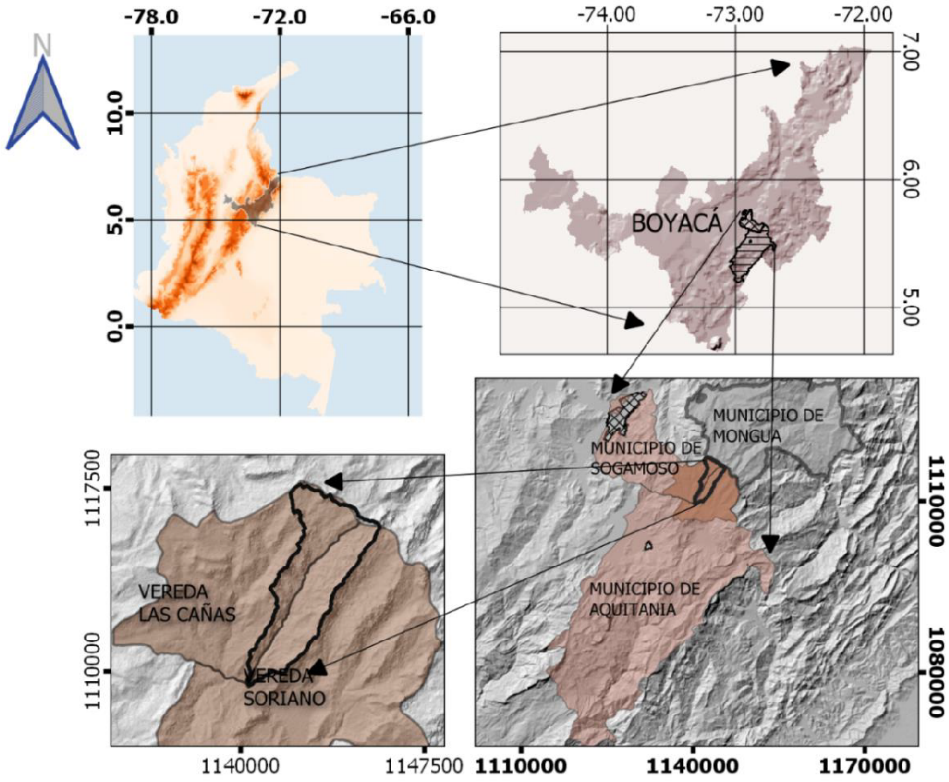

Fuente: Autores

Figura 1: Localización y delimitación área de estudio

2.1.2 Clasificación e identificación del cambio de coberturas y uso del suelo

Posteriormente, a partir del software QGIS se realizó la identificación del uso del suelo teniendo en cuenta las coberturas vegetales, empleando modelos de predicción. Para la caracterización de uso del suelo se aplicó la metodología Corine Land Cover escala 1:25000 y la información suministrada por el documento *Leyenda Nacional de Coberturas de la Tierra Metodología Corine Land Cover* escala 1:100000, adaptadas cada una a Colombia. Los datos fueron validados y rectificados con las visitas realizadas a campo.

En la figura 2, se presenta el diagrama metodológico para la clasificación e identificación del cambio de coberturas vegetales y uso del suelo.

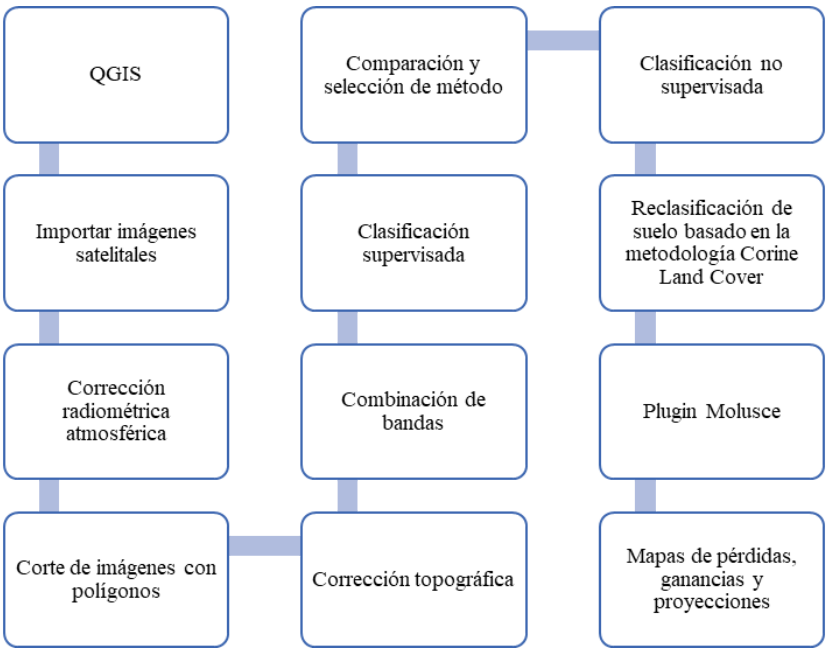

Fuente: Autores

Figura 2: Metodología usada para la clasificación e identificación del cambio de coberturas y uso del suelo

Por otra parte, la descarga y selección del mosaico de imágenes satelitales Landsat se realizó por medio del servicio geológico de Estados Unidos (USGS), teniendo en cuenta un porcentaje de nubosidad inferior al 20%. En la figura 3, se observan las imágenes multiespectrales.

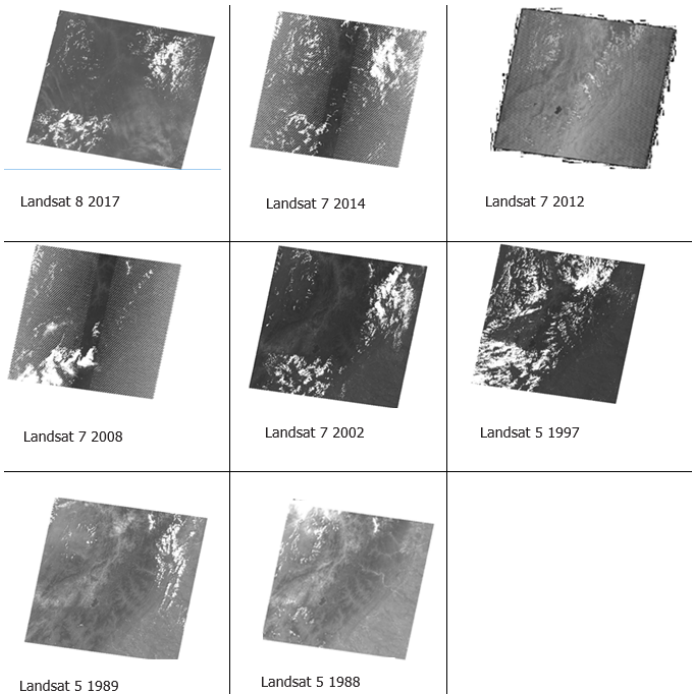

Fuente: Autores

Figura 3: Compendio de imágenes Landsat utilizadas

Es importante resaltar que se realizó una corrección y normalización de las imágenes satelitales debido a que estas presentaban contrastes diferentes, los cuales pudieron ser producidos por la posición en que se encontraba el sol al momento de su captura y por el relieve de la zona. La corrección topográfica se llevó a cabo por medio de la herramienta "Topographic correction" del software QGIS aplicando los métodos Coseno corrector (Civco, 1989) Minnaert correction with Slope (Law & Nichol, 2004) Corrección C y Normalización (Civco, modificada por Law & Nichol). De los métodos mencionados anteriormente, se optó por utilizar el de normalización ya que este fue el que presentó mejores resultados en términos de homogenización de las imágenes con el relieve.

a) Corrección Minnaert b) Corrección Coseno

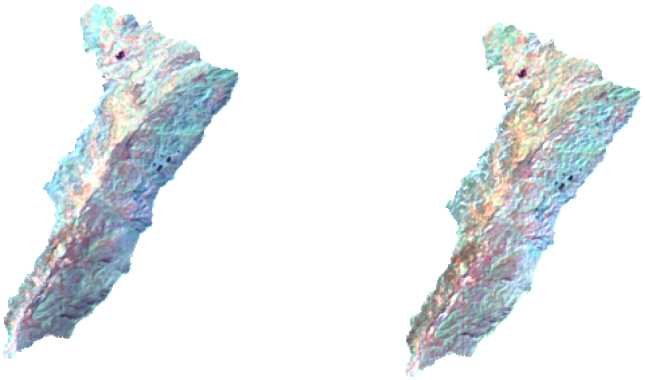

c) Corrección C d) Normalización

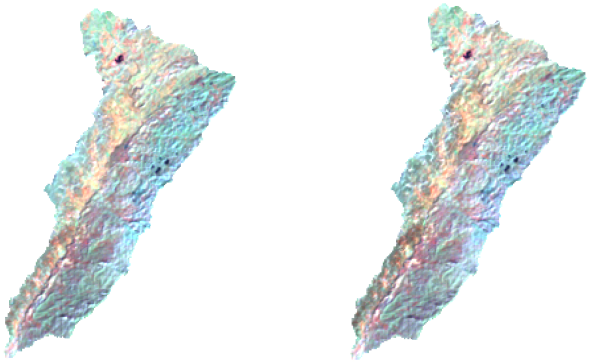

Fuente: Autores

Figura 4: Corrección de las imágenes satelitales

Posteriormente, se ajustó la clasificación de coberturas terrestres de manera supervisada. Esta clasificación es pertinente por la relación de las clases de cobertura existentes en el área de estudio. La reclasificación de las imágenes satelitales se realizó con la metodología Corine Land Cover adaptada para Colombia mencionada anteriormente (Menéndez & Núñez, 2009). En este proceso se tuvieron en cuenta, cuatro tipos de cobertura vegetal que fueron identificados en la microcuenca, presentados en la Tabla 1. Estas coberturas se relacionan con los usos de suelo presentes en la región, por medio del POT del municipio de Sogamoso, el EOT del municipio de Aquitania y el POMCA de la cuenca del río Cusiana.

Para verificar y corregir la información obtenida se hizo uso en el procesamiento geográfica en QGIS y de la información teórica descrita anteriormente, se realizó una visita al páramo de Siscunsí, donde se

identificó cada una de las clases de cobertura y uso del suelo, permitiendo ajustar los datos a las 4 clases de presentadas en la Tabla 1.

Tabla 1: Clasificación de cobertura vegetal y uso de suelo

Clssification	Cobertura Vegetal	Uso de suelo
1	Lagunas, lagos y ciénagas naturales	Cuerpos de aguas
2	Mosaico de pastos con espacios naturales	Actividades agropecuarias
3	Arbustal abierto mesófilo	Sistemas forestales
4	Herbazal denso alto de tierra firme no arbolado	Áreas para la conservación

Fuente: Autores

Con la información obtenida se elaboraron los mapas de uso de suelo de los años 1989,1997, 2002, 2008, 2014 y 2017, por medio de los cuales se llevó a cabo el análisis multitemporal. Se empleó el plugin Molusce del software QGIS para realizar las predicciones de los escenarios de uso del suelo, el cual permite analizar, modelar y simular las transformaciones de la cobertura vegetal y uso del suelo en una zona específica (Villalobos Chacón , 2019).

Para la aplicación de esta herramienta es necesario contar con las capas reclasificadas de dos años, así como una combinación de variables que están relacionas a la humedad, erosión y deslizamientos. Estas variables son la distancia a las vías empleando los datos de la red vial (figura 5), drenajes obtenidos del IGAC (figura 6), y también las pendientes dadas en porcentaje que presenta el terreno (figura 7).

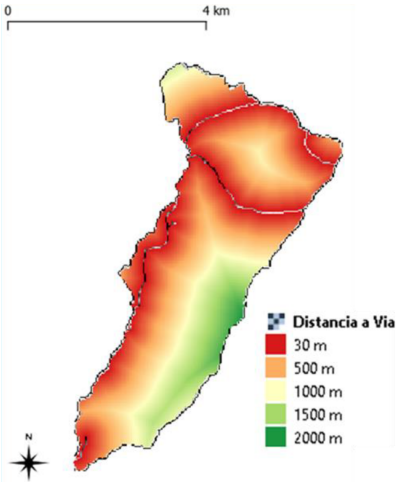

Fuente: Autores

Figura 5: Mapa distancia a vías

En la figura 6, se muestra la red de drenajes obtenida a partir del análisis de proximidad de cada cauce. El resultado es un nuevo ráster que simboliza la distancia euclidiana del terreno a cada uno de los cauces.

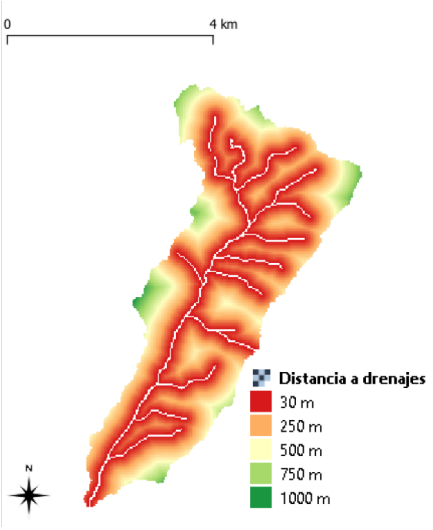

Fuente: Autores

Figura 6: Mapa distancia a drenajes

En la figura 7, se observa el mapa de pendientes en grados obtenido en QGIS, con la herramienta Slope.

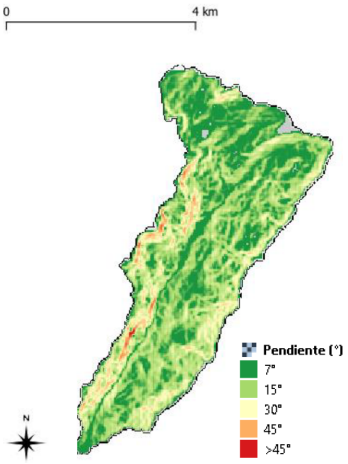

Fuente: Autores

Figura 7: Mapa pendiente de la cuenca expresada en grados

A partir de modelos matemáticos preestablecidos, la herramienta Molusce genera mapas de predicción de los años presentados en la tabla 2. Los periodos obtenidos por medio de los pares dan como resultado una diferencia temporal, la cual, al ser añadida al último año de los pares indica el año a proyectar.

Tabla 2: Predicciones realizadas de uso de suelos

Predicción
2014(2002-2008)
2020 (2008-2014)
2020(2014-2017)
2026 (2002-2014)
2027 (1989-2008)

Fuente: Autores.

La precisión del modelo se indica en el porcentaje del índice de Kappa. Este es un índice el cual mide la relación entre la clasificación y los píxeles de realidad en el terreno. Los valores de esta constante k indican la concordancia exacta, mientras que un valor de cero no representa ningún tipo de relación (Villalobos Chacón , 2019).

2.2 Análisis del cálculo del número de curva (CN)

La estimación de la precipitación efectiva se realizó por medio del método propuesto por el Soil Conservation Service (SCS), el cual emplea variables como la cobertura y uso de suelo, las condiciones de humedad antecedente (AMC) y la lluvia acumulada en el área de estudio con el fin de fijar un número de curva (CN) que representa tal interrelación. Para la formulación del CN, se tiene en cuenta que la escorrentía directa (Pe) siempre es menor o igual al agua que precipita en la cuenca (P); de igual manera, después de que comienza la precipitación efectiva, la profundidad adicional del agua retenida (Fa) es menor o igual a la retención potencial máxima (S) (Ven Te, 1984).

Con el método de la SCS la escorrentía directa (Q), o precipitación efectiva, es calculada a partir de la siguiente ecuación:

$$Q = \frac{(P-0.2S)}{(P+0.8S)} \quad (1)$$

Donde

Q es la escorrentía directa o precipitación efectiva, en pulgadas.

P es la precipitación considerada, en pulgadas.

S es la diferencia potencial máxima entre P y Q en el momento de inicio de la tormenta y representa proporcionalmente la pérdida de escorrentía por infiltración, intercepción y almacenamiento superficial.

Para el cálculo de la diferencia potencial máxima en pulgadas, se aplica la siguiente ecuación.

$$S = \frac{100}{CN} - 10 \quad (2)$$

Donde

CN es el número de curva.

2.2.1 Parámetros del modelo (AMC y Tipo de Suelo Hidrológico)

Las condiciones de humedad antecedente (Antecedent Moisture Conditions, AMC), se agrupan en tres condiciones básicas, como se observa en la Tabla 3.

Tabla 3: Condiciones de humedad antecedente básicas empleadas en el método SCS

Grupo AMC	Lluvia antecedente total de 5 días (pulgadas)		Tipo de condición
	Estación inactiva (seca)	Estación activa (de crecimiento)	
I	<0,5	<1,4	Seca
II	0,5 a 1,1	1,4 a 2,1	Normal
II	Sobre 1,1	Sobre 2,1	Húmeda

Fuente: (Avellaneda Córdova , 2020)

Los números de curva se aplican para condiciones de humedad antecedente normales (AMC II). Las otras dos condiciones se determinan a partir de las siguientes ecuaciones:

$$CN(I) = \frac{4{,}2\ CN(II)}{10 - 0{,}058 CN\ (II)} \quad (3)$$

$$CN(III) = \frac{23\ CN(II)}{0{,}13 CN\ (II)} \quad (4)$$

Por otra parte, el tipo de suelo hidrológico se determinó de acuerdo a las condiciones de infiltración subsuperficial que influyen en la precipitación efectiva en la cuenca, teniendo en cuenta el tipo agrológico que se encuentra en la misma. Además, se considera la cobertura vegetal, ya que la vegetación tiene una fuerte incidencia en el agua que escurre dentro de una zona, no solo por establecer el coeficiente de escorrentía sino también por la capacidad que presentan las plantas en absorber el agua en escenarios de humedad.

Para la clasificación de suelos se tuvo en cuenta las unidades geológicas del área de estudio identificadas a partir de la información suministrada por la plancha 192 del Servicio Geológico Colombiano, el POT del municipio de Sogamoso y EOT de Aquitania. En la figura 8 se observan las unidades geológicas de la microcuenca de la quebrada las Cañas.

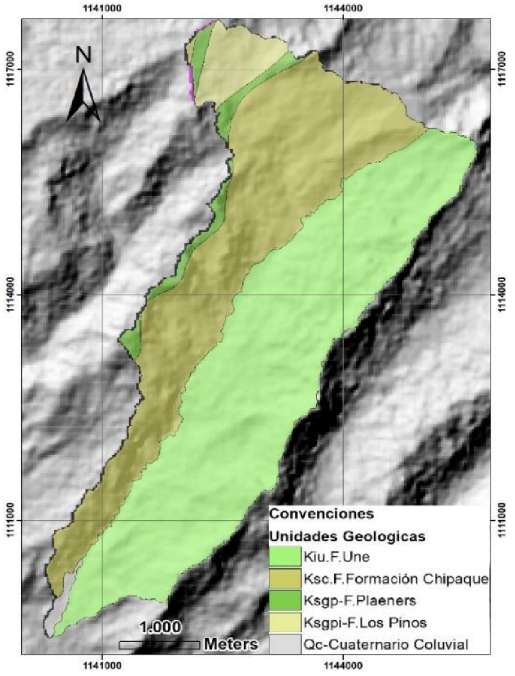

Fuente: Autores.

Figura 8: Unidades geológicas de la cuenca de estudio

Además, se clasificaron los tipos de suelo teniendo en cuenta las características litológicas de la zona, como se muestra en la tabla 4 y en la figura 9.

Tabla 4: Tipo de suelos y relación con unidades geológicas del área

Grupo Tipo de suelo	Infiltración	Formación	Tipo de roca
Tipo A	Alta capacidad de infiltración	Chipaque (Ksc) Los Pinos (Ksgpi) \Coluviales (Qc)	Arena limosa
Tipo B	Infiltración moderada	Une (Kiu)	Arena arcillosa
Tipo C	Infiltración baja	Plaeners (Ksgp)	Arcillo-arena limosa
Tipo D	Infiltración muy baja	Ninguna	Arcilla

Fuente: Autores

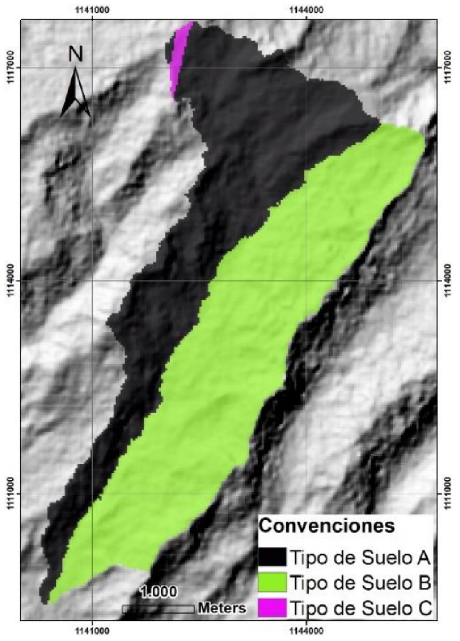

Fuente: Autores

Figura 9: Tipo de suelo de la cuenca

2.3 Cálculo de caudales a partir de intensidades obtenidas por los modelos de Dick Peschke y Frederich Bell

Se descargaron los datos pluviométricos de estaciones climáticas del IDEAM, de las cuales 5 son de clase meteorológica (MET) y 6 de clase hidrológica (HID), tal como se observa en la tabla 5. En la figura 10, se representan los polígonos de Thiessen obtenidos en el programa QGIS, donde se observa que la estación que presenta mayor aferencia sobre la microcuenca de estudio es la estación Puente Las Cañas.

Tabla 5: Estaciones climatológicas IDEAM utilizadas

Estación	Municipio	Clase
Aquitania	Aquitania	MET
Las Cintas	Sogamoso	MET
Criadero	Aquitania	HID
Hato Laguna	Aquitania	HID
La Horqueta	Pajarito	HID
Mongua	Mongua	MET
Monguí	Mongua	MET
Puente Colonial	Mongua	HID
Puente Las Cañas	Aquitania	HID
Toquilla	Aquitania	MET
Vado Hondo	Aquitania	HID

Fuente: Autores

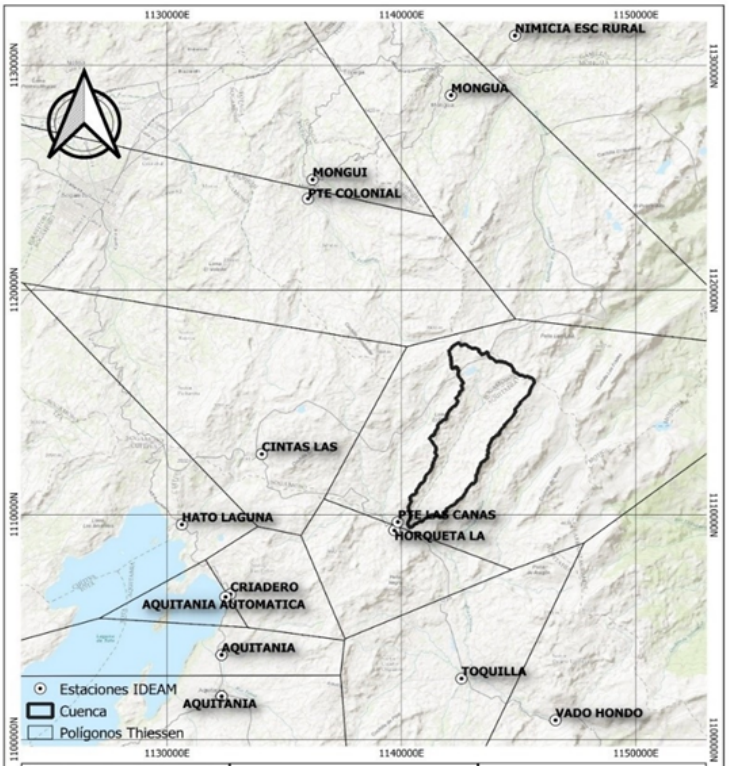

Fuente: Autores

Figura 10: Localización de estaciones climáticas y aferencias sobre la microcuenca

Las estaciones Puente Las Cañas y Toquilla, son las que se encuentran más cerca al área de estudio, y se ubican a una altitud similar a la cota promedio de la microcuenca, por lo tanto, se considera que los niveles de precipitación de estas dos estaciones son los más representativos.

Las curvas de intensidad, duración y frecuencia (IDF) se construyeron a partir de los valores de precipitación máxima en 24 horas de las estaciones Toquilla y Puente Las Cañas, durante el periodo de 1971 a 2018. Se llevó a cabo un muestreo estadístico de los datos en intervalos de tiempo de manera discreta y estable, con el objetivo de seleccionar para cada año los datos extremos de precipitación para diferentes valores de tiempo. Posteriormente se llevó a cabo un análisis de frecuencia a través de diferentes tipos de distribuciones tales como Gumbel y log-Gumbel, log-normal de 2 y 3 parámetros, probabilidad normal, gamma de 2 y 3 parámetros, log-Pearson tipo III, y finalmente para calcular los periodos de retorno de 5, 10, 20 y 50 años se realizó una prueba de ajuste de probabilidad Smirnov-Kolmogorov empleando los softwares Excel e Hidroesta 2 .

Con los datos de Pmax en 24 horas para los distintos periodos de retorno, se procedió a distribuir las precipitaciones en tiempos inferiores a 60 minutos y de 1 a 24 horas, y de este modo generar las curvas IDF, empleando los siguientes modelos:

2.3.1 Modelo de Dick Peschke

Este modelo es usado para el caso de duraciones de tormenta inferiores a 60 minutos, con datos pluviográficos con los que se pueda obtener las intensidades máximas o cuando no se cuente con registros pluviográficos que permitan obtener estas intensidades (Paredes Pinto, 2015). La ecuación que describe este modelo es la siguiente:

$$P_d = P_{24hr}\left(\frac{d}{1440}\right)^{0.25} \quad (5)$$

Donde

P_d es la precipitación total (mm).

d es la duración de la tormenta (min)

P_{24hr} es la precipitación máxima en 24 horas.

La intensidad es calcula a partir del cociente entre la precipitación P_d y la duración.

2.3.2 Modelo de Frederich Bell

De acuerdo con (Paredes Pinto, 2015), el modelo de Frederich Bell es empleado para calcular la lluvia máxima teniendo en cuenta la duración de la tormenta (min), la precipitación máxima de 1 hora de duración y el periodo de retorno de 10 años. La ecuación que describe este modelo es la siguiente:

$$P_T^t = (0.21LnT + 0.52)\left(0.54t^{0.25} - 0.50\right)P_{10}^{60}$$

Donde

P_T^t Es la precipitación de duración t minutos y periodo de retorno T (mm).

P_{10}^{60} Es la precipitación de duración 60 minutos y período de retorno 10 años (mm).

Al igual que (Paredes Pinto, 2015) para determinar P_{10}^{60} se empleó el Software Hidroesta2, teniendo en cuenta los valores de precipitación máxima durante 24 h para un periodo de retorno de 10 años, como se observa en la ecuación de Dick Peschke.

Por otra parte, la intensidad fue calculada empleando el modelo 2.3.1.

2.3.3 Método racional

Para la determinación de los caudales aplicando el método racional se empleó el Tc de la cuenca (Tiempo de concentración) y la intensidad respectiva a los periodos de retorno (TR) establecidos por medio del método de Dick Peschke y Frederich Bell para estación Puente las Cañas debido a que es la estación que presenta mayor aferencia en el área de estudio (Figura 10). A partir del tiempo de concentración de la microcuenca se realizó la interpolación de la intensidad para los TR correspondientes a 5, 10, 20 y 50 años.

La Intensidad de la Lluvia de Diseño se calculó por medio de la Ecuación 6. Es importante resaltar que se consideró la frecuencia como el periodo tiempo de retorno seleccionado y la duración igual al tiempo de concentración de la cuenca

$$I = \frac{615 \times Tr^{0.18}}{(D+5)^{0.685}} \quad (6)$$

Donde

I Es la intensidad de lluvia con duración igual al periodo de retorno (mm/h)

Tr Es el periodo de retorno en años

D Es la intensidad correspondiente al tiempo de concentración (min)

Posteriormente, se estableció el coeficiente promedio de escorrentía para el año 2017 por medio del procesamiento del tipo de suelo (Figuras 8 y 9), las pendientes del terreno, la cobertura vegetal obtenida de (Lemus & Navarro, 2003), los valores geográficos y el área de cada cobertura en el software QGIS. Teniendo en cuenta estas variables se determinó el caudal máximo, como se observa en la siguiente ecuación.

$$Q = \frac{CIA}{360} \quad (7)$$

Donde
Q Es el caudal máximo, en m^3/s.
C Es el coeficiente de escorrentía.
I Es la intensidad de lluvia con duración igual al periodo de retorno (mm/h)
A Es el área de la cuenca en hectáreas.

2.4 Comparación de caudales

Se llevó a cabo la comparación de los valores de los caudales obtenidos por el método racional con los datos hallados a partir del cálculo de la escorrentía superficial en el software QGIS.

Se utilizó el método de estimación inicial del umbral de escorrentía Po (mm) puesto que no se cuenta con la información suficiente para establecer la lluvia neta; por esta razón, el coeficiente se calculó a partir de las características de la zona de estudio. Por medio del valor inicial de Po (Tabla 6) se determinó el umbral de escorrentía de acuerdo con el tipo de cobertura vegetal, uso de suelo y los valores de pendientes de la cuenca (Figura 11).

Tabla 6: Valor inicial del umbral de escorrentía P_o

Uso de suelo	Pendiente	Grupo de suelo			
		A	B	C	D
Cuerpos de agua	No aplica	0	0	0	0
Actividades Agropecuarias	≥3	70	33	18	13
Actividades Agropecuarias	<3	120	55	22	14
Sistemas Forestales	No aplica	90	47	31	23
Áreas para la conservación	No aplica	2	2	2	2

Fuente: Autores.

A partir de la Tabla 6, se establecieron los valores del umbral de escorrentía de acuerdo a las condiciones del terreno. Posteriormente, mediante estos valores se procedió a calcular el CN.

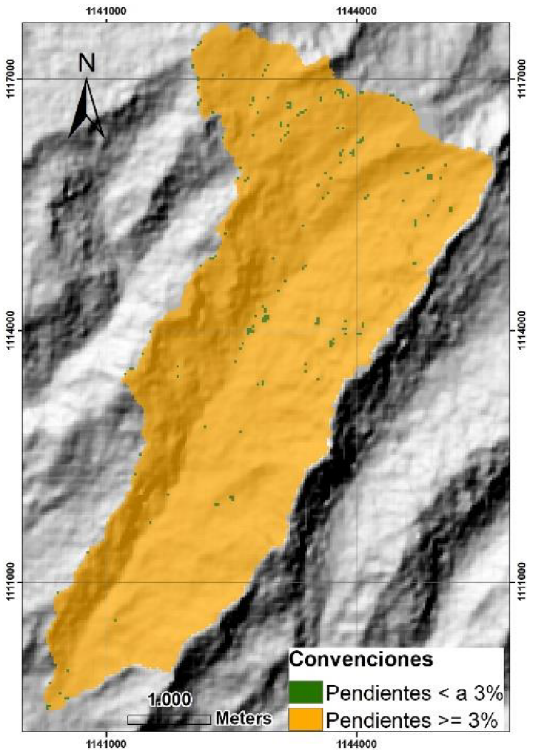

Fuente: Autores

Figura 11: Porcentaje de pendientes en la microcuenca de estudio

Empleando las ecuaciones 8 y 9 se calculó el número de curva por medio del P_o establecido para los años estudiados (1989,1997,2002,2008,2014,2017,2020, 2026,2027).

$$CN = \frac{25400}{254+\frac{P_0}{0.2}} \quad (8)$$

$$P_0 = \frac{5080}{CN} - 50.8 \quad (9)$$

El mapa resultante del procesamiento de estas variables mediante el software SIG se reclasificó de acuerdo con los valores de CN para condiciones normales. Luego, se obtuvieron los mapas de la diferencia potencial máxima por medio del uso de la herramienta "Algebra de mapas". No obstante, a pesar de que en esta metodología emplea el valor de precipitaciones de corta duración para poder evaluar escenarios máximos, en esta investigación se empleó la precipitación total mensual promedio de cada año obtenido a partir de la interpolación realizada con los datos de precipitación registrados por diversas estaciones climáticas en la zona.

A partir de los rásteres de la precipitación, CN y factor S se determinó la escorrentía mensual de la cuenca para los años estudiados por medio de la aplicación de la Ecuación 1. Además, mediante los valores promedios de la precipitación efectiva se calculó el volumen de agua. Por último, se determinó el caudal de la cuenca para cada periodo analizado teniendo en cuenta los valores de escorrentía directa y el área de la microcuenca.

III. RESULTADOS

3.1 Cambio de cobertura y uso del suelo

Con base a la visita realizada al páramo de Siscunsí, se pudo verificar y correlacionar las 4 categorías de acuerdo con la metodología Corine Land Cover adaptada para Colombia, esto se llevó a cabo con la

reclasificación de 15 puntos de observación distribuidos espacialmente a lo largo de la microcuenca Las Cañas. En la Figura 12 se puede evidenciar los puntos de control en la imagen satelital junto con la imagen ajustada y reclasificada en las 4 clases de uso de suelo para el año 2017.

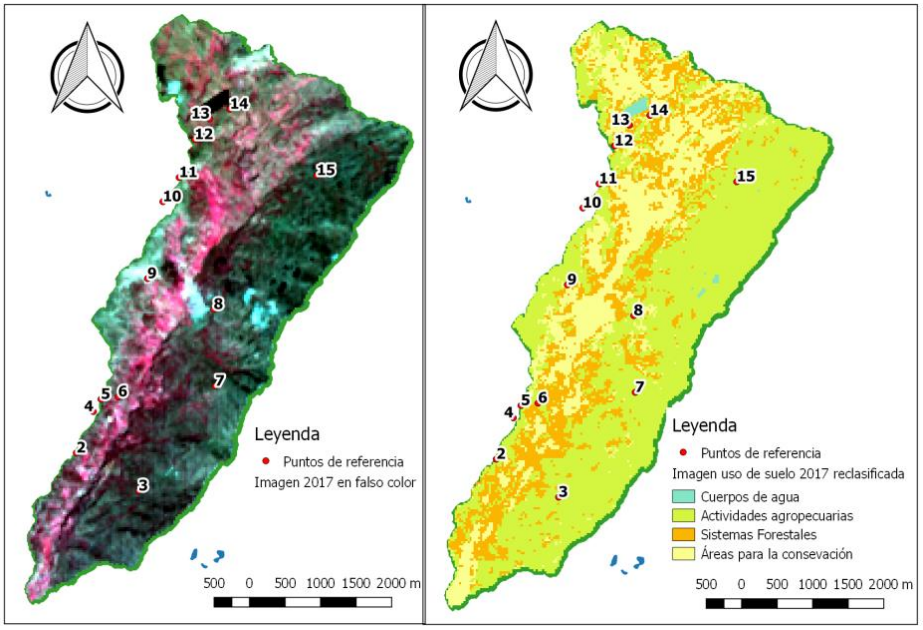

Fuente: Autores

Figura 12: Puntos de control en campo junto con imagen en falso color y uso del suelo reclasificado, año 201

Por otra parte, a partir del procesamiento de las imágenes satelitales en el software QGIS se pudo establecer los cambios de cobertura de los 4 tipos de uso de suelo que se presentan en el área de estudio durante el periodo 1989-2017. Como se observa en la Tabla 7, las actividades agropecuarias y las áreas para la conservación fueron las categorías que tuvieron un aumento en su extensión dentro de la microcuenca de 49,5 ha y 260,01 ha respectivamente. El incremento de cobertura de las actividades agropecuarias es la consecuencia de la expansión de la frontera agrícola y ganadera durante los 28 años analizados, dando como consecuencia la transformación de otros tipos de usos como los sistemas forestales, los cuales registraron una pérdida de 306,45 ha, en este tipo de uso de suelo. Por otra parte, la ganancia de cobertura de las áreas de conservación es el resultado de las diferentes actividades que se han planteado y desarrollado en la zona a lo largo de tiempo con miras a la conservación del páramo de Siscunsí.

En la Figura 13 se ilustran los cambios que presentó la microcuenca Las Cañas en los años 1989-2017 con respecto a las 4 categorías identificadas de uso de suelo.

Tabla 7: Cambios de uso de suelo durante el periodo de estudio

	Área (Ha)		Diferencia (Ha)	Área %		Diferencia (%)
	1989	2017	Δ	1989	2017	Δ
Cuerpos de agua	9,54	8,37	-1,17	0,54	0,48	-0,07
Actividades agropecuarias	929,7	979,2	49,5	52,27	55,00	2,73

Sistemas forestales	692,82	386,37	-306,45	38,95	21,70	-17,25
Áreas para la conservación	146,7	406,71	260,01	8,25	22,85	14,6

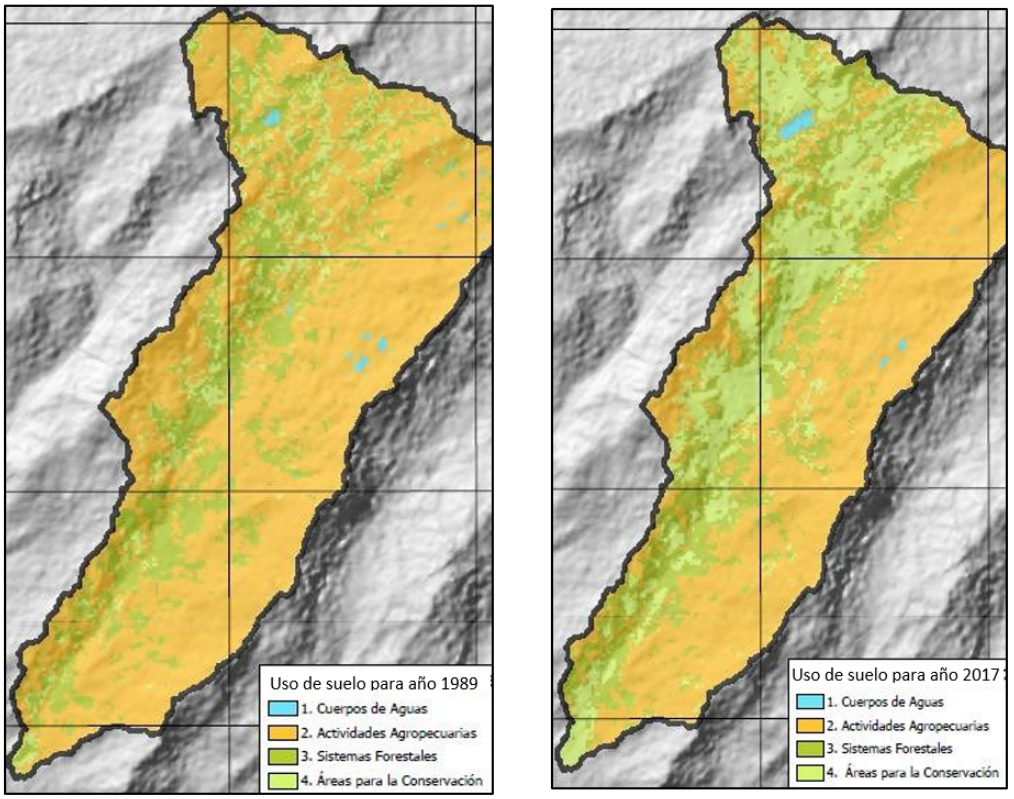

Fuente: Autores

Figura 13: Cambios de uso de suelo durante los años 1989 (Derecha) y 2017 (Izquierda)

Por otro lado, empleando las imágenes reclasificadas se realizó la simulación de uso de suelo para los años 2014, 2020, 2026 y 2027 desarrollando la metodología descrita en el apartado anterior.

Predicción uso de suelo 2014 a partir de imágenes 2002 y 2008

La proyección de la cobertura de uso de suelo del año 2014 se llevó a cabo con el fin de realizar una comparación de los resultados obtenidos de la simulación (Figura de la izquierda) con la imagen Landsat procesada en el software de este año (Figura de la derecha). Como se observa en la Tabla 8, las actividades agropecuarias y los sistemas forestales son las categorías de uso de suelo que presentaron una diferencia notable teniendo la información obtenida a partir de la simulación y el procesamiento de la imagen satelital. Los valores del área de cobertura dentro de la cuenca de estos dos usos difieren 122 ha y 90 ha respectivamente.

Es importante resaltar que la predicción realizada por medio de los resultados del cambio de uso del suelo entre el 2002 y 2008 no tuvo en cuenta la tasa de reforestación que se ha registrado en el páramo, es por esto por lo que los sistemas forestales y las áreas para la conservación son los usos de suelo que presentaron una mayor cobertura en la imagen simulada que en la imagen procesada de la zona de estudio.

Tabla 8: Cambios de uso de suelo predicción uso de suelo 2014

	Área (Ha)		Diferencia (Ha)	Área %		Diferencia%
	Predicción 2014	Procesada 2014	Δ	Predicción 2014	Procesada 2014	Δ%
Cuerpos de agua	9,14	9,63	0,99	0,48	0,54	0,06
Actividades agropecuarias	1065,23	943,12	-122,11	59,20	52,42	-6,79
Sistemas forestales	416,98	506,79	89,81	23,17	28,17	4,99
Áreas para la conservación	308,46	339,78	31,32	17,14	18,88	1,74

Fuente: Autor

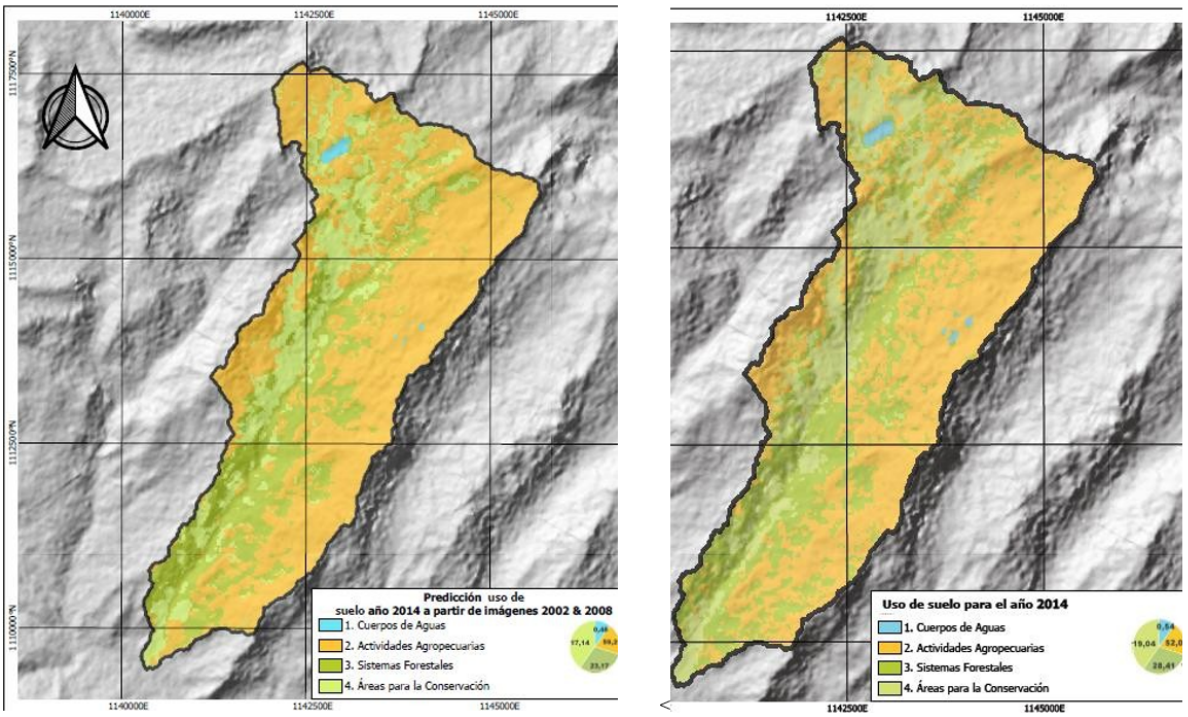

Fuente: Autores

Figura 14: Uso de suelo 2014 procesada (Derecha) y Simulación para el año 2014 a partir de imágenes 2002-2008 (Izquierda)

El índice de exactitud y el índice Kappa entre estas dos imágenes fue del 73.5% y 0.624 indicando un valor de concordancia bueno, lo cual significa que el comportamiento calculado y procesado del uso de suelo dentro de la cuenca presenta semejanza por esta razón los modelos de predicción de otros periodos presentaran resultados con una certeza aceptable.

Predicción uso de suelo 2020 a partir de imágenes 2008-2014 y 2014-2017

Como se observa en la Figura 15, debido al incremento de las áreas protegidas aledañas a la laguna de Siscunsí durante el periodo 2014- 2017, en la simulación los cuerpos de agua presentaron una reducción de su cobertura. En cuanto al modelo realizado con los periodos 2008-2014 se identifica una pequeña similitud en la zona centro y sur, debido a que los sistemas forestales y las áreas protegidas

presentan crecimiento de sus áreas. Los porcentajes de cambios ilustrados en la Tabla 9 permiten observar que las diferencias de las coberturas totales entre estos dos modelos no son mayores a 3.2%.

Además, al validar estas dos predicciones realizadas para el año 2020 se obtuvo un porcentaje de exactitud de 75.9% y un índice Kappa del 0.612 reflejando una correlación apropiada entre los datos. Estos valores ratifican que las simulaciones realizadas para los años posteriores aplicando el modelo de esta investigación generaran resultados confiables respecto al uso de suelo en la cuenca.

Tabla 9: Predicción 2020 a partir de (2008-2014), (2014-2017)

	Área (Ha)		Diferencia (Ha)	Área %		Diferencia %
	(2008-2014) 2020	(2014-2017) 2020	Δ	Predicción 2020	Predicción 2020	Δ%
Cuerpos de agua	10,17	9,23	5,94	0,57	0,24	0,33
Actividades agropecuarias	1079,8	1032,02	-47,78	60,65	57,97	-2,68
Sistemas forestales	358,76	355,53	-3,23	20,15	19,97	-0,18
Áreas para la conservación	331,59	388,55	56,96	18,63	21,82	3,20

Fuente: Autor

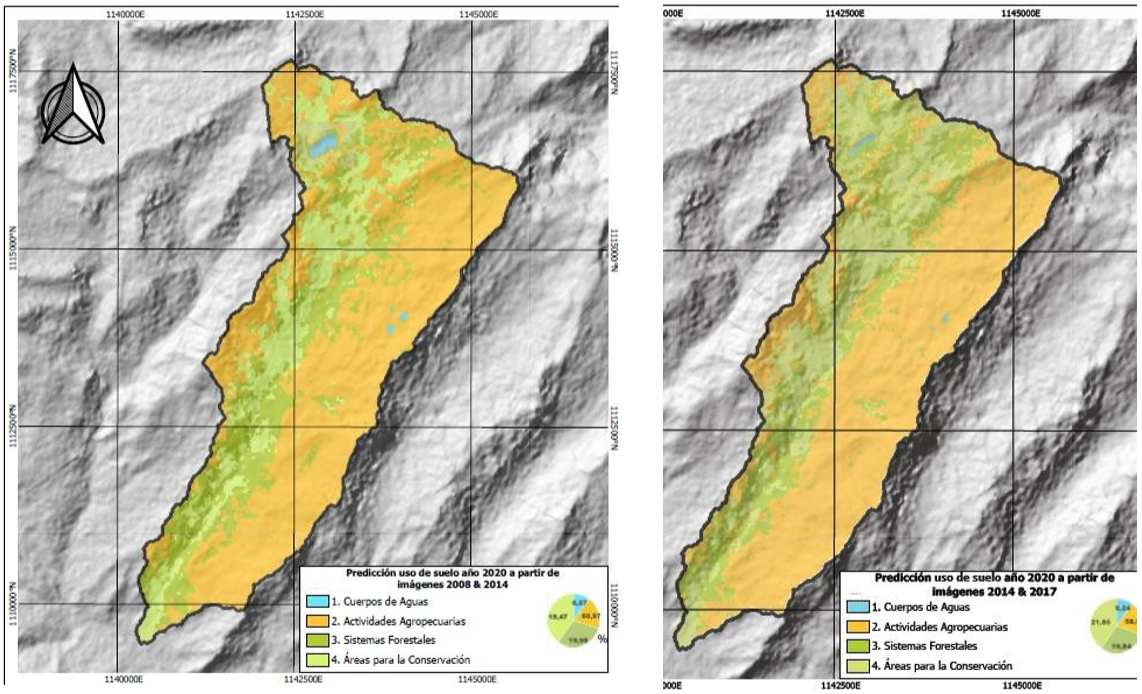

Fuente: Autores

Figura 15: Predicción 2020 a partir de 2008-2014(Izquierda), 2014- 2017 (Derecha)

Predicción uso de suelo 2026 y 2027 a partir de imágenes 2002-2014 y 1989-2008

Los modelos de predicción del uso del suelo para los años 2026 y 2027 difieren significativamente en algunas categorías debido a los distintos periodos empleados para la predicción de estos dos años. Como se observa en la Figura 26, las áreas de conservación en el año 2026 presentaron una mayor área

(484,11 ha) en relación con el año 2027 (382,88 ha) debido a que durante los años 2002 y 2014 (Años empleados para la predicción del modelo del 2026) se presentó una mayor expansión en este tipo de suelo dentro de la cuenca que entre los años 1989 y 2008 (Años empleados para la predicción del modelo del 2027). Por otra parte, los sistemas forestales mostraron una tendencia contraria al registrarse una mayor cobertura en el año 2027 (536,03 ha) en comparación con el año 2026 (426,52). En cuanto a los cuerpos de agua y las actividades agropecuarias las diferencias de coberturas de estos usos de suelo dentro de la cuenca en los dos años simulados tan solo difirieron en 0,63 ha y 8,91 ha respectivamente como se observa en la Tabla 10.

Tabla 10: Predicción 2026 a partir de (2002-2014), predicción 2027 a partir (1989-2008)

	Área (Ha)		Diferencia (Ha)	Área %		Diferencia %
	(2002-2014) 2026	(1989-2008) 2027	Δ	Predicción 2026	Predicción 2027	Δ%
Cuerpos de agua	9,91	9,54	0,63	0,50	0,53	0,04
Actividades agropecuarias	879,77	870,86	-8,91	48,89	48,40	-0,50
Sistemas forestales	426,52	536,03	109,51	23,70	29,79	6,09
Áreas para la conservación	484,11	382,88	-101,23	26,91	21,28	-5,63

Fuente: Autores

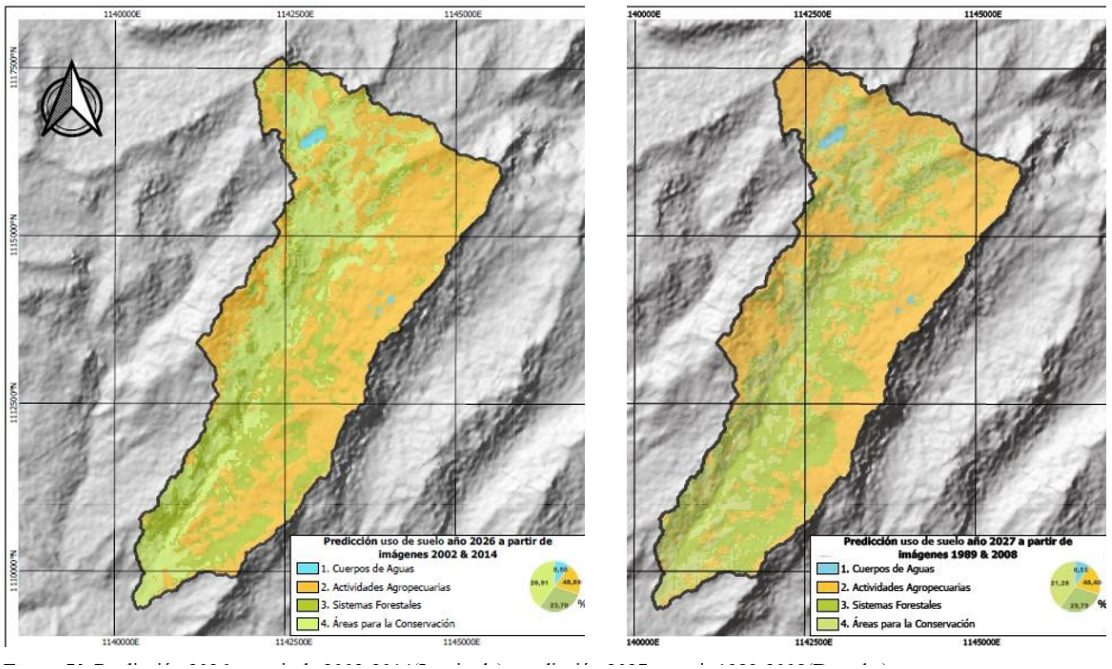

Fuente: Autores

Figura 16: Predicción 2026 a partir de 2002-2014 (Izquierda), predicción 2027 a partir 1989-2008 (Derecha)

Para la verificación , correlación y validación de estos modelos procesados se obtuvo un índice Kappa de 0.46 que representa una concordancia moderada en su desarrollo y una exactitud de 62.8 % de validación lo que indica que existe similitud en los mapas obtenidos, esto quiere decir, que si el proceso natural se mantiene se tendrán sistemas forestales y áreas de conservación como lo muestra cada mapa

de predicción para los años (2026-2027). Asimismo, los índices obtenidos de los modelos 2014 y 2020 arrojaron una concordancia buena, lo cual se debe a que la validación de estos datos se realizó con la imagen satelital del año 2002, lo que genera que el modelo de predicción del año 2026 se asemeje a la realidad.

3.2 Oferta hídrica de la cuenca empleando la precipitación efectiva

De acuerdo con el procesamiento de los datos en el software QGIS, en la Figura 17 se observan los mapas del número de curva obtenidos durante el periodo de estudio (1989-2017) y las predicciones (2020,2026 y 2027).

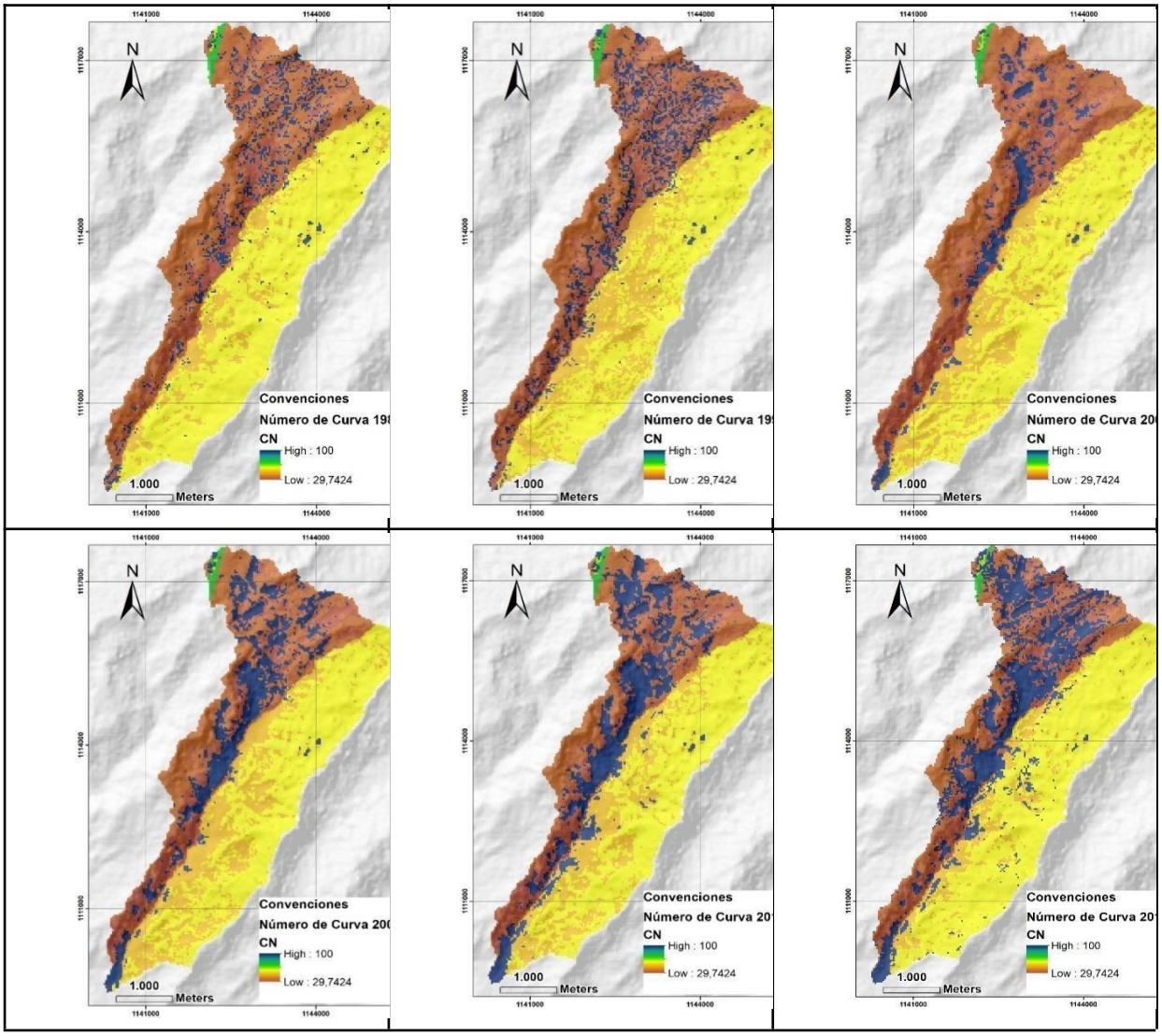

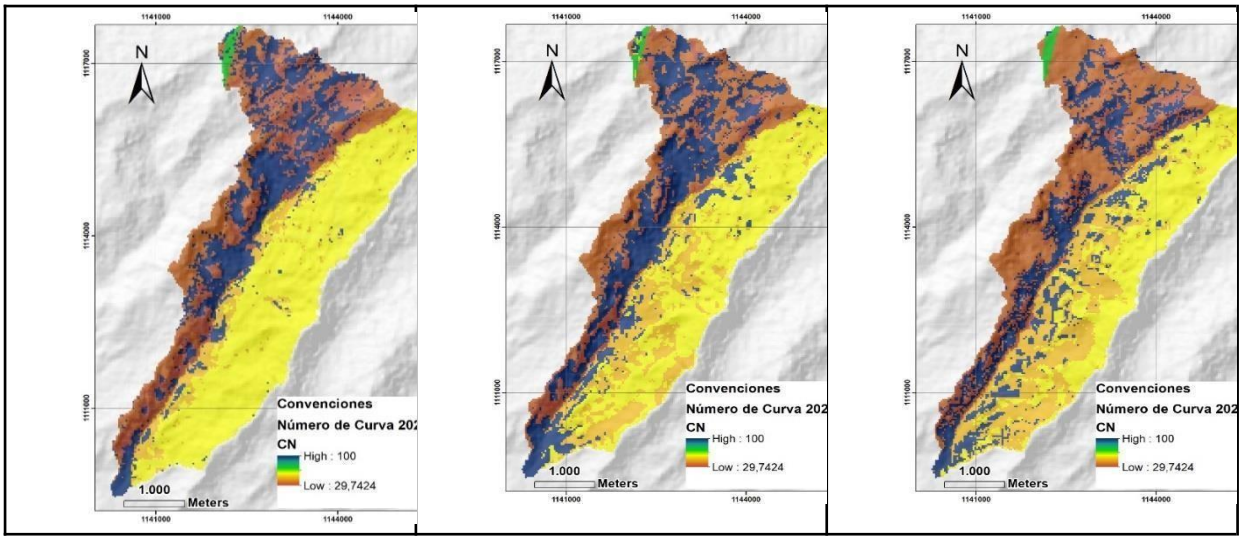

Fuente: Autores.

Figura 17: Raster de Número de curva para cada año

Por medio de los rásteres presentados anteriormente, se obtuvieron los resultados de diferencia potencial máxima (S) para la microcuenca Las Cañas, los cuales se ilustran en la Figura 18.

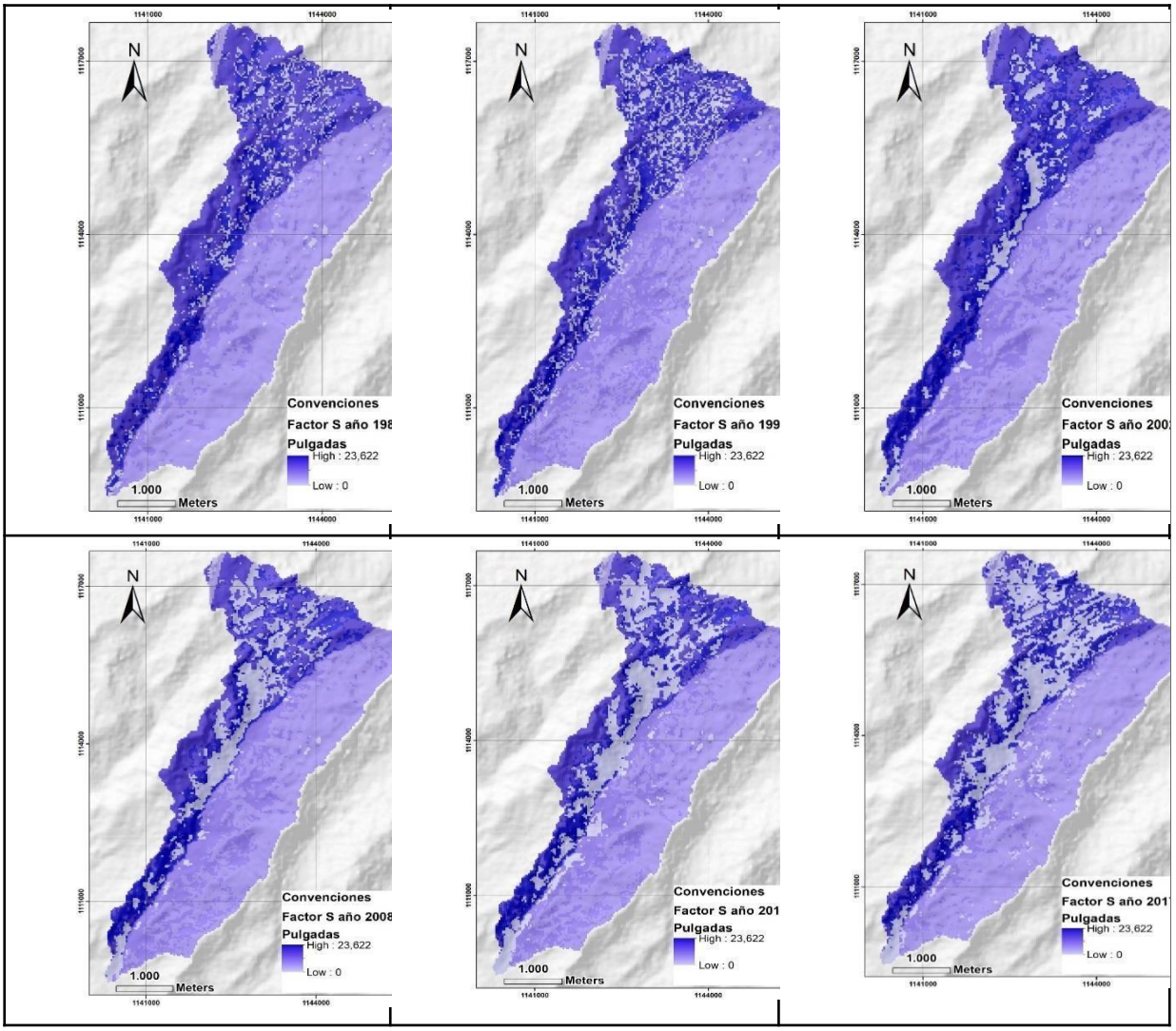

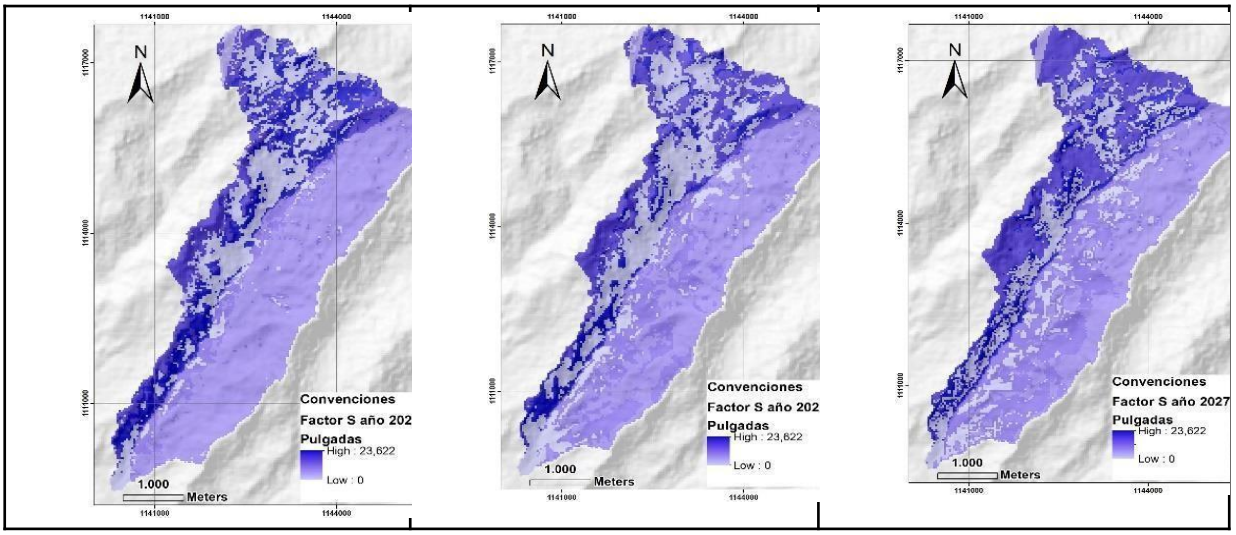

Fuente: Autores

Figura 18: Factor S calculado para cada año

Considerando la metodología empleada para calcular la precipitación efectiva en la zona de estudio durante el periodo analizado, se emplearon los valores interpolados de la precipitación media mensual de las distintas estaciones climáticas mencionadas en la Tabla 5. En la Figura 19 se observan los mapas de la precipitación media mensual para los años de estudio.

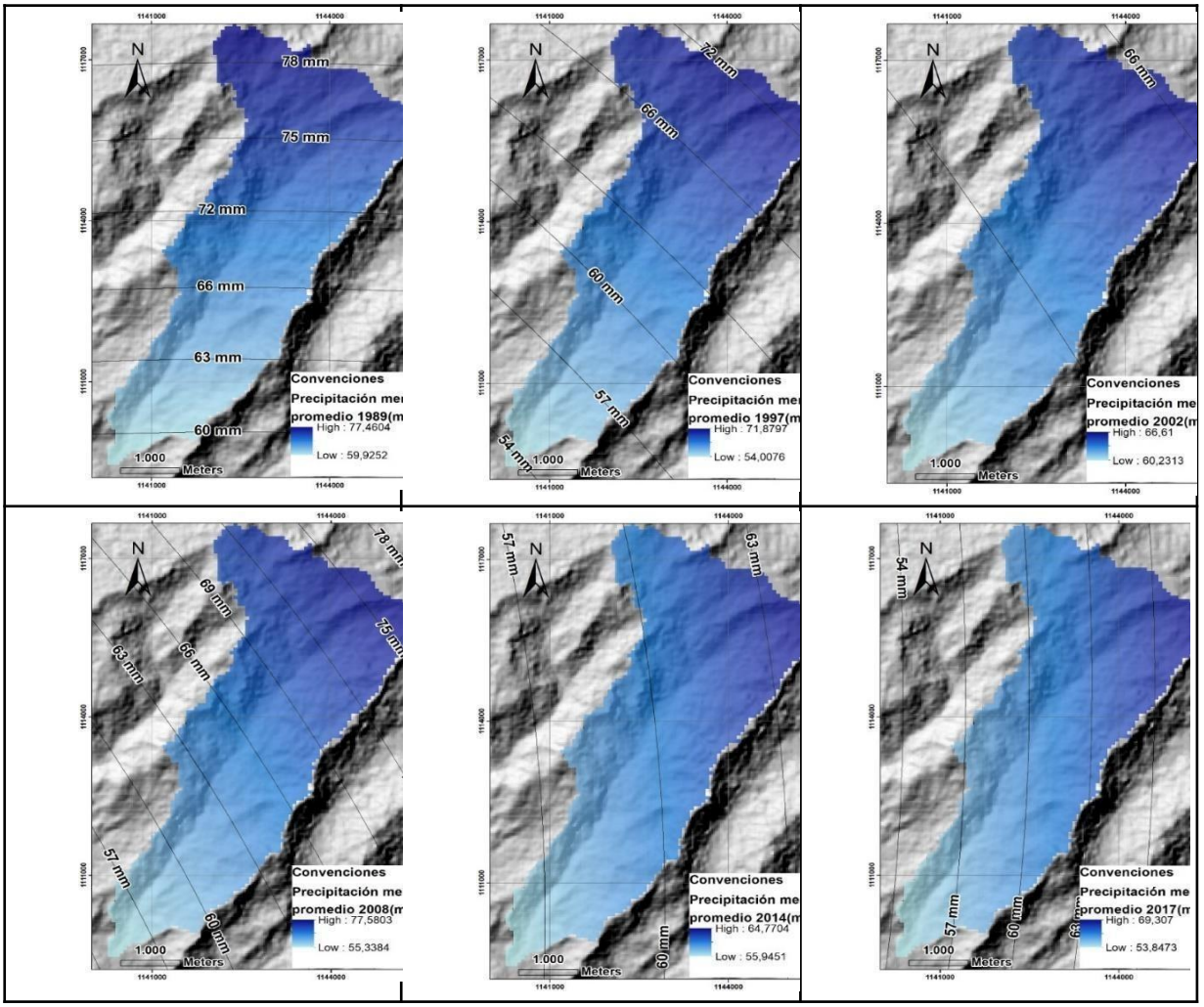

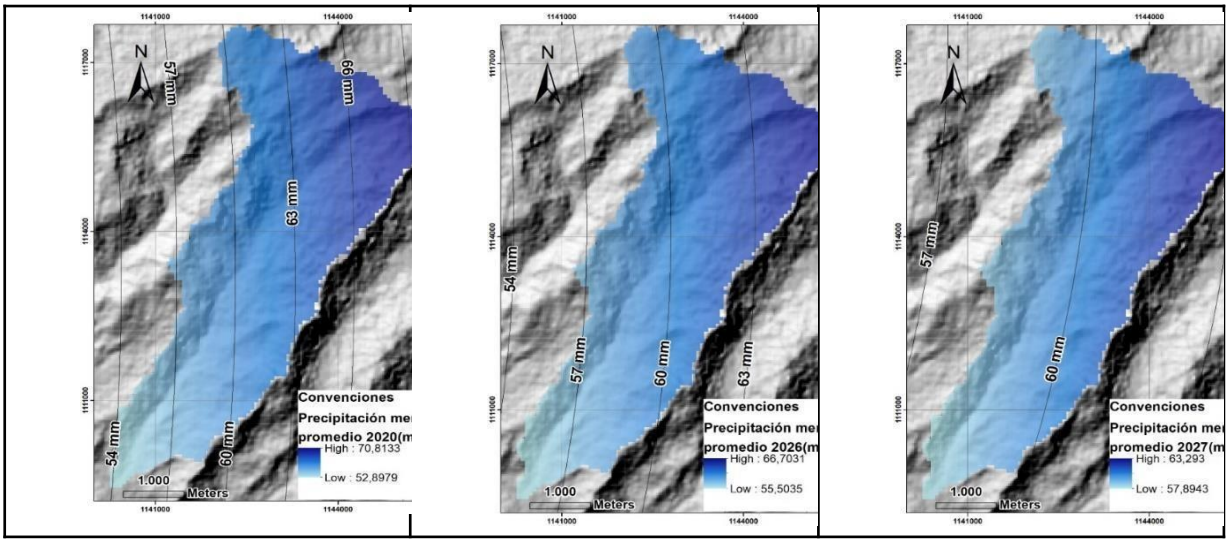

Fuente: Autores.

Figura 19: Precipitación media mensual para cada año

A partir del procesamiento de estas variables, en la Figura 20 se ilustran los mapas de precipitación efectiva promedio para cada año estudiado.

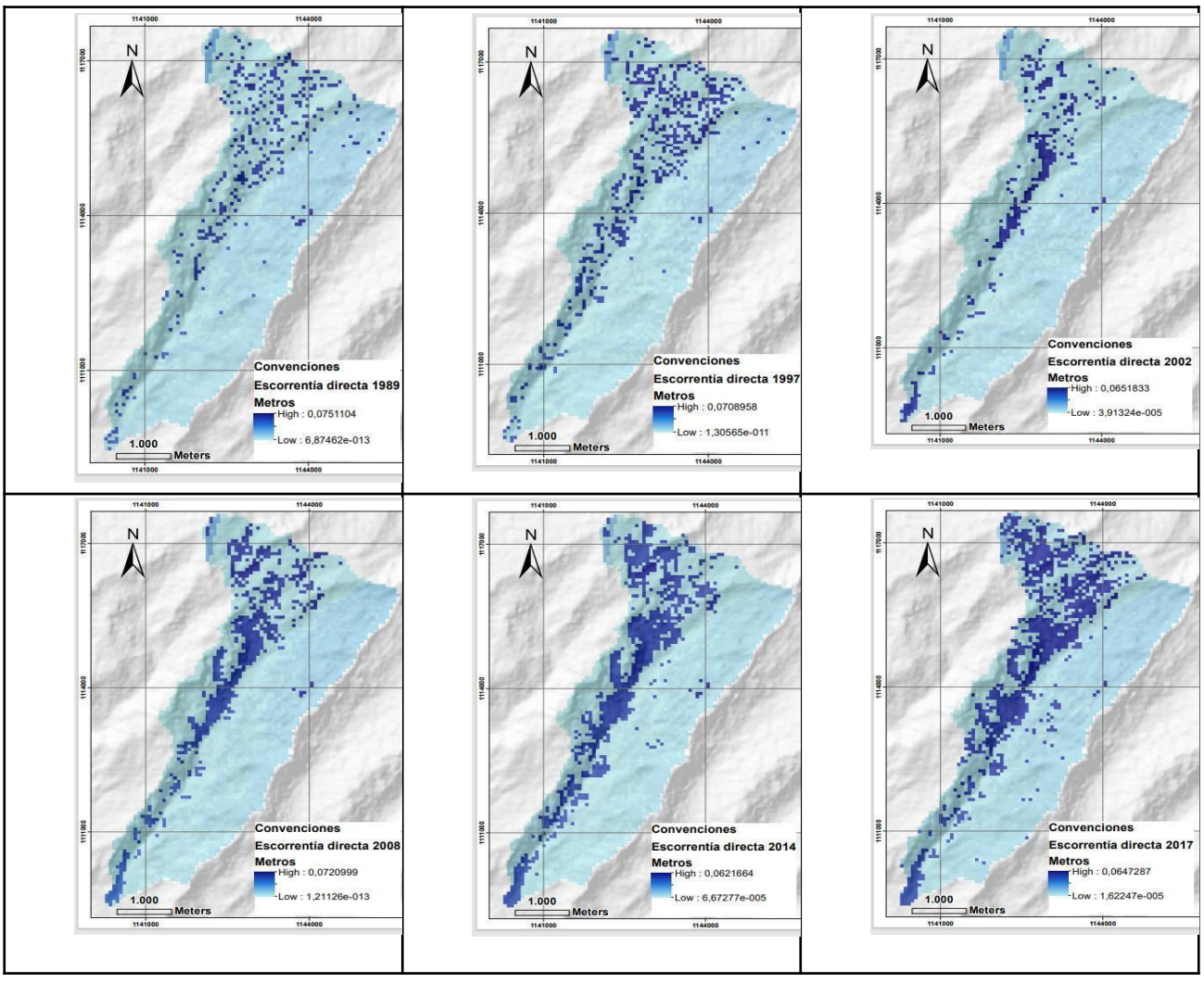

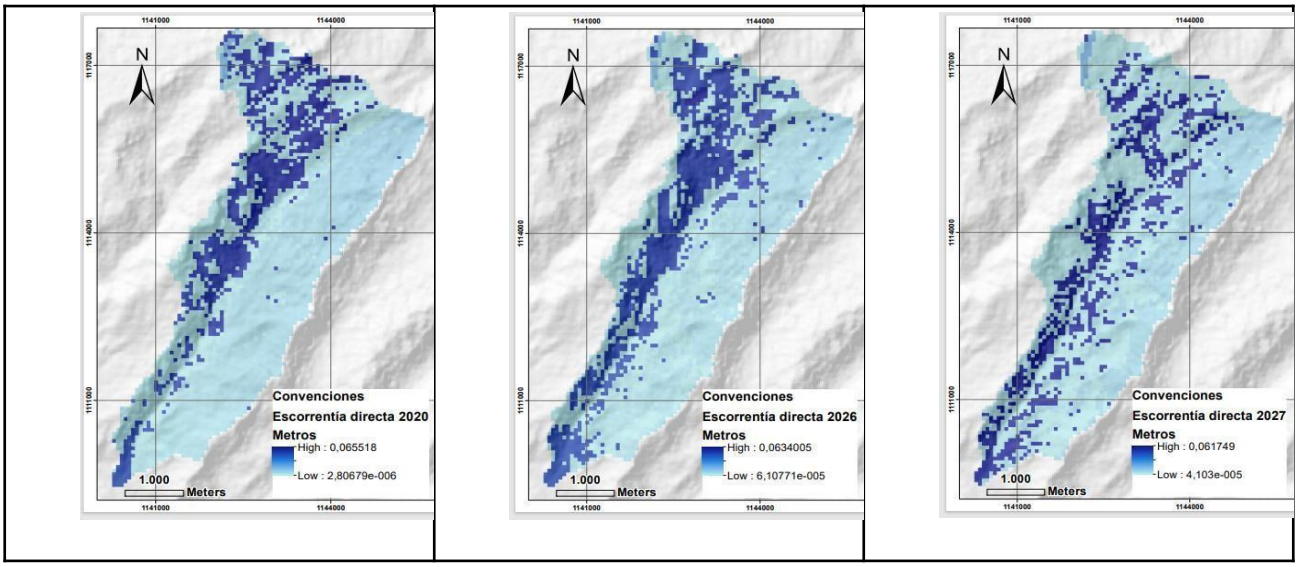

Fuente: Autores.

Figura 20: Precipitación efectiva media mensual para cada año

Teniendo en cuenta los valores promedio de cada una de las imágenes ráster de la precipitación efectiva determinados para el periodo analizado, en la Tabla 11 se presenta el volumen de la microcuenca Las Cañas.

Tabla 11: Volumen de agua calculado a partir de los valores promedio de la Precipitación Efectiva

Año	1989	1997	2002	2008	2014	2017	2020	2026	2027
Precipitación efectiva (mm)	8,01	8,56	6,30	11,19	12,01	13,99	13,80	16,00	12,59
Volumen estimado (m3)	14406,9	15403,3	11336,6	20130,1	21613,9	25171,5	24824,5	28792,6	22649,7

Fuente: Autores

La oferta hídrica de la microcuenca se calculó por medio de la conversión de los milímetros de escorrentía superficial a las unidades correspondientes de caudal, esto se obtuvo empleando el área total (1799 ha) y los valores máximos de precipitación efectiva para los distintos años estudiados, los resultados se ilustran en la Tabla 12. Mediante el programa Hidroesta2 se estimaron los valores de caudal; al mismo tiempo, por medio del software QGIS se determinó el tipo de uso de suelo, que, junto con los valores de área y precipitaciones de la microcuenca, se estimó el volumen de agua de esta.

Tabla 12: Caudal promedio calculado a partir de Escorrentía Superficial

Año	1989	1997	2002	2008	2014	2017	2020	2026	2027
Q(m^3/s)	0,521	0,486	0,451	0,500	0,430	0,444	0,451	0,437	0,423

Fuente: Autores

3.3 Oferta hídrica de la cuenca de estudio empleando el método racional

En la Tabla 13 y Figura 21 se presentan los resultados de intensidad, duración y frecuencia de la estación Puente Las Cañas durante los 4 periodos de retorno (5, 10,20 y 50 años), aplicando los modelos de Dick Peschke y Frederich Bell. Cabe la pena resaltar que estos cálculos también se realizaron para la estación Toquilla, sin embargo, solo se presentan los resultados de Puente Las Cañas por ser la que mejor representa las condiciones de la cuenca.

Tabla 13: Valores de intensidad, duración y frecuenta para la estación Puente Las Cañas empleando los modelos de Dick Peschke y Frederich Bell

	Modelo de Dick Peschke					Modelo de Frederich Bell			
Duración D (minutos)	T = 5 años	T= 10 años	T= 20 años	T=50 Años	Duración D (minutos)	T = 5 años	T=10 años	T=20 años	T= 50 años
	Intensidad (mm)					Intensidad (mm)			
10	493,62	603,23	737,18	960,95	10	195,94	225,7	259,98	313,41
20	293,51	358,68	438,33	571,38	20	133,51	153,78	177,14	213,54
30	216,54	264,63	323,39	421,56	30	106,67	122,87	141,53	170,62
40	174,52	213,27	260,63	339,75	40	90,97	104,78	120,7	145,5
50	147,63	180,41	220,47	287,39	50	80,4	92,61	106,67	128,6
60	128,76	157,35	192,29	250,66	60	72,68	83,72	96,43	116,25
70	114,7	140,17	171,3	223,29	70	66,74	76,87	88,55	106,74
80	103,77	126,81	154,97	202,01	80	61,98	71,39	82,24	99,14
90	95	116,09	141,87	184,93	90	58,07	66,89	77,05	92,88
100	87,78	107,27	131,09	170,88	100	54,78	63,1	72,68	87,62
110	81,72	99,87	122,05	159,09	110	51,97	59,86	68,95	83,12
120	76,56	93,56	114,34	149,04	120	49,52	57,04	65,71	79,21

Fuente: Autores

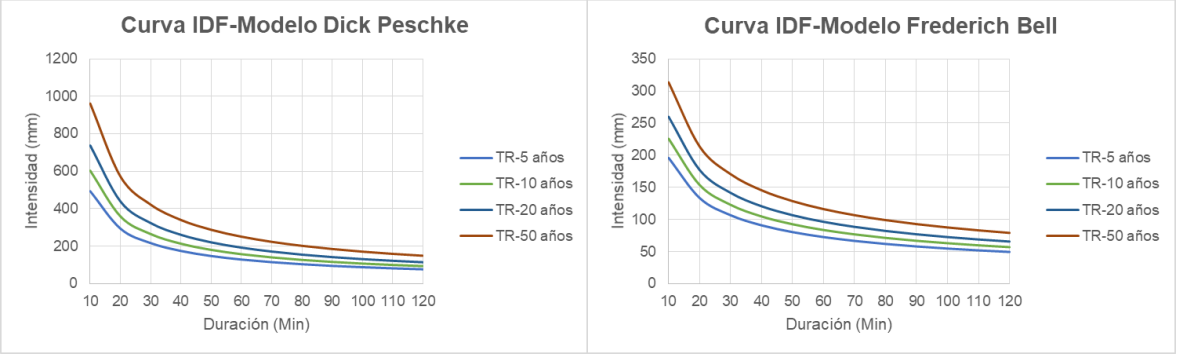

Fuente: Autores

Figura 21: Curvas IDF aplicando los modelos Dick Peschke y Frederich Bell

Con el fin de determinar los valores de intensidad durante el tiempo de concentración de la cuenca (67,2 minutos), se realizó una interpolación para cada uno de los periodos de retorno empleando los 2 modelos descritos anteriormente. Los resultados se registran en la Tabla 14.

Tabla 14: Intensidad D empleando los 2 modelos para cada periodo de retorno considerando el Tc

Intensidad (D) en mm/h				
Método	Tr (5 años)	Tr (10 años)	Tr (20 años)	Tr (50 años)
Frederich Bell	68.4	78.7	90.8	109.4
Dick Peschke	118.63	144.9	177.2	230.9

Fuente: Autores

En la Tabla 15 se presentan los resultados de la intensidad I calculada por medio de los valores de intensidad D.

Tabla 15: Intensidad I empleando los 2 modelos para cada periodo de retorno.

Intensidad (I) en mm/h				
Método	Tr (5 años)	Tr (10 años)	Tr (20 años)	Tr (50 años)
Frederich Bell	43.3	44.9	46.3	48.4
Dick Peschke	30.3	30.1	29.8	29.5

Fuente: Autores

Por medio de los valores de Intensidad I y el coeficiente de escorrentía determinado para la zona de estudio (0.39), se calculó la oferta hídrica de la cuenca teniendo en cuenta los 2 modelos empleados. En la Tabla 16 se registran los resultados obtenidos.

Tabla 16: Caudales calculados a partir del método racional

Método	Caudal (Q) m^3/s			
	Tr (5 años)	Tr (10 años)	Tr (20 años)	Tr (50 años)
Frederich Bell	0.235	0.243	0.251	0.262
Dick Peschke	0.164	0.163	0.161	0.160

Fuente: Autores

3.4 Comparación de la oferta hídrica empleando la precipitación efectiva y el método racional para el año 2027

Por medio de la Tabla 12 se puede evidenciar que teniendo en cuenta los cambios de uso del suelo y el cálculo de la precipitación efectiva, los caudales obtenidos para los años estudiados no presentan una tendencia uniforme debido a que se registran periodos en los cuales estos valores aumentan mientras que en otros la oferta hídrica de la cuenca disminuye.

Por otro lado, los caudales obtenidos por medio del método racional muestran que los resultados obtenidos aplicando el modelo de Frederich Bell aumentan a medida del transcurso de los periodos de retorno analizados, mientras que los valores obtenidos por medio del modelo de Dick Peschke descienden a medida del tiempo (Tabla 16).

En cuanto a la comparación de la oferta hídrica para el año 2027, en la Tabla 17 se presentan los resultados obtenidos tanto en la simulación teniendo en cuenta la precipitación efectiva de la microcuenca y los caudales calculados a partir del método racional en el tiempo de retorno de 10 años. Es necesario subrayar que la relación de caudal para el periodo de retorno de 10 años, que para el estudio es el año 2027, con el caudal obtenido por la simulación es de 1:2 por medio del modelo de Frederich Bell y aproximadamente de 1:2.5 empleando el método de Dick Peschke.

Tabla 17: Oferta hídrica para el año 2027 empleando el método racional y la precipitación efectiva

Método	Caudal (m^3/s)
Método Racional- Modelo Frederich Bell	0.243
Método Racional- Modelo Dick Peschke	0.163
Precipitación Efectiva	0.423

Fuente: Autores.

Para finalizar, teniendo los valores registrados en la Tabla 12, los cuales representan los caudales calculados por medio de la precipitación efectiva, presentan un promedio de 0.46 m^3/s. No obstante, el promedio de los caudales teniendo en cuenta los datos obtenidos con el método racional empleando el modelo Frederich Bell y Dick Peschke son de 0.247m^3/s y de 0.162m^3/s respectivamente.

IV. CONCLUSIONES

El incremento de áreas en las coberturas vegetales se ha dado significativamente en la microcuenca según los modelos analizados esto en áreas nativas y especies endémicas como lo son los frailejones (*Espeletia grandiflora*) representando un valor positivo agregado a la investigación y a la zona de estudio donde se puede reconocer el esfuerzo por la protección de estos parques naturales.

A partir del análisis multitemporal realizado por medio de software SIG, se logran identificar las transformaciones del uso del suelo durante un periodo de tiempo determinado, además de proveer información actualizada de las zonas en riesgo o con cierto grado de vulnerabilidad, lo cual permite contar con insumos útiles para la toma de decisiones por parte de las autoridades competentes.

La variación de los usos de suelos entre los años de 1989 y 2017 indican que los cuerpos de agua han disminuido en un 30% de su área, así como las actividades agropecuarias que se han visto reducidas en un 11% del total del área de estudio. Los sistemas forestales han aumentado en un 33%, mientras que las áreas para la conservación incrementaron en un 30%, esto gracias a la reforestación y a la población cercana al páramo.

Para estimar la oferta hídrica sobre la cobertura y uso de suelo a través del tiempo, se llevó a cabo un análisis multitemporal de estos usos, donde se registran las ganancias y pérdidas de cada uno. El número de curva se evaluó por medio de los caudales máximos empleando los registros históricos de la estación pluviométrica Toquilla y la estación Puente Las Cañas, con un análisis de frecuencia realizado por medio de diferentes distribuciones de probabilidad. La prueba de Kolmogórov-Smirnov reportó que en la estación Puente Las Cañas, la distribución más apropiada fue log-Gumbel (0.1195), mientras que para la estación Toquilla, la distribución normal fue la mejor puesto que presentó un ajuste con un valor de 0.0871.

Los resultados de la oferta hídrica empleando la precipitación efectiva y el método racional evidencian que con el método de la SCS el promedio de los valores de caudal fue mayor (0.46 m^3/s) en comparación con los resultados obtenidos a partir del método racional empleando los modelos de Frederich Bell y Dick Peschke donde se presentaron valores de caudal de 0.247m^3/s y de 0.162m^3/s respectivamente. Además, teniendo en cuenta el caudal simulado para un periodo de retorno de 10 años (2027) se identificó que la relación de la oferta hídrica por el método de escorrentía superficial con el método de Frederich Bell es de 1:2 mientras que con el método de Dick Peschke es de 1:2.5.

REFERENCIAS

1. Avellaneda Córdova , A. D. (2020). Análisis comparativo de los métodos Racional modificado Témez, Hidrogramas unitarios SCS, Clark y Snyder en la obtención de caudales máximos para las subcuencas Cañad y Alto Chancay Lambayeq Perú. Universidad Nacional Pedro Ruiz Gallo, 1-97.
2. Calvache, M. (2010). Física de suelos y su relación con los problemas ambientales. XII Congreso Ecuatoriano de la Ciencia del Suelo.
3. Castro López, J. (2011). El sistema de información geográfica aplicado a la investigación urbana en México: balance y formación técnica. Universidad Autónoma Metropolitana Unidad Azcapotzalco, México.
4. Civco, D. L. (1989). Topographic normalization of Landsat Thematic Mapper digital imagery. Photogrammetric Engineering & Remote Sensing, 55(9), 1303–1309.
5. Cuervo Barahona, E., Cely Reyes, G., & Moreno Pérez, D. (2016). Determinación de las fracciones de carbono orgánico en el suelo del páramo la Cortadera, Boyacá. Ingenio Magno, 7, 139-149.

6. Deshmukh, D. S., Chaube, U. C., Ekube Hailu, A., Aberra Gudeta, D., & Tegene Kassa. (2013). Estimation and comparision of curve numbers based on dynamic land use land cover change, observed rainfall-runoff data and land slope. Journal of Hydrology, 492, 89-101.
7. Díaz Carvajal , Á. (2017). Determinación del número de curva en la subcuenca de Betancí (Córdoba, Colombia) mediante teledetección y SIG. Ingeniería y Desarrollo(35), 452-470.
8. García Portilla, J. (2003). Análisis del potencial de emisión de dióxido de carbono del Páramo de Chingaza y lineamientos para su conservación en el contexto del mecanismo de desarrollo limpio. Bogotá, D.C: Universidad Javeriana.
9. Lao Ramos, B. (2018). La teledetección y los Sistemas de Información Geográfica para el manejo de las tierras. Revista Ciencias Técnicas Agropecuarias(27), 54-65.
10. Law, K. H., & Nichol, J. (2004). Topographic correction for differential illumination effects on IKONOS satellite imagery. Int. Arch. Photogramm. Remote Sens. Spat. Inform. Sci, 35, 641-646.
11. Lemus, M., & Navarro, V. G. (2003). Manual para el desarrollo de obras de conservación de suelo. San Fernando (Chile): Corporación Forestal Nacional.
12. Menéndez, M., & Núñez, V. (2009). El uso de los sensores remotos en los Recursos Naturales Primera parte: La fotografía aérea y la fotointerpretación Argentina. 3, 1-14.
13. Morad, M. (2001). Sistemas de Información Geográfica y modelizaciones hidrológicas. Una aproximación a las ventajas y dificultades de su aplicación. Boletín de la Asociación de Geógrafos Españoles, 31, 23-46.
14. Paredes Pinto, R. E. (2015). Generación de intensidades de precipitación máxima en estaciones sin información pluviográfica (cuenca del río Illpa- Puno). Puno-Perú: Universidad Nacional del Altiplano.
15. Rivera Ospina, D. (2013). Portafolio Nacional de Restauración de Páramos y Humedales de alta Montaña. Instituto de Investigación de Recursos Biológicos Alexander von Humboldt.
16. Rodríguez, A., Gaspari, F., Sinisterra, G., Delgado, M., & Besteiro, S. (2012). Evaluación del efecto de la restauración agro-hidrológica mediante la aplicación del modelo hidrológico GeoQ. Revista Investigaciones Agropecuarias, 38-39.
17. Romano Castillo, E. A. (2007). Algoritmo computacional para describir la dinámica del ciclo hidrológico superficial en una cuenca a partir de cartas temáticas topográficas, edafológicas, uso de suelo y vegetación. Foro-Red-Mat: Revista electrónica de contenido matemático(21).
18. Rubiano Galvis, S. (2015). Protección de páramos y derechos campesinos. Aportes jurídicos y de política Subdirección de Servicios Científicos y Proyectos Especiales . Bogotá, D.C: Instituto de Investigación de Recursos Biológicos Alexander von Humboldt.
19. Sánchez Palomino. (2015). Modelación precipitación escorrentía en cuencas urbanas-caso de estudio: Distrito de Carmen Alto. Universidad Nacional de San Cristóbal de Huamanga.
20. Sánchez Pérez, D. F. (2018). Propuesta de criterios de gestión territorial con base en el turismo de paisaje y senderismo como estrategia de desarrollo económico alternativo en el Páramo de Siscunsi en Sogamoso Boyacá. Universidad de Bogotá Jorge Tadeo Lozano.
21. Sedano Cruz, R. K. (2013). Gestión integrada del riesgo de inundaciones en Colombia. Universitat Politècnica de València(37), 75-77.
22. Ven Te, C. (1984). Handbook of Applied Hydrology. McGraw Hill Book Company.
23. Villalobos Chacón , A. (2019). Análisis del potencial de escurrimiento en la microcuenca del río Tiribí entre el 2005 al 2029 para la conservación de los servicios ecosistémicos de regulación hídrica. Heredia: Universidad Nacional de Costa Rica.

Results on Complex Valued Complete Fuzzy Metric Spaces

Praveen Kumar Sharma & Shivram Sharma

ABSTRACT

This work demonstrates certain standard fixed point theorems on complex-valued fuzzy metric spaces. We show certain fixed point findings in the situation of complex-valued fuzzy metric spaces, inspired by Singh et al. [25].

To begin, we extend some well-known existing conclusions from metric spaces to complex-valued fuzzy metric spaces and then prove them in the complex-valued complete fuzzy metric space context. We provide an example that supports our main result and supports our hypotheses.

Keywords: common fixed point; metric spaces; complex-valued fuzzy metric spaces (CVFMS).

Classification: DDC Code: 515.42 LCC Code: QA312

Language: English

Great Britain Journals Press

LJP Copyright ID: 925614
Print ISSN: 2631-8490
Online ISSN: 2631-8504

London Journal of Research in Science: Natural and Formal

Volume 23 | Issue 2 | Compilation 1.0

Results on Complex Valued Complete Fuzzy Metric Spaces

Praveen Kumar Sharma[α] & Shivram Sharma[σ]

ABSTRACT

This work demonstrates certain standard fixed point theorems on complex-valued fuzzy metric spaces. We show certain fixed point findings in the situation of complex-valued fuzzy metric spaces, inspired by Singh et al. [25].

To begin, we extend some well-known existing conclusions from metric spaces to complex-valued fuzzy metric spaces and then prove them in the complex-valued complete fuzzy metric space context. We provide an example that supports our main result and supports our hypotheses.

Keywords: common fixed point; metric spaces; complex-valued fuzzy metric spaces (CVFMS).

Author α: Department of Mathematics, SVIS, Shri Vaishnav Vidyapeeth Vishwavidyalaya, Indore-453111 (M.P.), India.
σ: Department of Mathematics, Govt. P.G. College, Guna-473001 (M.P.), India.

I. INTRODUCTION

In 1965, Zadeh [3] coined the term "fuzzy set." Following that, a slew of authors worked on fuzzy sets, expanding the fuzzy set theory and its applications [4-6]. The idea of fuzzy metric spaces was given by Kramosil and Michalik [7]. After then, George and Veeramani [9] updated this idea. Grabiec [8] investigated fuzzy metric space fixed-point theory. The idea of complex-valued metric spaces was introduced by Azam et al. [21].

Verma et al. [23] recently established 'Max' functions and the partial order relation'for complex numbers, and used properties (E-A) and CLRg to prove fixed point theorems in complex valued metric space. Singh et al. [25] were the first to present the concept of complex-valued fuzzy metric spaces and to create the complex-valued fuzzy version of some metric space results.

The goal of this study is to expand well-known metric-space results to complex-valued fuzzy metric spaces and then prove them in complex-valued complete fuzzy metric spaces.

II. PRELIMINARIES

Def.2.1.[21]. Let $\mathbb{C}$ be the set of complex numbers and $\eta_1, \eta_2 \in \mathbb{C}$, where $\eta = \mu + i\nu$. Then a partial order relation '$\lesssim$' on $\mathbb{C}$ is defined as follows:

$\eta_1 \lesssim \eta_2 \Leftrightarrow Re(\eta_1) \leq Re(\eta_2)$ and $Im(\eta_1) \leq Im(\eta_2)$

Hence $\eta_1 \lesssim \eta_2$ if one of the following satisfies;

London Journal of Research in Science: Natural and Formal

(PO1) $Re(\eta_1) = Re(\eta_2)$ and $Im(\eta_1) = Im(\eta_2)$

(PO2) $Re(\eta_1) < Re(\eta_2)$ and $Im(\eta_1) = Im(\eta_2)$

(PO3) $Re(\eta_1) = Re(\eta_2)$ and $Im(\eta_1) < Im(\eta_2)$

(PO4) $Re(\eta_1) < Re(\eta_2)$ and $Im(\eta_1) < Im(\eta_2)$

In particular, $\eta_1 \lesssim \eta_2$ if $\eta_1 \neq \eta_2$ and one of (PO2), (PO3), and (PO4) is satisfied, and we write $\eta_1 \prec \eta_2$ if only (PO4) is satisfied.

It can be noted that;

$0 \lesssim \eta_1 \lesssim \eta_2 \Rightarrow |\eta_1| < |\eta_2|,\ \eta_1 \lesssim \eta_2, \eta_2 \prec \eta_3 \Rightarrow \eta_1 \prec \eta_3.$

Def.2.2.[21]. Complex-Valued Metric Space (CVMS)

Let X be a non-empty set. Assume that the mappings $d: X \times X \to \mathbb{C}$ satisfies:

(CV1) $0 \lesssim d(a, b),$ for all $a, b \in X$ and $d(a, b) = 0$ iff $a = b$;

(CV2) $d(a, b) = d(b, a),$ for all $a, b \in X$;

(CV3) $d(a, c) \lesssim d(a, b) + d(b, c),$ for all $a, b, c \in X$

Then d is called a complex-valued metric on X, and (X, d) is called a CVMS.

Def.2.3.[23]. The 'max' function with partial order relation '$\lesssim$' is defined as

(1) $max\{\eta_1, \eta_2\} = \eta_2 \Leftrightarrow \eta_1 \lesssim \eta_2$
(2) $\eta_1 \lesssim max\{\eta_2, \eta_3\} \Rightarrow \eta_1 \lesssim \eta_2$ or $\eta_1 \lesssim \eta_3$

And the 'min' functions can be defined as

(1) $min\{\eta_1, \eta_2\} = \eta_1 \Leftrightarrow \eta_1 \lesssim \eta_2$
(2) $min\{\eta_1, \eta_2\} \lesssim \eta_3 \Rightarrow \eta_1 \lesssim \eta_3$ or $\eta_2 \lesssim \eta_3$.

Following Zadeh's [3] contribution to fuzzy set theory, a number of scholars [4-6] contributed to the field's basics and core theories.

Buckley [10] was the first to present the concept of fuzzy complex numbers. Other authors were inspired by Buckley's work and continued their research on fuzzy complex numbers. Ramot et al. [1] expanded fuzzy sets to complex fuzzy sets in this chain.

Singh et al. [25], inspired by Ramot et al. [1,] constructed complex-valued fuzzy metric spaces using continuous t - norms, defined a Hausdorff topology on complex - valued fuzzy metric space, and gave the concept of Cauchy sequences in CVFMS.

We establish certain fixed-point conclusions in the situation of complex -valued fuzzy metric spaces, inspired by Singh et al. [25]. We begin by extending several well-known metric-space results to complex-valued fuzzy metric spaces, and then we prove those results in the setting of CVFMS.

Def.2.4.[1]. The complex fuzzy set S is given by $S = \{(x, \mu_s(x))/x \in U\}$.

Where U is a universe of discourse, $\mu_s(x)$ is a membership function and defined as $\mu_s(x) = r_s(x).e^{iw_s(x)}$, $(i = \sqrt{-1})$ where $r_s(x)$ and $w_s(x)$ both real-valued, with $r_s(x) \in [0,1]$.

Def.2.5. [25]. Complex Valued Continuous t-norm

A binary operation $*$: $r_s e^{i\theta} \times r_s e^{i\theta} \to r_s e^{i\theta}$, wherein $r_s \in [0,1]$ and a fix $\theta \in [0, \frac{\pi}{2}]$, is called complex valued continuous t-norm if it satisfies the following conditions:

(1) $*$ is associative and commutative,
(2) $*$ is continuous,
(3) $a * e^{i\theta} = a, \forall a \in r_s e^{i\theta}$, where $r_s \in [0,1]$,
(4) $a * b \lesssim c * d$ whenever $a \lesssim c$ and $b \lesssim d$, for all $a, b, c, d \in r_s e^{i\theta}$, where $r_s \in [0,1]$.

Ex.2.5. [25]. The following binary operations defined in (i), (ii) and (iii) are complex valued continuous t-norm

(i) $a * b = min(a, b)$.
(ii) $a * b = max(a + b - e^{i\theta}, 0)$, for a fix $\theta \in [0, \frac{\pi}{2}]$.
(iii) $a * b = \begin{cases} \min\{a,b\}, if\ \max\{a,b\} = e^{i\theta}; \\ 0, otherwise, \end{cases}$ for a fix $\theta \in [0, \frac{\pi}{2}]$.

Def.2.6. [25]. Complex Valued Fuzzy Metric Spaces (CVFMS)

The triplet $(X, M, *)$ is said to be CVFMS if a complex valued fuzzy set M : $X \times X \times (0, \infty) \to r_s e^{i\theta}$ (where $X \neq \emptyset$, $*$ is a complex valued continuous t-norm) fulfil the following criteria:

(CF1) $M(a, b, t) > 0$,

(CF2) $M(a, b, t) = e^{i\theta}$ for all $t > 0 \Leftrightarrow a = b$,

(CF3) $M(a, b, t) = M(b, a, t)$,

(CF4) $M(a, b, t) * M(b, c, s) \gtrsim M(a, c, t + s)$,

(CF5) $M(a, b, .) : (0, \infty) \to r_s e^{i\theta}$ is continuous,

for all $a, b, c \in X, s, t > 0, r_s \in [0,1]$ and $\theta \in [0, \frac{\pi}{2}]$.

Note- Wherever appropriate to our study, we refer to [25] and the references mentioned in [25] for further basic definitions, examples, and fundamental features of CVMS.

Singh et al. [25] demonstrated the following lemmas in CVFMS before establishing the result on complex-valued fuzzy metric space, i.e. Theorem 2.7.

Lemma 2.7 [25]. Let $(X, M,*)$ be a CVFMS such that $\lim_{t\to\infty} M(a, b, t) = e^{i\theta}$, for all $a, b \in X$, if $M(a, b, \mathcal{K}t) \gtrsim M(a, b, t)$, for all $a, b \in X, 0 < \mathcal{K} < 1, t \in (0, \infty)$ then $a = b$.

Lemma 2.8 [25]. Let $\{b_n\}$ be a sequence in a CVFMS $(X, M,*)$ with $\lim_{t\to\infty} M(a, b, t) = e^{i\theta}$, for all $a, b \in X$. If there exists a number $\mathcal{K}$ which lies on $(0, 1)$such that

$M(b_{n+1}, b_{n+2}, \mathcal{K}t) \gtrsim M(b_n, b_{n+1}, t), \forall t > 0, n = 0, 1, 2, \ldots$ Then $\{b_n\}$ is a Cauchy sequence in X.

The following theorem was established by Singh et al. [25], which is the resetting of the Banach contraction principle in CVFMS.

Theorem 2.7 [25]. Let $(X, M,*)$ be a CVFMS such that $\lim_{t\to\infty} M(a, b, t) = e^{i\theta}, \forall a, b \in X$, and $t > 0$. Let $T: X \to X$ be a mapping that satisfies $M(Ta, Tb, \mathcal{K}t) \gtrsim M(a, b, t)$, $\forall \mathcal{K} \in (0, 1)$. Then T has a fixed point that is unique.

III. MAIN RESULTS

Fisher [24] established the following theorem in complete metric space for three mappings.

Theorem A [24]. Let S and T be continuous mappings of a complete metric space (X, d) into themselves. Then S and T have a common fixed point in X iff a continuous mapping A of X into S(X) ∩T(X) exists, which commutes with S and T and satisfies;

$d(Ax, Ay) \leq \alpha\, d(Sx, Ty)$ for all $x, y \in X$ and $0 < \alpha < 1$. Indeed S, T and A have a unique common fixed point.

We can now extend the preceding theorem/result to complex-valued complete fuzzy metric space as follows:

Theorem -3.1. Let $(X, M,*)$ be a complex-valued complete fuzzy metric space (CVCFMS). S and T are continuous mappings from X to X. If A is a continuous mapping from X to $S(X) \cap T(X)$, it commutes with S and T, and if detailed maps satisfy the following contractive condition.

$M(Ax, Ay, kt) \gtrsim Min\{M(Ty, Ay, t), M(Sx, Ax, t), M(Sx, Ty, t)\}$ for all $x, y \in X, t \in (0, \infty)$ and $0 < k < 1$

... (3.11)

London Journal of Research in Science: Natural and Formal

Additionally, $\lim_{t\to\infty} M(x,y,t) = e^{i\theta}$, for all $x, y \in X$ and $\theta \in [0, \frac{\pi}{2}]$
... (3.12)

Then S, T, and A have a unique common fixed point.

Proof: Ax_n is a Cauchy sequence?

Since A is a continuous mapping from X to $S(X) \cap T(X)$ so for $x_1 \in X$, there exists any $x_0 \in X$ such that $Ax_0 = Sx_1$ and $Ax_0 = Tx_1$

On keep repeating this process for different x_1 and x_0, we get a sequence $\{x_n\}$ such that

$Ax_n = Sx_{n+1}$ and $Ax_n = Tx_{n+1}$

Or $Ax_{2n} = Sx_{2n+1}$ and $Ax_{2n} = Tx_{2n+1}$, $n = 1,2,3, \ldots$

On setting $x = x_{2r}$ and $y = x_{2r+1}$ in (3.11), we get for $r = 1,2,3, \ldots$

$$M(Ax_{2r}, Ax_{2r+1}, kt) \gtrsim Min\{M(Tx_{2r+1}, Ax_{2r+1}, t), M(Sx_{2r}, Ax_{2r}, t), M(Sx_{2r}, Tx_{2r+1}, t)\}$$

$$M(Ax_{2r}, Ax_{2r+1}, kt) \gtrsim Min\{M(Ax_{2r}, Ax_{2r+1}, t), M(Ax_{2r-1}, Ax_{2r}, t), M(Ax_{2r-1}, Ax_{2r}, t)\}$$

$$M(Ax_{2r}, Ax_{2r+1}, kt) \gtrsim Min\{M(Ax_{2r}, Ax_{2r+1}, t), M(Ax_{2r-1}, Ax_{2r}, t)\} \ldots (I)$$

Now suppose $Min\{M(Ax_{2r}, Ax_{2r+1}, t), M(Ax_{2r-1}, Ax_{2r}, t)\} = M(Ax_{2r}, Ax_{2r+1}, t)$

Then by (I), we have $M(Ax_{2r}, Ax_{2r+1}, kt) \gtrsim M(Ax_{2r}, Ax_{2r+1}, t)$

By lemma (4.1) or (5.1), we have $Ax_{2r} = Ax_{2r+1}$

Which is not possible

Hence by (I), we must have $M(Ax_{2r}, Ax_{2r+1}, kt) \gtrsim M(Ax_{2r-1}, Ax_{2r}, t), \forall\, t > 0 \ldots (II)$

In general, we get $M(Ax_{r+1}, Ax_{r+2}, kt) \gtrsim M(Ax_r, Ax_{r+1}, t), \forall\, t > 0 \ldots (III)$

Hence by lemma (4.2), $\{Ax_n\}$ is a Cauchy sequence in X.

Since the space X is complete, so there exists some $p \in X$ such that $\lim_{n\to\infty} Ax_n = p$

and $p = \lim_{n\to\infty} Sx_{n+1} = \lim_{n\to\infty} Tx_{n+1}$

It follows that $Ap = Sp = Tp$, and

$$M(Ap, A^2p, kt) \gtrsim Min\{M(TAp, AAp, t), M(Sp, Ap, t), M(Sp, TAp, t)\}$$

$$M(Ap, A^2p, kt) \gtrsim M(Sp, ATp, t)$$

$$M(Ap, A^2p, kt) \gtrsim M(Ap, A^2p, t)$$

$$\vdots$$

$$M(Ap, A^2p, kt) \gtrsim M\left(Ap, A^2p, \frac{t}{k^n}\right) \ldots (IV)$$

On taking $n \to \infty$, then by lemma (4.1), we have; $Ap = A^2p$

London Journal of Research in Science: Natural and Formal

This implies that $Ap = p$

Thus p is a common fixed point of A, S, and T.

Uniqueness: - let $q(\neq p)$ be another fixed point of A, S, and T. Then, by (3.11), we have

$$M(Ap, Aq, kt) \gtrsim Min\{M(Tq, Aq, t), M(Sp, Ap, t), M(Sp, Tq, t)\}$$

Which implies that

$$M(p, q, kt) \gtrsim Min\{e^{i\theta}, e^{i\theta}, M(p, q, t)\}$$

As $M(p, q, t) \in r_s e^{i\theta}$, $r_s \in [0, 1]$ and $\theta \in [0, \frac{\pi}{2}]$, also $M(p, q, t) \lesssim e^{i\theta}$

Then certainly we get, $Min\{e^{i\theta}, e^{i\theta}, M(p, q, t)\} = M(p, q, t)$

$$M(p, q, kt) \gtrsim M(p, q, t)$$

Which implies that $p = q$.

As a result, p is unique.

Ex. 3.1. Let $X = [3,21]$ with the metric d defined by $d(x, y) = |x - y|, \forall x, y \in X$.

For all $x, y \in X$ and $t \in (0, \infty)$, we define $M(x, y, t) = e^{i\theta}[\frac{t}{t + d(x,y)}]$ or $M(x, y, t) = e^{i\theta}\left[\frac{t}{kt + d(x,y)}\right]$, $k = \frac{1}{2}$, and t -norm $' * '$ is defined as $a * b = min\{a, b\}$ where $a, b \in r_s e^{i\theta}$, for $r_s \in [0, 1]$ and $\theta \in [0, \frac{\pi}{2}]$. Here, $\lim_{t\to\infty} M(x, y, t) = e^{i\theta}$, for all $x, y \in X$.

$(X, M, *)$ is a CVCFMS with a given t-norm $*$.

$S, T : X \to X$ are defined as:

$$S(X) = \begin{cases} 3; at\ \ x = 3 \\ \frac{x}{3} + 2;\ \ 3 < x \leq 21 \end{cases}, \text{and } T(X) = \begin{cases} 3; at\ \ x = 3 \\ \frac{2x}{3} + 1;\ \ 3 < x \leq 21 \end{cases}$$

And $A: X \to S(X) \cap T(X)$ as:

$$A(X) = \begin{cases} 3; at\ \ x = 3 \\ \frac{3x + 21}{10};\ \ 3 < x \leq 21 \end{cases}$$

The mappings S and T are continuous. A is continuous from X to $S(X) \cap T(X)$.

Clearly, $A(X) \subseteq S(X)$ and $A(X) \subseteq T(X)$

This implies that $A(X) \subseteq S(X) \cap T(X)$.

IV. CONCLUSION

Existing results from complete metric space have been extended to complex-valued complete fuzzy metric spaces in this study. We tested the extended version of the result using a new form of weaker contractive condition. We've offered an example that backup our major finding and proves our hypotheses. In this line, various complete metric space results can be extended and demonstrated in the context of complex-valued complete fuzzy metric spaces.

REFERENCES

1. D. Ramot, R. Milo, M. Friedman, and A. Kandel, IEEE Transactions of Fuzzy Systems 10(2) (2002), 171–186.
2. G. Jungck, Commuting maps and fixed points, Amer Math Monthly 83 (1976), 261– 263.
3. L.A. Zadeh, Fuzzy sets, Inform Control 8 (1965), 338–353.
4. A. Kandel, Fuzzy Mathematical Techniques and Applications. Reading, MA: Addison- Wesley, 1986.
5. G.J. Klir and B. Yuan, Fuzzy Sets and Fuzzy Logic: Theory and Applications, NJ: Prentice-Hall, 1995. [6] J.M. Mendel, Fuzzy logic systems for engineering: A tutorial, Proc IEEE 83 (1995), 345–377.
6. I. Kramosil and J. Michalek, Fuzzy metric and statistical metric spaces, Kybernetica 11 (1975), 336–344.
7. M. Grabiec, Fixed points in fuzzy metric spaces, Fuzzy Sets and System 27 (1988), 385–399.
8. A. George and P. Veeramani, On some results in fuzzy metric spaces, Fuzzy Sets System 64 (1994), 395–399.
9. J.J. Buckley, Fuzzy complex numbers, in Proc ISFK, Guangzhou, China, 1987, 597aˆASˇ ¸700
10. J.J. Buckley, Fuzzy complex numbers, Fuzzy Sets System 33 (1989), 333aˆASˇ ¸345.
11. J.J. Buckley, Fuzzy complex analysis I: Differentiation, Fuzzy Sets System 41 (1991), 269aˆASˇ ¸284. [13]
12. J.J. Buckley, Fuzzy complex analysis II: Integration, Fuzzy Sets System 49 (1992), 171aˆASˇ ¸179.
13. M. Ousmane and C. Wu, Semi-continuity of complex fuzzy function, Tsinghua Science and Technology 8 (2003), 65–70.
14. N. Sethi, S.K. Das and D.C. Panda, Probabilistic interpretation of complex fuzzy set, IJCSEIT 2(2) (2012), 31–44.
15. D. Qiu and L. Shu, Notes on aˆAIJon the restudy of fuzzy ˇ complex analysis: Part I and part IIaˆAˇ ˙I, Fuzzy Sets System 159 (2008), 2185–2189.
16. D. Qiu, L. Shu and Z. Wen Mo, Notes on fuzzy complex analysis, Fuzzy Sets System 160 (2009), 1578–1589.
17. J. Qiu, C. Wu and F. Li, On the restudy of fuzzy complex analysis: Part I. The sequence and series of fuzzy complex numbers and their convergences, Fuzzy Sets System 115 (2000), 445–450.
18. J. Qiu, C. Wu and F. Li, On the restudy of fuzzy complex analysis: Part II. The continuity and differentiation of fuzzy complex functions, Fuzzy Sets System 120 (2001), 517–521.
19. C. Wu and J. Qiu, Some remarks on fuzzy complex analysis, Fuzzy Sets System 106 (1999),231-238
20. A. Azam, B. Fisher, and M. Khan, Common fixed point theorems in complex valued metric spaces, Numerical Functional Analysis and Optimization 32(3) (2011), 243–253.

21. F. Rouz ar an M. Im a , Some common ixe point t eorems on comp ex-va ue metric spaces, Computer and Mathematics with Applications 64 (1012), 1866–1874.
22. R.K. Verma and H.K. Pathak, Common fixed point theorems using property (E.A) in complex-valued metric spaces, Thai Journal of Mathematics 11(2) (2013), 347–355.
23. B. Fisher; Mapping with a common fixed point, Math. Sem. Notes Kobe Univ., Vol.7,81-84 (1979).
24. D. Singh, V. Joshi, M. Imdad, and P. Kumam; A novel framework of complex-valued fuzzy metric spaces and fixed-point theorems, Journal of Intelligent and fuzzy system, Vol.30, 3227-3238,2016.

An Energy Level with Principal Quantum Number *n*=0 Exists in a Hydrogen Atom

Dr. Koshun Suto

ABSTRACT

The classical quantum theory of Bohr does not take the theory of relativity into account. The energy levels of a hydrogen atom, derived by Bohr, are known to be approximations. In this paper, the kinetic energy and momentum of an electron in a hydrogen atom are treated relativistically. This paper predicts the existence of an n=0 energy level present in a hydrogen atom. However, the state where n=0 is not an energy level of the electron comprising the hydrogen atom. It is thought that an electron in the n=0 state forms a pair with a positron, and constitutes the vacuum inside the hydrogen atom.

Keywords: hydrogen atom, energy levels, classical quantum theory, einstein's energy-momentum relationship, relativistic kinetic energy, *n*=0 energy level.

Classification: DDC Code: 333.794 LCC Code: TP359.H8

Language: English

Great Britain Journals Press

LJP Copyright ID: 925614
Print ISSN: 2631-8490
Online ISSN: 2631-8504

London Journal of Research in Science: Natural and Formal

Volume 23 | Issue 2 | Compilation 1.0

An Energy Level with Principal Quantum Number n=0 Exists in a Hydrogen Atom

Dr. Koshun Suto

ABSTRACT

The classical quantum theory of Bohr does not take the theory of relativity into account. The energy levels of a hydrogen atom, derived by Bohr, are known to be approximations. In this paper, the kinetic energy and momentum of an electron in a hydrogen atom are treated relativistically. This paper predicts the existence of an n=0 energy level present in a hydrogen atom. However, the state where n=0 is not an energy level of the electron comprising the hydrogen atom. It is thought that an electron in the n=0 state forms a pair with a positron, and constitutes the vacuum inside the hydrogen atom.

Keywords: hydrogen atom, energy levels, classical quantum theory, einstein's energy-momentum relationship, relativistic kinetic energy, n=0 energy level.

I. INTRODUCTION

In 1913, Bohr derived the following formulas for the energy levels of a hydrogen atom, and the orbital radius of the electron orbiting inside the hydrogen atom [1].

$$E_{\mathrm{BO},n} = -\frac{1}{2}\left(\frac{1}{4\pi\varepsilon_0}\right)^2 \frac{m_e e^4}{\hbar^2}\cdot\frac{1}{n^2} = -\frac{\alpha^2 m_e c^2}{2n^2}, \quad n = 1, 2, \cdots. \tag{1}$$

$$r_{\mathrm{BO},n} = 4\pi\varepsilon_0 \frac{\hbar^2}{m_e e^2}\cdot n^2, \quad n = 1, 2, \cdots. \tag{2}$$

Here, m_e is the rest mass of the electron, c is the speed of light, and n is the principal quantum number. Also, α is the following fine-structure constant.

$$\alpha = \frac{e^2}{4\pi\varepsilon_0\hbar c}. \tag{3}$$

The subscript "BO" signifies a physical quantity predicted by Bohr.

When deriving Eqs. (1) and (2), Bohr assumed the following quantum condition.

$$m_e v_n \cdot 2\pi r_{\mathrm{BO},n} = 2\pi n\hbar. \tag{4}$$

Using this assumption, Bohr explained why the energy levels in a hydrogen atom are discontinuous.

Subsequently, quantum mechanics developed further, and it became possible to explain more complicated energy levels. However, even in quantum mechanics with improved precision, the minimum value of the principal quantum number remains at 1.

The author has previously pointed out that an energy level with n=0 exists in a hydrogen atom [2]. However, that paper did not attract much notice. In that paper, the author assumed the following relationship.

$$\frac{v_n}{c} = \frac{\alpha}{n}. \tag{5}$$

Due to Eq. (5), it is possible to identify discontinuous states that are permissible in terms of quantum mechanics in the continuous motions of classical theory.

However, it later became clear that Eq. (5) can be derived logically [3]. Therefore, this paper rewrites the originally published paper [2] based on newly obtained results.

II. A NEW QUANTUM CONDITION TO REPLACE THE QUANTUM CONDITION OF BOHR

In Bohr's theory, the energy levels of the hydrogen atom is treated non-relativistically, and thus here the momentum of the electron is taken to be $m_e v$. Also, the Planck constant h can be written as follows [4].

$$\hbar = \frac{h}{2\pi} = \frac{m_e c \lambda_C}{2\pi}. \tag{6}$$

λ_C is the Compton wavelength of the electron.

When Eq. (6) is used, the fine-structure constant α can be expressed as follows.

$$\alpha = \frac{e^2}{4\pi\varepsilon_0 \hbar c} = \frac{e^2}{2\varepsilon_0 m_e c^2 \lambda_C}. \tag{7}$$

Also, the classical electron radius r_e is defined as follows.

$$r_e = \frac{e^2}{4\pi\varepsilon_0 m_e c^2}. \tag{8}$$

If r_e / α is calculated here,

$$\frac{r_e}{\alpha} = \frac{\lambda_C}{2\pi}. \tag{9}$$

If Eq. (2) is written using r_e and α, the result is as follows.

$$r_{BO,n} = \frac{e^2}{4\pi\varepsilon_0 m_e c^2}\left(\frac{4\pi\varepsilon_0 \hbar c}{e^2}\right)^2 n^2 = \frac{r_e}{\alpha^2} n^2. \tag{10}$$

Next, if $\hbar$ in Eq. (6) and $r_{BO,n}$ in Eq. (10) are substituted into Eq. (4),

$$m_e v_n \cdot 2\pi \frac{r_e}{\alpha^2} n^2 = 2\pi n \frac{m_e c \lambda_C}{2\pi}. \tag{11}$$

If Eq. (9) is also used, then Eq. (11) can be written as follows.

$$m_e v_n \cdot 2\pi \frac{r_e}{\alpha^2} n^2 = 2\pi n \frac{m_e c r_e}{\alpha}. \tag{12}$$

Next, if we multiply both sides of Eq. (12) by $\alpha / 2\pi n m_e r_e$ and simplify, the following relationship can be derived [5].

$$\frac{v_n}{c} = \frac{\alpha}{n}. \tag{13}$$

If Eq. (13) is taken as a departure point, the energy levels of the hydrogen atom derived by Bohr can be derived immediately.

According to the famous virial theorem, if K is taken to be the kinetic energy of the entire system, and V is taken to be the potential energy of the entire system, then the following relation holds between K and V:

$$\langle K \rangle = -\frac{1}{2}\langle V \rangle. \tag{14}$$

The time average of K is equal to $-1/2$ the time average of V. Also, the sum of the time average K of the kinetic energy of the entire system and the time average of the total mechanical energy E of the entire system becomes 0. That is,

$$\langle K \rangle + \langle E \rangle = 0. \tag{15}$$

Next, if Eqs. (14) and (15) are combined, the result is as follows:

$$\langle E \rangle = -\langle K \rangle = \frac{1}{2}\langle V \rangle. \tag{16}$$

When both sides of Eq. (13) are squared, and then multiplied by $m_e/2$,

$$\frac{1}{2}\frac{m_e v_n^2}{c^2} = \frac{1}{2}\frac{m_e \alpha^2}{n^2}. \tag{17}$$

Hence,

$$E_{\mathrm{BO},n} = -K_{\mathrm{cl},n} = -\frac{1}{2}m_e v_n^2 = -\frac{\alpha^2 m_e c^2}{2n^2}. \tag{18}$$

The "cl" in K_{cl} is an abbreviation for "classical". However, from a relativistic perspective, $(1/2)m_e v_n^2$ is an approximation of the relativistic kinetic energy of the electron.

III. TWO FORMULAS FOR RELATIVISTIC KINETIC ENERGY OF PARTICLES MOVING IN FREE SPACE

Einstein and Sommerfeld defined the relativistic kinetic energy K_{re} as follows [6].

$$K_{\mathrm{re}} = mc^2 - m_0 c^2. \tag{19}$$

Here, $m_0 c^2$ is the rest mass energy of the body. And mc^2 is the relativistic energy.

The "re" subscript of K_{re} stands for "relativistic."

According to the STR, the following relation holds between the energy and momentum of a body moving in free space [7].

$$\left(mc^2\right)^2 = \left(m_0 c^2\right)^2 + c^2 p^2. \tag{20}$$

Now, Eq. (20) is rewritten as follows.

$$\left(mc^2\right)^2 = m_0^2 c^4 + \left(m^2 c^4 - m_0^2 c^4\right) = \left(m_0 c^2\right)^2 + c^2 p^2. \tag{21}$$

Comparing Eqs. (20) and (21), the relativistic momentum p_{re} can be defined as follows.

$$p_{re}^2 = m^2c^2 - m_0^2c^2. \tag{22}$$

Hence,

$$p_{re}^2 = (m+m_0)(mc^2 - m_0c^2). \tag{23}$$

The following relation holds due to Eqs. (19) and (23).

$$K_{re} = \frac{p_{re}^2}{m+m_0}. \tag{24}$$

Based on the above discussion, it was found that the relativistic kinetic energy of particles moving in isolated systems in free space can be described with Eqs. (19) and (24).

IV. AN ENERGY-MOMENTUM RELATIONSHIP APPLICABLE TO THE ELECTRON IN A HYDROGEN ATOM

An energy-momentum relationship applicable to the electron in a hydrogen atom has already been derived in a previous paper [8]. That relationship is derived again by another method, including the significance of the review in Section 4.

Now, consider the case where an electron at rest in an isolated system in free space is attracted by the electrostatic attraction of the proton (hydrogen atom nucleus), and forms a hydrogen atom.

The electron at rest has a rest mass energy of $m_e c^2$. When this electron is taken into the region of the hydrogen atom, it acquires an amount of kinetic energy K_{re} equivalent to the emitted photon.

Both energy sources must satisfy the law of energy conservation. The energy source here has been thought to be potential energy.

However, the only energy an electron has when at rest is rest mass energy. There is no possible source for supplying the photon emitted by the electron, and the acquired kinetic energy, aside from the rest mass energy of the electron.

We take this decrease in energy to be $-\Delta m_e c^2$, the energy of the photon emitted by the electron to be $h\nu,$ and the kinetic energy gained by the electron to be K_{re} .

For the law of conservation of energy to hold, the following relation must hold between these energies.

$$-\Delta m_e c^2 + h\nu + K_{re} = 0. \tag{25}$$

London Journal of Research in Science: Natural and Formal

The author presented the following equation as an equation indicating the relationship between the rest mass energy and potential energy of the electron in a hydrogen atom [9, 10].

$$V(r) = -\Delta m_e c^2. \tag{26}$$

According to this equation, the potential energy of a bound electron in a hydrogen atom is equal to the reduction in rest mass energy of that electron.

There is a lower limit to potential energy, and the range which energy can assume is as follows.

$$-m_e c^2 \le V(r) < 0. \tag{27}$$

When describing the motion of a bound electron in a hydrogen atom, a term must be included in that equation for the potential energy. From this $E_{\mathrm{ab},n}$ can be defined as follows.

$$E_{\mathrm{ab},n} = m_n c^2 = m_e c^2 - h\nu = m_e c^2 + V(r_n) + K_{\mathrm{re},n}, \qquad n = 1, 2, \cdots. \tag{28}$$

Here, m_n is the relativistic mass of the electron. $E_{\mathrm{ab},n}$ gives the relativistic energy of the electron, but this is also the absolute energy of the electron. The “ab” subscript of $E_{\mathrm{ab},n}$ stands for “absolute.”

The relativistic energy of an electron in a hydrogen atom $m_n c^2$ becomes smaller than the rest mass energy $m_e c^2$. That is,

$$m_n c^2 < m_e c^2. \tag{29}$$

The behavior of an electron inside an atom, where there is potential energy, cannot be described with the relationship of Einstein (1). Caution is necessary because it is completely overlooked in Eq. (29).

Now, referring to Eq. (19), it is natural to define the relativistic kinetic energy of an electron in a hydrogen atom as follows [3]

$$K_{\mathrm{re},n} = -E_{\mathrm{re},n} = m_e c^2 - m_n c^2. \tag{30}$$

This paper defines $E_{\mathrm{re},n}$ as the relativistic energy levels of the hydrogen atom derived at the level of classical quantum theory. (The quantum number used here is just the principal quantum number. Therefore, $E_{\mathrm{re},n}$ is not a formula which predicts all the relativistic energy levels of the hydrogen atom.) However, the term "relativistic" used here does not mean based on the STR. It means that the expression takes into account the fact that the mass of the electron varies due to velocity. According to the STR, the electron's mass increases when its velocity increases. However, inside the hydrogen atom, the mass of the electron decreases when the velocity of the electron increases.

Next, the relativistic kinetic energy of an electron in a hydrogen atom is defined as follows by referring to Eq. (24).

$$K_{\mathrm{re},n} = \frac{p_{\mathrm{re},n}^2}{m_e + m_n}, \qquad p_{\mathrm{re},n} = m_n v_n. \tag{31}$$

Here, $p_{\mathrm{re},n}$ indicates the relativistic momentum of the electron.

In this way, two formulas have been obtained for the relativistic kinetic energy of the electron in a hydrogen atom (Eqs. (30), and (31)).

The following equation can be derived from Eqs. (30) and (31).

$$\frac{p_{\mathrm{re},n}^2}{m_{\mathrm{e}}+m_n}=m_{\mathrm{e}}c^2-m_nc^2. \tag{32}$$

Rearranging this, the following relationship can be derived.

$$\left(m_nc^2\right)^2+p_{\mathrm{re},n}^2c^2=\left(m_{\mathrm{e}}c^2\right)^2. \tag{33}$$

Equation (33) is the energy-momentum relationship applicable to the electron in a hydrogen atom.

V. ENERGY LEVELS OF A HYDROGEN ATOM IN LIGHT OF THE THEORY OF RELATIVITY

In the past, Dirac derived the following negative solution from Eq. (20).

$$E=\pm mc^2=\pm m_0c^2\left(1-\frac{v^2}{c^2}\right)^{-1/2}. \tag{34}$$

If the same logic is applied to Eq. (33), then the following formula can be derived.

$$E_{\mathrm{ab},n}^{\pm}=\pm m_{\mathrm{e}}c^2\left(1+\frac{v_n^2}{c^2}\right)^{-1/2}. \tag{35}$$

However, Eq. (35) does not incorporate the discontinuity peculiar to the micro world. Therefore, Eq. (35) must be rewritten into a relationship where energy is discontinuous.

Using the relation in Eq. (13), Eq. (35) can be written as follows [2].

$$E_{\mathrm{ab},n}^{\pm}=\pm m_nc^2=\pm m_{\mathrm{e}}c^2\left(1+\frac{\alpha^2}{n^2}\right)^{-1/2}. \tag{36a}$$

$$=\pm m_{\mathrm{e}}c^2\left(\frac{n^2}{n^2+\alpha^2}\right)^{1/2}. \tag{36b}$$

The following relation holds between $E_{\mathrm{re},n}$ and $E_{\mathrm{ab},n}$.

$$E_{\mathrm{ab},n}-E_{\mathrm{re},n}=m_nc^2+K_{\mathrm{re},n}=m_{\mathrm{e}}c^2. \tag{37}$$

Here, m_nc^2 is the residual part of the rest mass energy of the electron, and $E_{\mathrm{re},n}$ corresponds to the reduction in rest mass energy of the electron.

Also, the relationship of these energies can be illustrated as follows (see Fig.1) [11].

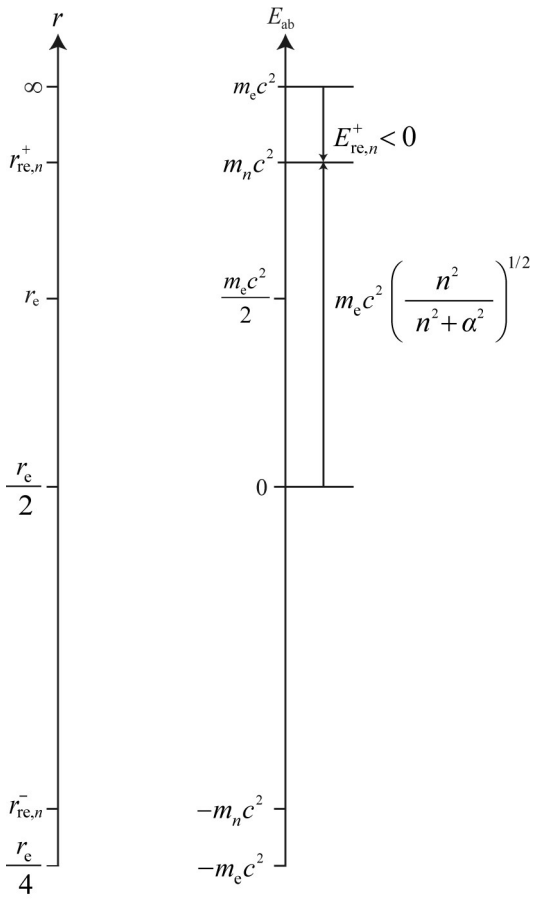

Figure 1: Relationship of $E_{re,n}$ and $E_{ab,n}$ $E_{re,n}$ corresponds to the decrease in rest mass energy of the electron, and $E_{ab,n}$ $(m_n c^2)$ corresponds to the remaining part.

The relativistic energy levels of an ordinary hydrogen atom, $E_{re,n}$ can be expressed as follows.

$$E_{re,n} = m_n c^2 - m_e c^2 = m_e c^2 \left[\left(1 + \frac{\alpha^2}{n^2} \right)^{-1/2} - 1 \right] \tag{38a}$$

$$= m_e c^2 \left[\left(\frac{n^2}{n^2 + \alpha^2} \right)^{1/2} - 1 \right], \quad n = 0, 1, 2, \cdots. \tag{38b}$$

Ordinarily, there is no problem in omitting the + of $E_{re,n}$ Note the difference between the relativistic energy levels of the hydrogen atom $E_{re,n}$ and the relativistic energy of the electron $E_{ab,n}$ [3].

To simplify the discussion in this paper, the only quantum number addressed is n In Eq. (38), the principal quantum number *n* starts from 0. Energy in the state where *n*=0 are as follows.

$$E_{re,0} = -m_e c^2. \tag{39}$$

Next, when the part of Eq. (38a) in parentheses is expressed as a Taylor expansion,

$$E_{\mathrm{re},n} \approx m_{\mathrm{e}}c^2\left[\left(1-\frac{\alpha^2}{2n^2}+\frac{3\alpha^4}{8n^4}-\frac{5\alpha^6}{16n^6}\right)-1\right] \tag{40a}$$

$$\approx -\frac{\alpha^2 m_{\mathrm{e}}c^2}{2n^2}. \tag{40b}$$

From this, it is evident that Eq. (1) derived by Bohr is an approximation of Eq. (38).

Incidentally, in Eq. (1) for the energy levels of the hydrogen atom derived by Bohr, the energy of an electron at rest infinitely far from the proton was regarded as zero (Figure 2) [12].

The rest mass energy of the electron is not taken into account in Bohr's theory. Thus, the author derived a Eq. (38) for the energy levels of the hydrogen atom, taking into account the rest mass energy of the electron (Figure 3) [12].

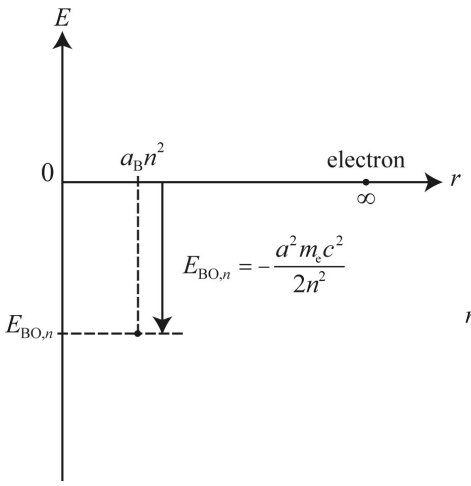

Figure 2

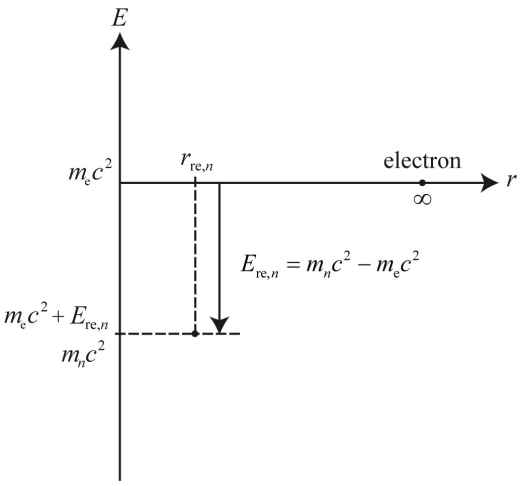

Figure 3

Figure 2: In Bohr's theory, the energy when the electron is at rest at a position infinitely distant from the atomic nucleus is defined to be zero.

Figure 3: According to the STR, the energy of an electron at rest at a position where $r=\infty$ is $m_{\mathrm{e}}c^2$. $E_{\mathrm{re},n}$ is given by the difference between $m_{\mathrm{e}}c^2$ and $m_n c^2$.

Now, the total mechanical energy of the hydrogen atom is given by the following formula.

$$E_{\mathrm{re},n} = K_{\mathrm{re},n} + V(r_n) = -K_{\mathrm{re},n}. \tag{41}$$

Also, if the formula for potential energy is used, then $E_{\mathrm{re},n}$ can be written as follows.

$$E_{\mathrm{re},n} = \frac{1}{2}V(r_n) = -\frac{1}{2}\frac{1}{4\pi\varepsilon_0}\frac{e^2}{r_n} = -\frac{1}{2}m_{\mathrm{e}}c^2\frac{r_{\mathrm{e}}}{r_n} = -m_{\mathrm{e}}c^2\left(\frac{r_{\mathrm{e}}/2}{r_n}\right). \tag{42}$$

From Eq. (42), $m_n c^2$ is:

$$m_n c^2 = m_e c^2 + E_{re,n} = m_e c^2 - m_e c^2 \left(\frac{r_e / 2}{r_n} \right) = m_e c^2 \left(\frac{r_n - r_e / 2}{r_n} \right). \tag{43}$$

Here, if $-m_e c^2$ is substituted for $E_{re,n}$ in Eq. (42), then the r where $E_{ab,0} = 0$ is:

$$r_0 = \frac{r_e}{2}. \tag{44}$$

The radius r where $E_{ab,0} = 0$ is $r_e / 2$ due to Eq. (43). Dirac predicted that the vacuum energy E satisfies the relation $E < -m_e c^2$, but actually $E_{ab,0} = 0$ is the energy of the virtual electron-positron pair which make up the vacuum (Figure 4)[13].

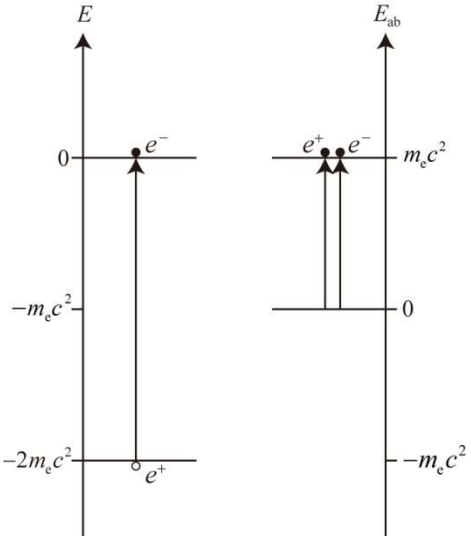

Figure 4a Figure 4b

Figure 4: Differences between Dirac's hole theory and the interpration in this paper

In Dirac's hole theory, when the γ-ray gives all of its energy to the virtual particles ($E = -2m_e c^2$) comprising the vacuum around the atomic nucleus, a virtual particle acquires rest mass, and is emitted as an electron into free space, while the hole opened in the vacuum is the positron (Figure 4a).

In the author's interpretation, an electron-positron pair is created because a γ-ray with an energy of 1.022 MeV gives rest mass to a virtual electron-positron pair at the position $r = r_e / 2$ (Figure 4b).

Next, the following table summarizes the energies of a hydrogen atom obtained from Eqs. (1) and (38). (Table.1) [14].

Table 1: Comparison of the energies of a hydrogen atom predicted by Bohr's classical quantum theory and this Paper

n	Bohr's Energy Levels, $E_{\mathrm{BO},n}$	This Paper, $E_{\mathrm{re},n}$
0	—	-0.511 MeV
1	-13.60569eV	-13.60515eV
2	-3.40142eV	-3.40139eV
3	-1.511744eV	-1.511737eV

VI. ORBITAL RADIUS OF AN ELECTRON IN A HYDROGEN ATOM

The following equation holds due to Eqs. (36b) and (43).

$$\frac{n^2}{n^2+\alpha^2}=\left(\frac{r_n-r_{\mathrm{e}}/2}{r_n}\right)^2. \tag{45}$$

From this, the following quadratic equation is obtained.

$$r_n^2-\left(\frac{n^2+\alpha^2}{\alpha^2}\right)r_{\mathrm{e}}r_n+\left(\frac{n^2+\alpha^2}{\alpha^2}\right)\frac{r_{\mathrm{e}}^2}{4}=0. \tag{46}$$

If this equation is solved for r_n ,

$$r_n^{\pm}=\frac{r_{\mathrm{e}}}{2}\left(1+\frac{n^2}{\alpha^2}\right)\left[1\pm\left(1+\frac{\alpha^2}{n^2}\right)^{-1/2}\right]. \tag{47}$$

Next, if the electron orbital radii corresponding to the energy levels in Eq. (38) are taken to be, respectively, $r_{\mathrm{re},n}^{+}$ and $r_{\mathrm{re},n}^{-}$,

$$r_{\mathrm{re},n}^{+}=\frac{r_{\mathrm{e}}}{2}\frac{\left(n^2+\alpha^2\right)^{1/2}}{\left(n^2+\alpha^2\right)^{1/2}-n}. \tag{48}$$

$$r_{\mathrm{re},n}^{-}=\frac{r_{\mathrm{e}}}{2}\frac{\left(n^2+\alpha^2\right)^{1/2}}{n^2+\alpha^{2\ 1/2}+n}. \tag{49}$$

Also, Eqs. (48) and (49) can be written as follows [15].

$$r_{\mathrm{re},n}^{+}=\frac{r_{\mathrm{e}}}{2}\left[1+\frac{n}{\left(n^2+\alpha^2\right)^{1/2}-n}\right]. \tag{50}$$

$$r_{\mathrm{re},n}^{-}=\frac{r_{\mathrm{e}}}{2}\left[1-\frac{n}{\left(n^2+\alpha^2\right)^{1/2}+n}\right]. \tag{51}$$

In this paper, $r_{\mathrm{re},n}^{+}$ is called the orbital radius, as is customary. However, a picture of the motion of the electron cannot be drawn, even if that motion is discussed at the level of classical quantum theory. The electron in a hydrogen atom is not in orbital motion around the atomic nucleus. The domain of the ordinary hydrogen atom that we all know starts from $r=r_{\mathrm{e}}/2\ \left(E_{\mathrm{ab},0}=0\right)$

The negative solutions for E and r have been discussed in another paper [16]. Therefore, that problem is not considered in this paper.

VII. DISCUSSION

A. First, if both sides of Eq. (13) are squared, and multiplied by $m_n^2/(m_e+m_n)$,

$$\frac{m_n^2}{m_e+m_n}\cdot\frac{v_n^2}{c^2}=\frac{\alpha^2}{n^2}\cdot\frac{m_n^2}{m_e+m_n}. \tag{52}$$

From this, the relativistic kinetic energy of the electron $K_{re,n}$ is,

$$K_{re,n}=-E_{re,n}=\frac{m_n^2v_n^2}{m_e+m_n}=\frac{\alpha^2c^2}{n^2}\cdot\frac{m_n^2}{m_e+m_n}. \tag{53}$$

Incidentally, the following relationship holds between m_e and m_n.

$$m_n=m_e\left(1+\frac{\alpha^2}{n^2}\right)^{-1/2}. \tag{54}$$

Equation (54) can be written as follows.

$$\left(\frac{\alpha^2}{n^2+\alpha^2}\right)^{1/2}=\frac{m_n}{m_e}. \tag{55}$$

If the relationship in Eq. (55) is used here,

$$K_{re,n}=-E_{re,n}=\frac{\alpha^2c^2}{n^2}\left(\frac{n^2}{n^2+\alpha^2}\right)m_e^2\cdot\frac{1}{m_e\left[1+\left(\frac{n^2}{n^2+\alpha^2}\right)^{1/2}\right]}. \tag{56}$$

Next, the following formula is multiplied with the numerator and denominator,.

$$1-\left(\frac{n^2}{n^2+\alpha^2}\right)^{1/2}.$$

When this is done,

$$E_{re,n}=-\frac{\alpha^2m_ec^2}{n^2}\left(\frac{n^2}{n^2+\alpha^2}\right)\left[1-\left(\frac{n^2}{n^2+\alpha^2}\right)^{1/2}\right]\left(1-\frac{n^2}{n^2+\alpha^2}\right)^{-1} \tag{57a}$$

$$=-\frac{\alpha^2m_ec^2}{n^2}\left(\frac{n^2}{n^2+\alpha^2}\right)\left[1-\left(\frac{n^2}{n^2+\alpha^2}\right)^{1/2}\right]\left(\frac{n^2+\alpha^2}{\alpha^2}\right) \tag{57b}$$

$$=m_ec^2\left[\left(\frac{n^2}{n^2+\alpha^2}\right)^{1/2}-1\right] \tag{57c}$$

$$=m_nc^2-m_ec^2. \tag{57d}$$

This enables derivation of Eq. (38) from Eq. (13).

B. If the energy levels derived by Bohr Eq. (1) are multiplied by the classical orbital radius Eq. (10),

$$E_{\mathrm{BO},n} r_{\mathrm{BO},n} = -\frac{\alpha^2 m_e c^2}{2n^2} \cdot \frac{r_e}{\alpha^2} n^2 = -m_e c^2 \cdot \frac{r_e}{2}. \tag{58}$$

Incidentally, the following equation holds due to Eqs. (42) and (30).

$$\frac{1}{2} \frac{1}{4\pi\varepsilon_0} \frac{e^2}{r_{\mathrm{re},n}} = m_e c^2 - m_n c^2. \tag{59}$$

Finding $r_{\mathrm{re},n}$ from Eq. (59),

$$r_{\mathrm{re},n} = \frac{r_e}{2} \frac{m_e}{m_e - m_n}. \tag{60}$$

Next, if we calculate the denominator of Eq. (60),

$$\frac{m_e}{m_e - m_n} = \frac{1}{1 - \frac{1}{\left(1 - \alpha^2 / n^2\right)^{1/2}}} = \frac{\left(n^2 + \alpha^2\right)^{1/2}}{\left(n^2 + \alpha^2\right)^{1/2} - n}. \tag{61}$$

Next, if we find the product of the relativistic energy levels derived in this paper (30) and the relativistic orbital radius (60),

$$E_{\mathrm{re},n}\, r_{\mathrm{re},n} = \left(m_n - m_e\right) c^2 \cdot \frac{r_e}{2} \frac{m_e}{m_e - m_n} = -m_e c^2 \cdot \frac{r_e}{2}. \tag{62}$$

The following relationship holds based on Eqs. (58) and (62).

$$E_{\mathrm{BO},n}\, r_{\mathrm{BO},n} = E_{\mathrm{re},n}\, r_{\mathrm{re},n}, \quad n = 1, 2, \cdots. \tag{63}$$

The points above are summarized in the following table.

Table 2: Products of $E_{\mathrm{BO},n}$ and $r_{\mathrm{BO},n}$ derived by Bohr

n	$E_{\mathrm{BO},n}$	$r_{\mathrm{BO},n}$	$E_{\mathrm{BO},n} r_{\mathrm{BO},n}$
0	—	—	—
1	$-\frac{\alpha^2 m_e c^2}{2}$	$\frac{r_e}{\alpha^2}$	$-m_e c^2 \cdot \frac{r_e}{2}$
n	$-\frac{\alpha^2 m_e c^2}{2n^2}$	$\frac{r_e}{\alpha^2} n^2$	$-m_e c^2 \cdot \frac{r_e}{2}$

Table 3: Products of $E_{\mathrm{re},n}$ and $r_{\mathrm{re},n}$ derived in this paper

n	$E_{\mathrm{re},n}$	$r_{\mathrm{re},n}$	$E_{\mathrm{re},n}r_{\mathrm{re},n}$
0	$-m_{\mathrm{e}}c^2$	$\frac{r_{\mathrm{e}}}{2}$	$-m_{\mathrm{e}}c^2\cdot\frac{r_{\mathrm{e}}}{2}$
1	$m_{\mathrm{e}}c^2\left[\left(\frac{1}{1+\alpha^2}\right)^{1/2}-1\right]$	$\frac{r_{\mathrm{e}}}{2}\left[1+\frac{1}{\left(1+\alpha^2\right)^{1/2}-1}\right]$	$-m_{\mathrm{e}}c^2\cdot\frac{r_{\mathrm{e}}}{2}$
n	$m_{\mathrm{e}}c^2\left[\left(\frac{n^2}{n^2+\alpha^2}\right)^{1/2}-1\right]$, $m_nc^2-m_{\mathrm{e}}c^2$	$\frac{r_{\mathrm{e}}}{2}\left[1+\frac{n}{\left(n^2+\alpha^2\right)^{1/2}-n}\right]$, $\frac{r_{\mathrm{e}}}{2}\frac{m_{\mathrm{e}}}{m_{\mathrm{e}}-m_n}$	$-m_{\mathrm{e}}c^2\cdot\frac{r_{\mathrm{e}}}{2}$

C. Rewriting Eq. (33) into a relation for momentum yields the following.

$$\left(m_nc\right)^2+p_{\mathrm{re},n}^2=\left(m_{\mathrm{e}}c\right)^2. \tag{64}$$

Also, $p_{\mathrm{re},n}$ can be written as follows.

$$p_{\mathrm{re},n}=m_nv_n=m_{\mathrm{e}}\left(\frac{n^2}{n^2+\alpha^2}\right)^{1/2}\frac{\alpha c}{n}=m_{\mathrm{e}}c\left(\frac{\alpha^2}{n^2+\alpha^2}\right)^{1/2}. \tag{65}$$

Therefore, Eq. (64) can be written:

$$\left[m_{\mathrm{e}}c\left(\frac{n^2}{n^2+\alpha^2}\right)^{1/2}\right]^2+\left[m_{\mathrm{e}}c\left(\frac{\alpha^2}{n^2+\alpha^2}\right)^{1/2}\right]^2=\left(m_{\mathrm{e}}c\right)^2. \tag{66}$$

Here, taking the ratio of the first term and the momentum of the second term on the left side of Eq. (64),

$$\frac{p_{\mathrm{re},n}}{m_nc}=\frac{v_n}{c}. \tag{67}$$

Similarly, taking the ratio of the first term and the momentum of the second term on the left side of Eq. (66),

$$m_{\mathrm{e}}c\left(\frac{\alpha^2}{n^2+\alpha^2}\right)^{1/2}\cdot\frac{1}{m_{\mathrm{e}}c}\left(\frac{n^2+\alpha^2}{n^2}\right)^{1/2}=\frac{\alpha}{n}. \tag{68}$$

From Eqs. (67) and (68),

$$\frac{p_{\mathrm{re},n}}{m_nc}=\frac{\alpha}{n}. \tag{69}$$

The author has previously presented Eq. (13) as a new quantum condition to replace Bohr's quantum condition. However, the reason why Eq. (13) holds is because Eq. (69) holds. Therefore, Eq. (69) is actually a quantum condition to replace the quantum condition of Bohr.

VIII. CONCLUSION

As indicated by Eq. (40), Eq. (1) for the energy levels of a hydrogen atom derived classically by Bohr is an approximation of Eq. (38), the formula for the relativistic energy levels of a hydrogen atom. In Eq. (38), the principal quantum number n starts from 0. Energy and r in the state where n=0 are as follows.

$$E_{\mathrm{ab},0} = 0, \quad E_{\mathrm{re},0} = -m_{\mathrm{e}}c^2. \tag{70}$$

$$r_{\mathrm{re},0} = \frac{r_{\mathrm{e}}}{2}. \tag{71}$$

It is thought that an electron in the n=0 state forms a pair with a positron, and constitutes the vacuum inside the hydrogen atom.

Also, this paper has shown that the relativistic energy levels $E_{\mathrm{re},n}$ and $r_{\mathrm{re},n}$ of an ordinary hydrogen atom can be described using the following two types of formulas.

$$E_{\mathrm{re},n} = m_n c^2 - m_{\mathrm{e}}c^2, \quad n = 0,1,2,\cdots. \tag{72}$$

$$r_{\mathrm{re},n} = \frac{r_{\mathrm{e}}}{2}\frac{m_{\mathrm{e}}}{m_{\mathrm{e}} - m_n}. \tag{73}$$

$$E_{\mathrm{re},n} = m_{\mathrm{e}}c^2\left[\left(\frac{n^2}{n^2+\alpha^2}\right)^{1/2} - 1\right], \quad n = 0,1,2,\cdots. \tag{74}$$

$$r_{\mathrm{re},n} = \frac{r_{\mathrm{e}}}{2}\left[1 + \frac{n}{\left(n^2+\alpha^2\right)^{1/2} - n}\right]. \tag{75}$$

Multiplying E and r, we obtain:

$$E_{\mathrm{BO},n}\, r_{\mathrm{BO},n} = E_{\mathrm{re},n}\, r_{\mathrm{re},n} = -m_{\mathrm{e}}c^2 \cdot \frac{r_{\mathrm{e}}}{2}, \quad n = 1,2,\cdots. \tag{76}$$

$$E_{\mathrm{re},0}\, r_{\mathrm{re},0} = -m_{\mathrm{e}}c^2 \cdot \frac{r_{\mathrm{e}}}{2}. \tag{77}$$

$$E_{\mathrm{BO},0}\, r_{\mathrm{BO},0} \neq -m_{\mathrm{e}}c^2 \cdot \frac{r_{\mathrm{e}}}{2}. \tag{78}$$

As is evident from Eqs. (76) to (78), the products of the energy levels E and r of a hydrogen atom are always fixed values. In a hydrogen atom, Eqs. (70) and (71) become important quantities. Those important quantities are involved in the formulas (74) and (75) derived in this paper.

However, there is no relation between the solution derived by Bohr and Eqs. (70) and (71).

In the end, Bohr's formulas (1) and (2) are just approximations of Eqs. (74) and (75), and they are not accurate. Since the n=0 energy level is missing, quantum mechanics is an inadequate theory.

REFERENCES

1. Bohr, N. (1913). On the Constitution of Atoms and Molecules. *Philosophical Magazine*, *26,* 1. https://doi.org/10.1080/14786441308634955
2. Suto, K. (2014). *n*=0 Energy Level Present in the Hydrogen Atom. *Applied Physics Research,* 6, 109-115. https://doi.org/10.5539/apr.v6n5p109
3. Suto, K. (2019). The Relationship Enfolded in Bohr's Quantum Condition and a Previously Unknown Formula for Kinetic Energy. *Applied Physics Research,* 11(1), 19-34. https://doi.org/10.5539/apr.v11n1p19
4. Suto, K. (2020). The Planck Constant Was Not a Universal Constant. *Journal of Applied Mathematics and Physics*, 8, 456-463. https://doi.org/10.4236/jamp.2020.83035
5. Suto, K. (2021). The Quantum Condition That Should Have Been Assumed by Bohr When Deriving the Energy Levels of a Hydrogen Atom. *Journal of Applied Mathematics and Physics,* 9, 1230-1244. https://doi.org/10.4236/jamp.2021.96084
6. Sommerfeld, A. (1923). Atomic Structure and Spectral Lines, Methuen & Co. Ltd., London, 528.
7. Einstein, A. (1961). Relativity. Crown, New York, 43.
8. Suto, K. (2011). An Energy-Momentum Relationship for a Bound Electron inside a Hydrogen Atom. *Physics Essays,* 24, 301-307. https://doi.org/10.4006/1.3583810
9. Suto, K. (2009). True nature of potential energy of a hydrogen atom. *Physics Essays*, *22*(2),135-139. http://dx.doi.org/10.4006/1.3092779
10. Suto, K. (2018). Potential Energy of the Electron in a Hydrogen Atom and a Model of a Virtual Particle Pair Constituting the Vacuum, *Applied Physics Research,* 10 (4), 93-101. https://doi.org//10.5539/apr.v10n4p93
11. Suto, K. (2022). A Compelling Formula Indicating the Existence of Ultra-low Energy Levels in the Hydrogen Atom, *Global Journal of science frontier research*: A. 22 (5). DOI: 10.34257/gjsfrevol22is5pg7
12. Suto, K. (2022). A Surprising Physical Quantity Involved in the Phase Velocity and Energy Levels of the Electron in a Hydrogen Atom. *Applied Physics Research,* 14 (2), 1-17. https://doi.org//10.5539/apr.v14n2p1
13. Suto, K. (2021). Dark Matter Has Already Been Discovered. *Applied Physics Research*, 13 (6), 36-47. https://doi.org/10.5539/apr.v13n3p36
14. Suto, K. (2020). The Incompleteness of Quantum Mechanics Demonstrated by Considerations of Relativistic Kinetic Energy. *Journal of Applied Mathematics and Physics,* 8, 210-217. https://doi.org/10.4236/jamp.2020.82016
15. Suto, K. (2017). Region of Dark Matter Present in the Hydrogen Atom, *Journal of Physical Mathematics,* 8 (4), 1-6. doi: 10.4172/2090-0902.1000252
16. Suto, K. (2020). Theoretical Prediction of Negative Energy Specific to the Electron. *Journal of Modern Physics,* 11, 712-724. https://doi.org/10.4236/jmp.2020.115046